Inside PROLITH™

A Comprehensive Guide to Optical Lithography Simulation

For the PROLITH Family of Lithography Simulation Tools, v5.0

Chris A. Mack
FINLE Technologies, Inc.
Austin, Texas

Published by FINLE Technologies, Inc., Austin, Texas, USA

First Published 1997
Second Printing, 1997

Mack, Chris A., 1960-
Inside PROLITH: A Comprehensive Guide to Optical Lithography Simulation / Chris A. Mack

ISBN 0-9650922-0-8
Library of Congress Catalog Card No. 97-060438

1. Optical Lithography. 2. Lithography Simulation I. Title

Printed in the United States of America

Table of Contents

Chapter 1

Introduction

Optical lithography modeling began in the early 1970s when Rick Dill started an effort at IBM Yorktown Heights Research Center to describe the basic steps of the lithography process with mathematical equations. At a time when lithography was considered a true art, such an approach was met with much skepticism. The results of their pioneering work were published in a landmark series of papers in 1975 [1.1-1.4], now referred to as the "Dill papers." These papers not only gave birth to the field of lithography modeling, they represented the first serious attempt to describe lithography not as an art, but as a science. These papers presented a simple model for image formation with incoherent illumination, the first order kinetic "Dill model" of exposure, and an empirical model for development coupled with a cell algorithm for photoresist profile calculation. The Dill papers are still the most referenced works in the body of lithography literature.

While Dill's group worked on the beginnings of lithography simulation, a professor from the University of California at Berkeley, Andy Neureuther, spent a year on sabbatical working with Dill. Upon returning to Berkeley, Neureuther and another professor, Bill Oldham, started their own modeling effort. In 1979 they presented the first result of their effort, the lithography modeling program SAMPLE [1.5]. SAMPLE improved the state of the art in

lithography modeling by adding partial coherence to the image calculations and by replacing the cell algorithm for dissolution calculations with a string algorithm. But more importantly, SAMPLE was made available to the lithography community. For the first time, researchers in the field could use modeling as a tool to help understand and improve their lithography processes.

The author began working in the area of lithographic simulation in 1983 and in 1985 introduced the model PROLITH (the Positive Resist Optical LITHography model) [1.6]. This model added an analytical expression for the standing wave intensity in the resist, a prebake model, a kinetic model for resist development (now known as the Mack model), and the first model for contact and proximity printing. PROLITH was also the first lithography simulator to run on a personal computer (the IBM PC), making lithography modeling accessible to all lithographers, from advanced researchers to process development engineers to manufacturing engineers. Over the years, PROLITH advanced to include a model for contrast enhancement materials, the extended source method for partially coherent image calculations, and an advanced focus model for high numerical aperture imaging.

In 1990, a commercial version of PROLITH was introduced by FINLE Technologies and was called PROLITH/2, the second generation optical lithography model. This model combined the advanced calculations of PROLITH with an easy-to-use interface and impressive graphics to provide a complete modeling package. In the years since its introduction, PROLITH/2 has continued to advance the state-of-the-art in lithography simulation while becoming the world's most popular lithography model. PROLITH/2 has become the cornerstone of the PROLITH family of lithography simulation software. In addition to PROLITH/2, PROXLITH/2 has been developed to simulate contact and proximity printing, and PROLITH/3D extends the two-dimensional modeling of PROLITH/2 into three dimensions. ProCD performs statistical analysis of simulated linewidth data to predict linewidth distributions across the wafer. Finally, ProABC and ProDRM analyze experimental resist data to extract the exposure and development modeling parameters of the resist.

The PROLITH family provides an extensive suite of software applications for predicting and analyzing lithography. This book, however, is focused mostly on PROLITH/2 and PROLITH/3D. Chapter 4 describes the diffraction models specific to PROXLITH/2, and some information about

ProABC and ProDRM can be found in Chapters 5 and 7, respectively. ProCD is not discussed but is mentioned in Chapter 10.

PROLITH/2 simulates the basic lithographic steps of image formation, resist exposure, post-exposure bake diffusion, and development to obtain a final resist profile. Figure 1-1 shows a basic schematic of the calculation steps required for lithography modeling. Below is a brief overview of the physical models found in PROLITH/2. More details on these models can be found in subsequent chapters.

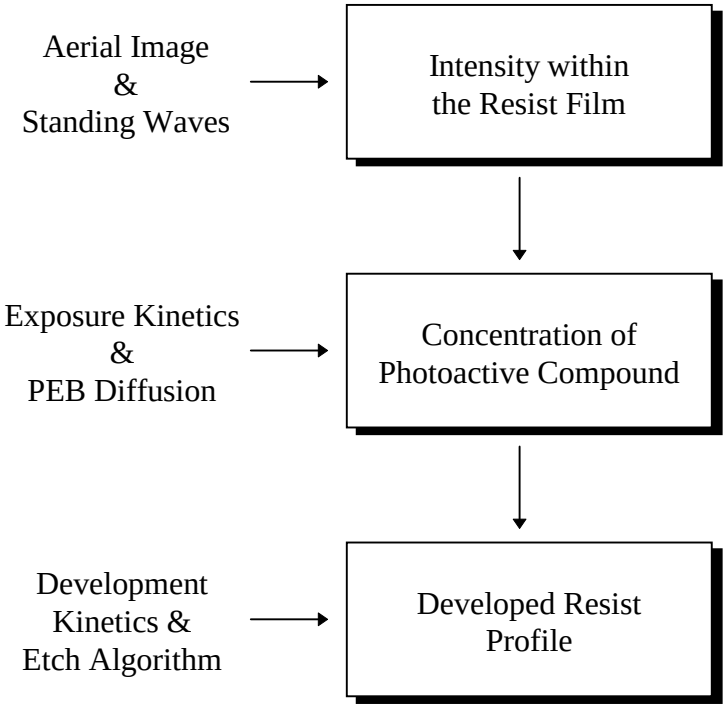

Figure 1-1. Flow diagram of a lithography model.

Aerial Image: The extended source method is used to predict the aerial image of a partially coherent diffraction limited or aberrated projection system based on scalar and/or vector diffraction theory. Single wavelength or broadband illumination can be used. The standard image model accounts for the important effect of image defocus through the resist film. Mask patterns can be one-dimensional lines and spaces or small two dimensional contacts and islands. Phase-shifting masks and off-axis illumination can be simulated with optional modules. Pupil filters can be defined. The user can also select the high-NA scalar model to increase the accuracy of calculations for numerical apertures of 0.5 or greater, and an optional vector model can be used for very high numerical apertures. An optional module allows the user to simulate arbitrarily complex two-dimensional mask features as well.

Standing Waves: An analytical expression is used to calculate the standing wave intensity as a function of depth into the resist, including the effects of resist bleaching, on planar substrates. Film stacks can be defined below the resist with up to 14 layers between the resist and substrate. Contrast enhancement layers or top-layer anti-reflection coatings can also be included. The high NA models include the effects of non-vertical light propagation.

Prebake: Thermal decomposition of the photoresist photoactive compound during prebake is modeled using first order kinetics resulting in a change in the resist's optical properties (the Dill parameters A and B). Many important bake effects, however, are not yet well understood.

Exposure: First order kinetics are used to model the chemistry of exposure using the standard Dill ABC parameters. Both positive and negative resists can be simulated.

Post-Exposure Bake: A two-dimensional (or three-dimensional for PROLITH/3D) diffusion calculation allows the post-exposure bake to reduce the effects of standing waves. For chemically amplified resists, this diffusion is accompanied by an amplification reaction which accounts for crosslinking, blocking, or deblocking in an acid catalyzed reaction. Acid loss mechanisms and non-constant diffusivity can also be simulated.

Development: The Mack kinetic model or the enhanced Mack model for resist dissolution are used in conjunction with an etching algorithm to determine the resist profile. Surface inhibition or enhancement can also be taken into account. Alternatively, a data file of development rate information can be used.

CD Measurement: Three models for measurement of the photoresist linewidth gives accuracy and flexibility to match the model to an actual CD measurement tool.

Lumped Parameter Model: This simple two-parameter model of resist exposure and development allows for extremely fast calculation of a focus-exposure matrix and the resulting process window. Although not as accurate as the full PROLITH/2 models, the LPM is ideal for quick results and optimization work.

The combination of the models described above provides a complete mathematical description of the optical lithography process. Use of the models incorporated in PROLITH/2 allows the user to investigate many interesting and important aspects of optical lithography. The following chapters describe each of the models in detail, including derivations of most of the mathematical models as well as physical descriptions of their basis. The final chapter describes a variety of uses for lithography simulation.

References

1.1. F. H. Dill, "Optical Lithography," *IEEE Trans. Electron Devices*, ED-22, No. 7 (1975) pp. 440-444.

1.2. F. H. Dill, W. P. Hornberger, P. S. Hauge, and J. M. Shaw, "Characterization of Positive Photoresist," *IEEE Trans. Electron Devices*, ED-22, No. 7 (July, 1975) pp. 445-452.

1.3. K. L. Konnerth and F. H. Dill, "In-Situ Measurement of Dielectric Thickness During Etching or Developing Processes," *IEEE Trans. Electron Devices*, ED-22, No. 7 (1975) pp. 452-456.

1.4. F. H. Dill, A. R. Neureuther, J. A. Tuttle, and E. J. Walker "Modeling Projection Printing of Positive Photoresists," *IEEE Trans. Electron Devices*, ED-22, No. 7 (1975) pp. 456-464.

1.5. W. G. Oldham, S. N. Nandgaonkar, A. R. Neureuther and M. O'Toole, "A General Simulator for VLSI Lithography and Etching Processes: Part I - Application to Projection Lithography," *IEEE Trans. Electron Devices*, ED-26, No. 4 (April, 1979) pp. 717-722.

1.6. C. A. Mack, "PROLITH: A Comprehensive Optical Lithography Model," *Optical Microlithography IV, Proc.*, SPIE Vol. 538 (1985) pp. 207-220.

Chapter 2

Aerial Image Formation

Projection printing means projecting the image of a photomask (also called a reticle) onto a resist coated wafer. The imaging process is a well-studied optical phenomenon. We will begin at the most basic level with a mathematical description of light.

A. Mathematical Description of Light

Light is an electromagnetic wave with coupled electric and magnetic fields traveling through space. Since the electric and magnetic fields are related to each other (the magnetic field is always perpendicular to the electric field and both fields are always perpendicular to the direction of propagation) and since photoresist reacts chemically to the electric field only, we can describe light by describing just the electric field. A general electric field E (due to monochromatic light of frequency ω) at any point P and time t can be described by a deceptively simple sinusoidal equation.

$$E(P,t) = A(P)\cos(\omega t + \Phi(P)) \tag{2.1}$$

where A is the amplitude and Φ is the phase, both of which are position dependent, in general. Equation (2.1) is a general solution to the Helmholtz wave equation, which is itself a simplification and combination of Maxwell's equations for the propagation of electromagnetic waves. As an example of one form of equation (2.1), consider a "plane wave" of light traveling in the $+z$ direction. The term plane wave refers to the shape of the wavefront, i.e., the shape of the function $\Phi(P)$ = constant. Thus, a plane wave traveling in the $+z$ direction would require a constant phase (and, incidentally, a constant amplitude) in the x-y plane. Such a plane wave would be described by the equation

$$E(P,t) = A\cos(\omega t - kz) \tag{2.2}$$

where k is a constant called the *propagation constant* or the *wave number*.

How does the wave represented by equation (2.2) propagate? We can think of the wave as having a certain shape, and this shape travels through time. Thus, this wave will have the given shape at all points in space and time such that $\omega t - kz$ = constant, giving the same electric field. In other words, the wavefront (a plane in this case) travels through space and time according to

$$z - z_0 = \frac{\omega}{k} t \tag{2.3}$$

where z_o is a constant corresponding to the position of the plane wave at t=0. This is simply a plane of light traveling in the $+z$ direction at speed ω/k.

Although equation (2.1) completely describes an arbitrary electromagnetic field, a more compact and convenient representation is possible based on the assumption that the frequency of the light does not change (quite a good assumption under normal optical conditions). A sinusoid can be related to a complex exponential by

$$E(P,t) = A(P)\cos(\omega t + \Phi(P)) = \mathrm{Re}\left\{ U(P)e^{-i\omega t} \right\} \tag{2.4}$$

where $$U(P) = A(P)e^{-i\Phi(P)}$$

and *U(P)* is called the *phasor* representation of the sinusoidal electric field *E(P,t)*. Notice that this phasor representation shows no time dependence. Study of the basic behavior of light has shown that the time dependence of the electric field typically does not change as light travels, interferes, and interacts with matter. Thus, suppressing the time dependence and expressing the electric field as a phasor has become quite common in the mathematical analysis of optical systems.

Since converting back to the time domain involves taking the real part of the phasor, the sign of the phase in *U(P)* and in the time dependent term could just as easily have been chosen to be positive rather than negative. The sign convention chosen is not consistent among authors and there is no absolute standard. The sign convention represented by equation (2.4) is used by Goodman [2.1] and in other standard optics textbooks dealing with imaging. Using this convention, a plane wave traveling in the +*z* direction (i.e., equation (2.2)) would be written as

$$U(P) = Ae^{ikz} \tag{2.5}$$

The negative phase sign convention of equation (2.4) is the most common for imaging applications. Unfortunately, most publications and textbooks in the area of thin film interference effects and coatings use the positive phase sign convention. For this thin film sign convention, equation (2.5) would represent a plane wave traveling in the -*z* direction. Lithography simulation uses both imaging calculations and thin film interference calculations. As such, both of these competing "standard" sign conventions will be used in this book, mainly for historical reasons. Of course, this is terribly confusing, but I will try to alleviate the confusion by clarifying the sign convention used throughout this book.

B. Basic Imaging Theory

Consider the generic projection system shown in Figure 2-1. It consists of a *light source*, a *condenser lens*, the *mask*, the *objective lens*, and finally the resist-coated wafer. The combination of the light source and the condenser lens

is called the *illumination system*. In optical design terms a lens is a system of (possibly many) lens elements. Each lens element is an individual piece of glass (refractive element) or a mirror (reflective element). The purpose of the illumination system is to deliver light to the mask (and eventually into the objective lens) with sufficient intensity, the proper directionality and spectral characteristics, and adequate uniformity across the field. The light then passes through the clear areas of the mask and diffracts on its way to the objective lens. The purpose of the objective lens is to pick up a portion of the diffraction pattern and project an image onto the wafer which, one hopes, will resemble the mask pattern.

The first and most basic phenomenon occurring here is the diffraction of light. Diffraction is usually thought of as the bending of light as it passes through an aperture, which is certainly an appropriate description for diffraction by a lithographic mask. More correctly, diffraction theory simply describes how light propagates. This propagation includes the effects of the surroundings (boundaries). Maxwell's equations describe how electromagnetic waves propagate, but result in partial differential equations of vector quantities which, for general boundary conditions, are extremely difficult to solve without the aid of a powerful computer. A simpler approach is to artificially decouple the electric and magnetic field *vector* components and describe light as a *scalar* quantity. Under most conditions scalar diffraction theory is surprisingly accurate.

Scalar diffraction theory was first rigorously used by Kirchoff in 1882, and involves performing one numerical integration (much simpler than solving partial differential equations!). Kirchoff diffraction was further simplified by Fresnel for the case when the distance away from the diffracting plane (that is, the distance from the mask to the objective lens) is much greater than the wavelength of light. Finally, if the distance to the objective lens is very large, or if the mask is illuminated by a spherical wave which converges to a point at the entrance to the objective lens, Fresnel diffraction simplifies to *Fraunhofer diffraction*. Comparison of these different diffraction regions is given in Figure 2-2.

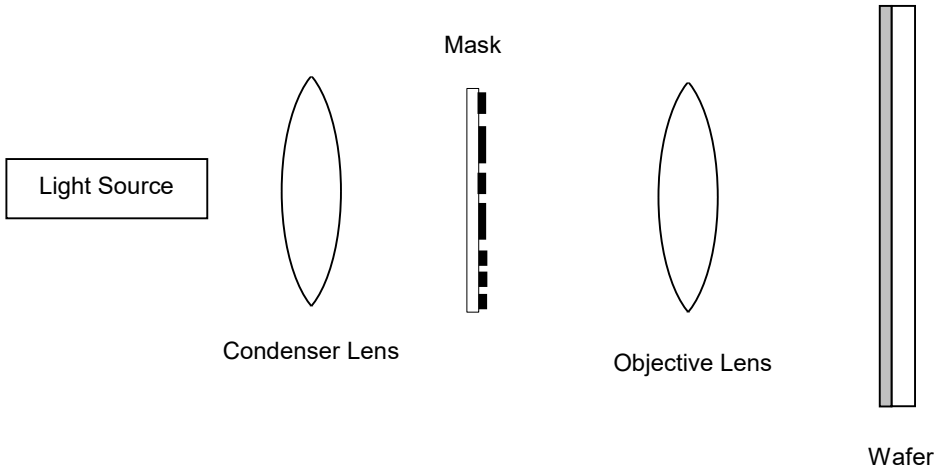

Figure 2-1. Block diagram of a generic projection system.

In order to establish a mathematical description of diffraction by a mask, let us describe the electric field transmittance of a mask pattern as *m(x,y)*, where the mask is in the *x,y*-plane and *m(x,y)* has in general both magnitude and phase. For a simple chrome-glass mask, the mask pattern becomes binary: *m(x,y)* is 1 under the glass and 0 under the chrome. Let the *x′,y′*-plane be the diffraction plane, that is, the entrance to the objective lens, and let *z* be the distance from the mask to the objective lens. Finally, we will assume monochromatic light of wavelength λ and that the entire system is in air (so that its index of refraction can be dropped). Then, the electric field of our diffraction pattern, *E(x′,y′)*, is given by the Fraunhofer diffraction integral:

$$E(x',y') = \int_{-\infty}^{\infty}\int_{-\infty}^{\infty} m(x,y)\, e^{-2\pi i(f_x x + f_y y)}\, dx\, dy \qquad (2.6)$$

where $f_x = x'/(z\lambda)$ and $f_y = y'/(z\lambda)$ and are called the *spatial frequencies* of the diffraction pattern.

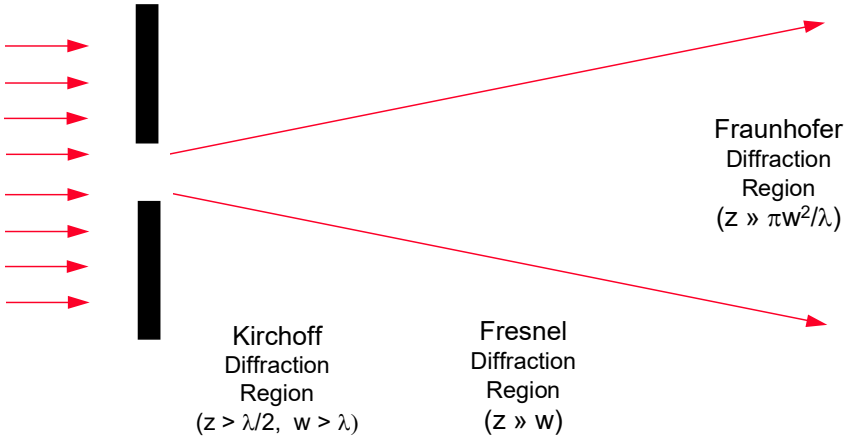

Figure 2-2. Comparison of the diffraction "regions" where various approximations become accurate. Diffraction is for a slit of width *w* illuminated by light of wavelength λ, and *z* is the distance away from the mask.

For many scientists and engineers (and especially electrical engineers), this equation should be quite familiar: it is simply a *Fourier transform*. Thus, the diffraction pattern (i.e., the electric field distribution as it enters the objective lens) is just the Fourier transform of the mask pattern. This is the principle behind an entire field of science called Fourier Optics (for more information, consult Goodman's classic textbook [2.1]).

Figure 2-3 shows two mask patterns, one an isolated space, the other a series of equal lines and spaces, both infinitely long in the *y*-direction (the direction out of the page). The resulting mask pattern functions, *m(x)*, look like a square pulse and a square wave, respectively. The Fourier transforms are easily found in tables or textbooks and are also shown in Figure 2-3. The isolated space gives rise to a *sinc* function diffraction pattern, and the equal lines and spaces yield discrete *diffraction orders*.

$$E_{isolated\ space}(x') = \frac{\sin(\pi w f_x)}{\pi f_x}$$

$$E_{dense\ space}(x') = \sum_{n=-\infty}^{\infty} \frac{\sin(\pi w f_x)}{\pi f_x} \delta\left(f_x - \frac{n}{p}\right) \tag{2.7}$$

where δ is the Dirac delta function.

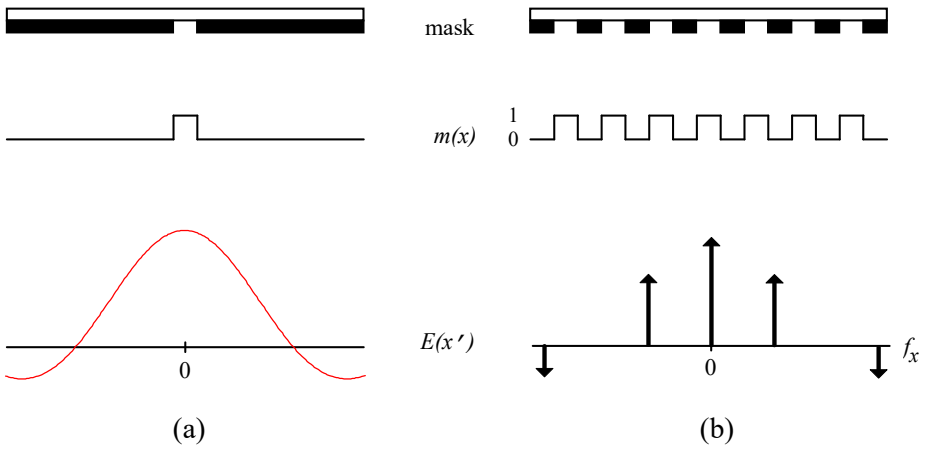

Figure 2-3. Two typical mask patterns, an isolated space and an array of equal lines and spaces, and the resulting Fraunhofer diffraction patterns assuming normally incident plane wave illumination.

Let's take a closer look at the diffraction pattern for equal lines and spaces. Notice that the graphs of the diffraction patterns in Figure 2-3 use spatial frequency as its x-axis. Since z and λ are fixed for a given optical system, the spatial frequency is simply a scaled x'-coordinate. At the center of the objective lens entrance ($f_x = 0$) the diffraction pattern has a bright spot called the *zero order*. The zero order is the light which passes through the mask and is not diffracted. The zero order can be thought of as "D.C." light, providing power but no information as to the size of the features on the mask. To either side of the zero order are two peaks called the *first diffraction orders*. These peaks occur at spatial frequencies of $\pm 1/p$ where p is the pitch of the mask pattern (linewidth plus spacewidth). Since the position of these diffraction orders

depends on the mask pitch, their position contains information about the pitch. It is this information that the objective lens will use to reproduce the image of the mask. In fact, in order for the objective lens to form a true image of the mask it must have the zero order and at least one higher order. In addition to the first order, there can be many higher orders, with the n^{th} order occurring at a spatial frequency of n/p.

Summarizing, given a mask in the x-y plane described by its electric field transmission $m(x,y)$, the electric field M as it enters the objective lens (the x'-y' plane) is given by

$$M(f_x, f_y) = \mathcal{F}\{m(x,y)\} \tag{2.8}$$

where the symbol $\mathcal{F}$ represents the Fourier transform and f_x and f_y are the spatial frequencies and are simply scaled coordinates in the x'-y' plane.

We are now ready to describe what happens next and follow the diffracted light as it enters the objective lens. In general, the diffraction pattern extends throughout the x'-y' plane. However, the objective lens, being only of finite size, cannot collect all of the light in the diffraction pattern. Typically, lenses used in microlithography are circularly symmetric and the entrance to the objective lens can be thought of as a circular aperture. Only those portions of the mask diffraction pattern which fall inside the aperture of the objective lens go on to form the image. Of course we can describe the size of the lens aperture by its radius, but a more common and useful description is to define the maximum angle of diffracted light which can enter the lens. Consider the geometry shown in Figure 2-4. Light passing through the mask is diffracted at various angles. Given a lens of a certain size placed a certain distance from the mask, there is some maximum angle of diffraction, α, for which diffracted light just makes it into the lens. Light emerging from the mask at larger angles misses the lens and is not used in forming the image. The most convenient way to describe the size of the lens aperture is by its *numerical aperture*, defined as the sine of the maximum half-angle of diffracted light which can enter the lens times the index of refraction of the surrounding medium. In the case of lithography, all of the lenses are in air and the numerical aperture is given by $NA = \sin\alpha$. (Note that the spatial frequency is the sine of the diffracted angle divided by the wavelength of light. Thus, the maximum spatial frequency which can enter the objective lens is given by NA/λ.)

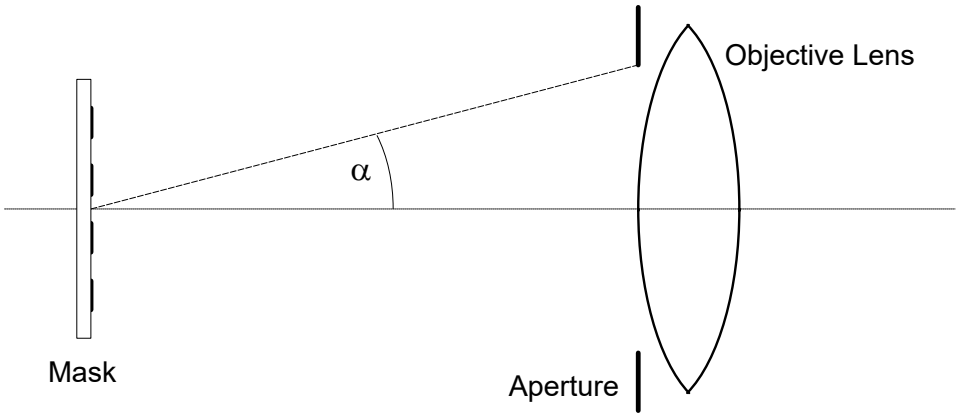

Figure 2-4. The numerical aperture is defined as $NA = sin\alpha$ where α is the maximum half-angle of the diffracted light which can enter the objective lens (the lens and mask are in air).

Obviously, the numerical aperture is going to be quite important. A large numerical aperture means that a larger portion of the diffraction pattern is captured by the objective lens. For a small numerical aperture, much more of the diffracted light is lost. In fact, we can use this viewpoint to define *resolution*, at least from the limited perspective of image formation. Consider the simple case of a mask pattern of equal lines and spaces. As we have seen, the resulting diffraction pattern is a series of discrete diffraction orders. In order to produce an image which even remotely resembles the original mask pattern it is necessary for the objective lens to capture the zero order (i.e., the undiffracted light) and at least one higher diffraction order. If the light illuminating the mask is a normally incident plane wave, the diffraction pattern will be centered in the objective lens. Since the position of the ± 1 diffraction orders are given by $\pm 1/p$ where p is the pitch of the mask pattern, the requirement that a lens of a finite size must capture these diffraction orders to form an image puts a lower limit on the pitch which can be imaged. Thus, the smallest pitch (p_{min}) which still produces an image would put the first diffraction order at the outer edge of the objective lens. Thus,

$$\frac{1}{p_{\min}} = \frac{NA}{\lambda} \tag{2.9}$$

If we let R represent the resolution element (the linewidth or the spacewidth) of our equal line/space pattern, the resolution will be given by

$$R = 0.5\frac{\lambda}{NA} \tag{2.10}$$

This classic equation is often called the *theoretical resolution* of an imaging system. Note that several very specific assumptions were made in deriving this resolution equation: a mask pattern of equal lines and spaces was used, and the illumination was a single wavelength normally incident plane wave (called coherent illumination). For other features, for example an isolated line, there is no clear resolution cut-off. For other types of illumination, this cut-off will change.

To proceed further, we must now describe how the lens affects the light entering it. Obviously, we would like the image to resemble the mask pattern. Since diffraction gives the Fourier transform of the mask, if the lens could give the *inverse* Fourier transform of the diffraction pattern, the resulting image would resemble the mask pattern. In fact, spherical lenses do behave precisely in this way. We can define an ideal imaging lens as one which produces an image which is identically equal to the inverse Fourier transform of the light distribution entering the lens. It is the goal of lens designers and manufacturers to create lenses as close as possible to this ideal. Does an ideal lens produce a perfect image? No. Because of the finite size of the numerical aperture, only a portion of the diffraction pattern enters the lens. Thus, even an ideal lens cannot produce a perfect image unless the lens is infinitely big. Since in the case of an ideal lens the image is limited only by the diffracted light which does not make it through the lens, we call such an ideal system *diffraction limited*.

In order to write our final equation for the formation of an image, let us define the objective lens *pupil function P* (a pupil is just another name for an aperture). The pupil function of an ideal lens simply describes what portion of light enters the lens: it is one inside the aperture and zero outside:

$$P(f_x, f_y) = \begin{cases} 1, & \sqrt{f_x^2 + f_y^2} < NA / \lambda \\ 0, & \sqrt{f_x^2 + f_y^2} > NA / \lambda \end{cases} \tag{2.11}$$

Thus, the product of the pupil function and the diffraction pattern describes the light entering the objective lens. Combining this with our description of how a lens behaves gives us our final expression for the electric field at the image plane (that is, at the wafer):

$$E(x,y) = \mathcal{F}^{-1}\{M(f_x, f_y)P(f_x, f_y)\} \tag{2.12}$$

where the symbol $\mathcal{F}^{-1}$ represents the inverse Fourier transform.

The *aerial image* is defined as the intensity distribution at the wafer and is simply the square of the magnitude of the electric field.

Consider the full imaging process. First, light passing through the mask is diffracted. The diffraction pattern can be described as the Fourier transform of the mask pattern. Since the objective lens is of finite size, only a portion of the diffraction pattern actually enters the lens. The numerical aperture describes the maximum angle of diffracted light which enters the lens and the pupil function is used to mathematically describe this behavior. Finally, the effect of the lens is to take the inverse Fourier transform of the light entering the lens to give an image which resembles the mask pattern. If the lens is ideal, the quality of the resulting image is only limited by how much of the diffraction pattern is collected. This type of imaging system is called diffraction limited.

Although we have completely described the behavior of a simple ideal imaging system, we must add one more complication before we have described the operation of a projection system for lithography. So far, we have assumed that the mask is illuminated by *spatially coherent* light. Coherent illumination means simply that the light striking the mask arrives from only one direction. We have further assumed that the coherent illumination on the mask is normally incident. The result was a diffraction pattern which was centered in the entrance to the objective lens. What would happen if we changed the direction of the illumination so that the light struck the mask at some angle θ'? The effect is

simply to shift the position of the diffraction pattern with respect to the lens aperture (in terms of spatial frequency, the amount shifted is $\sin\theta'/\lambda$), as seen in Figure 2-5. Recalling that only the portion of the diffraction pattern passing through the lens aperture is used to form the image, it is quite apparent that this shift in the position of the diffraction pattern can have a profound effect on the resulting image. Letting f_x' and f_y' be the shift in the spatial frequency due to the tilted illumination, equation (2.12) becomes

$$E(x, y, f_x', f_y') = \mathcal{F}^{-1}\{M(f_x - f_x', f_y - f_y')P(f_x, f_y)\}$$

$$I(x, y, f_x', f_y') = |E(x, y, f_x', f_y')|^2 \qquad (2.13)$$

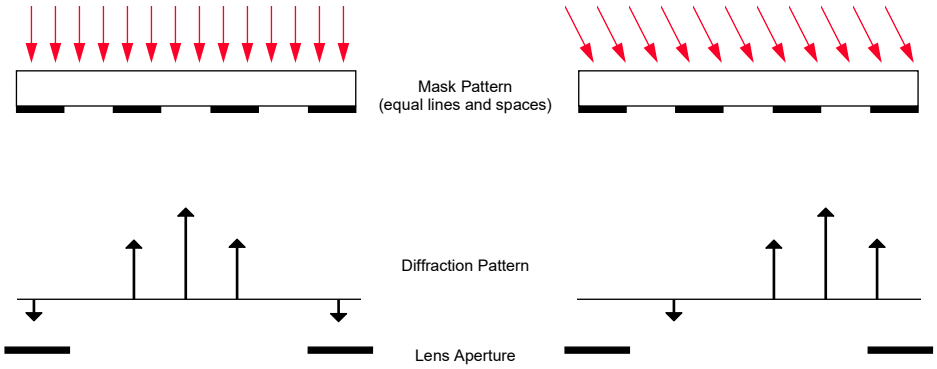

Figure 2-5. The effect of changing the angle of incidence of plane wave illumination on the diffraction pattern is simply to shift its position in the lens aperture.

If the illumination of the mask is composed of light coming from a range of angles rather than just one angle, the illumination is called *partially coherent*. If one angle of illumination causes a shift in the diffraction pattern, a range of

angles will cause a range of shifts, resulting in broadened diffraction orders (Figure 2-6). One can characterize the range of angles used for the illumination in several ways, but the most common is the *partial coherence factor*, σ (also called the degree of partial coherence, or the pupil filling function, or just the partial coherence). The partial coherence is defined as the sine of the half-angle of the illumination cone divided by the objective lens numerical aperture. It is thus a measure of the angular range of the illumination relative to the angular acceptance of the lens. Finally, if the range of angles striking the mask extends from -90° to 90° (that is, all possible angles), the illumination is said to be *incoherent*. Table I helps define the terminology of spatial coherence.

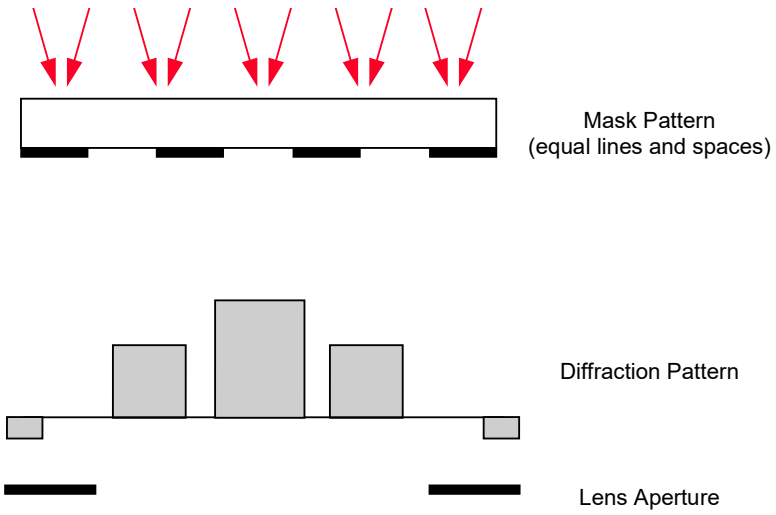

Figure 2-6. The diffraction pattern is broadened by the use of partially coherent illumination (plane waves over a range of angles striking the mask).

PROLITH/2 uses the extended source method for partially coherent image calculations. In this method, the full source is divided into individual point sources. Each point source is coherent and results in an aerial image given by equation (2.13). Two point sources from the extended source, however, do not interact coherently with each other. Thus, the contributions of these two sources must be added to each other incoherently (that is, the intensities are added together). The full aerial image is determined by calculating the coherent aerial image from each point on the source, and then integrating the intensity over the source. The source can be defined by a source function, $S(f_x', f_y')$, which is just the intensity of the source as a function of position (or angle). The total intensity of the image is then

$$I_{total}(x,y) = \frac{\iint_{source} I(x,y,f_x',f_y')\,S(f_x',f_y')\,df_x'\,df_y'}{\iint_{source} S(f_x',f_y')\,df_x'\,df_y'} \qquad (2.14)$$

Table I. Partial coherence types

Illumination Type	Partial Coherence Factor	Source Shape
Coherent	$\sigma = 0$	point source
Incoherent	$\sigma = \infty$	infinite size source
Partially Coherent	$0 < \sigma < \infty$	disk shaped source

C. Aberrations and Pupil Filters

Aberrations can be defined as the deviation of the real behavior of an imaging system from its ideal behavior (the ideal behavior was described above using Fourier optics as diffraction limited imaging). Aberrations are inherent in the behavior of all lens systems and come from three basic sources: defects of construction, defects of use, and defects of design. Defects of construction include rough or inaccurate lens surfaces, inhomogeneous glass, incorrect lens thicknesses or spacings, and tilted or decentered lens elements. Defects of use include use of the wrong illumination or tilt of the lens system with respect to the optical axis of the imaging system. Also, changes in the environmental conditions during use, such as the temperature of the lens or the barometric pressure of the air, result in defects of use. Defects of design may be a bit of a misnomer, since the aberrations of a lens design are not mistakenly designed *into* the lens, but rather were not designed *out* of the lens. All lenses have aberrated behavior since the Fourier optics behavior of a lens is only approximately true and is based on a linearized Snell's law for small angles. It is the job of a lens designer to combine elements of different shapes and properties so that the aberrations of each individual lens element tends to cancel in the sum of all of the elements, giving a lens system with only a small residual amount of aberrations. It is impossible to design a lens system with absolutely no aberrations.

Mathematically, aberrations are described as a *wavefront deviation*, the difference in phase (or path difference) of the actual wavefront emerging from the lens compared to the ideal wavefront as predicted from Fourier optics. This phase difference is a function of the position within the lens pupil, most conveniently described in polar coordinates. This wavefront deviation is in general quite complicated, so the mathematical form used to describe it is also quite complicated. The most common model for describing the phase error across the pupil is the *Zernike polynomial*, an infinite polynomial series, usually cut off at 36 terms, with powers of the radial pupil position R and trigonometric functions of the polar angle θ. The Zernike polynomial can be arranged in many ways, but most lens design software and lens measuring equipment in use today employ the fringe or circle Zernike polynomial, defined below:

$$
\begin{aligned}
W(R,\theta) = \;& Z1*R*\cos\theta \\
& + Z2*R*\sin\theta \\
& + Z3*(2*R*R-1) \\
& + Z4*R*R*\cos 2\theta \\
& + Z5*R*R*\sin 2\theta \\
& + Z6*(3*R*R-2)*R*\cos\theta \\
& + Z7*(3*R*R-2)*R*\sin\theta \\
& + Z8*(6*R**4-6*R*R+1) \\
& + Z9*R**3*\cos 3\theta \\
& + Z10*R**3*\sin 3\theta \\
& + Z11*(4*R*R-3)*R*R*\cos 2\theta \\
& + Z12*(4*R*R-3)*R*R*\sin 2\theta \\
& + Z13*(10*R**4-12*R*R+3)*R*\cos\theta \\
& + Z14*(10*R**4-12*R*R+3)*R*\sin\theta \\
& + Z15*(20*R**6-30*R**4+12*R*R-1) \\
& + Z16*R**4*\cos 4\theta \\
& + Z17*R**4*\sin 4\theta \\
& + Z18*(5*R*R-4)*R**3*\cos 3\theta \\
& + Z19*(5*R*R-4)*R**3*\sin 3\theta \\
& + Z20*(15*R**4-20*R*R+6)*R*R*\cos 2\theta \\
& + Z21*(15*R**4-20*R*R+6)*R*R*\sin 2\theta \\
& + Z22*(35*R**6-60*R**4+30*R*R-4)*R*\cos\theta \\
& + Z23*(35*R**6-60*R**4+30*R*R-4)*R*\sin\theta \\
& + Z24*(70*R**8-140*R**6+90*R**4-20*R*R+1) \\
& + Z25*R**5*\cos 5\theta \\
& + Z26*R**5*\sin 5\theta \\
& + Z27*(6*R*R-5)*R**4*\cos 4\theta \\
& + Z28*(6*R*R-5)*R**4*\sin 4\theta \\
& + Z29*(21*R**4-30*R*R+10)*R**3*\cos 3\theta \\
& + Z30*(21*R**4-30*R*R+10)*R**3*\sin 3\theta \\
& + Z31*(56*R**6-105*R**4+60*R**2-10)*R*R*\cos 2\theta \\
& + Z32*(56*R**6-105*R**4+60*R**2-10)*R*R*\sin 2\theta \\
& + Z33*(126*R**8-280*R**6+210*R**4-60*R*R+5)*R*\cos\theta \\
& + Z34*(126*R**8-280*R**6+210*R**4-60*R*R+5)*R*\sin\theta \\
& + Z35*(252*R**10-630*R**8+560*R**6-210*R**4+30*R*R-1) \\
& + Z36*(924*R**12-2772*R**10+3150*R**8-1680*R**6+420*R**4- \\
& 42*R*R+1) \qquad (2.15)
\end{aligned}
$$

where $W(R,\theta)$ is the optical path difference relative to the wavelength and Zi is called the ith Zernike coefficient. It is the magnitude of the Zernike coefficients that determine the aberration behavior of a lens. They have units of optical path length relative to the wavelength. (Note that different notational schemes are in use for the Zernike coefficients. Another popular scheme includes a constant offset as the first term, then calls the rest of the coefficients Z2 - Z37. Unfortunately, there is no universal standard and naming conventions can vary.)

The impact of aberrations on the aerial image can be calculated by modifying the pupil function of the lens to include the aberration phase error given by equation (2.15).

$$P(f_x, f_y) = P_{ideal}(f_x, f_y) e^{i2\pi W(R,\theta)} \tag{2.16}$$

Figure 2-7 shows several examples of plots of $W(R,\theta)$ for different simple aberrations.

Pupil filters are special filters placed inside the objective lens in order to purposely modify the pupil function $P(f_x, f_y)$. In general, the ideal pupil function will provide the best overall imaging capabilities. However, under special circumstances (for example, when imaging one specific mask pattern), a change in the pupil function may result in desirable imaging properties such as enhanced depth of focus. The pupil filter function $F(f_x, f_y)$ can have both a variation in transmission (T) and phase (θ) across the pupil.

$$F(f_x, f_y) = T(f_x, f_y) e^{i\theta(f_x, f_y)} \tag{2.17}$$

The final pupil function is then the pupil function given by equation (2.16) multiplied by the filter function given in equation (2.17).

put Figure 2-7 here

D. Defocus

Previous expressions for calculating the aerial image (such as equation 2.12) apply only to the image at the focal plane. What happens when the imaging system is out of focus? What is the image intensity distribution some small distance away from the plane of best focus? The impact of focus errors on the resulting aerial image can be described as an aberration of a sort. Consider a perfect spherical wave converging (i.e., focusing) down to a point. An ideal projection system would create such a wave coming out of the lens aperture (called the *exit pupil*), as shown in Figure 2-8a. If the wafer to be printed were placed in the same plane as the focal point of this wave, we would say that the wafer was in focus. What happens if the wafer were removed from this plane by some distance δ, called the defocus distance? Figure 2-8b shows such a situation. The spherical wave with the solid line represents the actual wave focused to a point a distance δ away from the wafer. If, however, the wave had a different shape, as given by the dotted curve, then the wafer would be in focus. Note that the only difference between these two different waves is the radius of curvature. Since the dotted curve is the wavefront we want for the given wafer position, we can say that the actual wavefront is in error because it does not focus where the wafer is located. (This is just a variation of "the customer is always right" attitude -- the wafer is always right, it is the optical wavefront that is out of focus.)

By viewing the actual wavefront as having an error in curvature relative to the desired wavefront (i.e., the one that focuses on the wafer), we can quantify the effect of defocus. Looking at Figure 2-8b, it is apparent that the distance from the desired to the "defocused" wavefront goes from zero at the center of the exit pupil and increases as we approach the edge of the pupil. This distance between wavefronts is called the *optical path difference* (OPD). The OPD is a function of the defocus distance and the position within the pupil and can be obtained from the geometry shown in Figure 2-9. Describing the position within the exit pupil by an angle θ, the optical path difference (assuming $R >> \delta$) is given by

$$OPD = \delta(1 - \cos\theta) \tag{2.18}$$

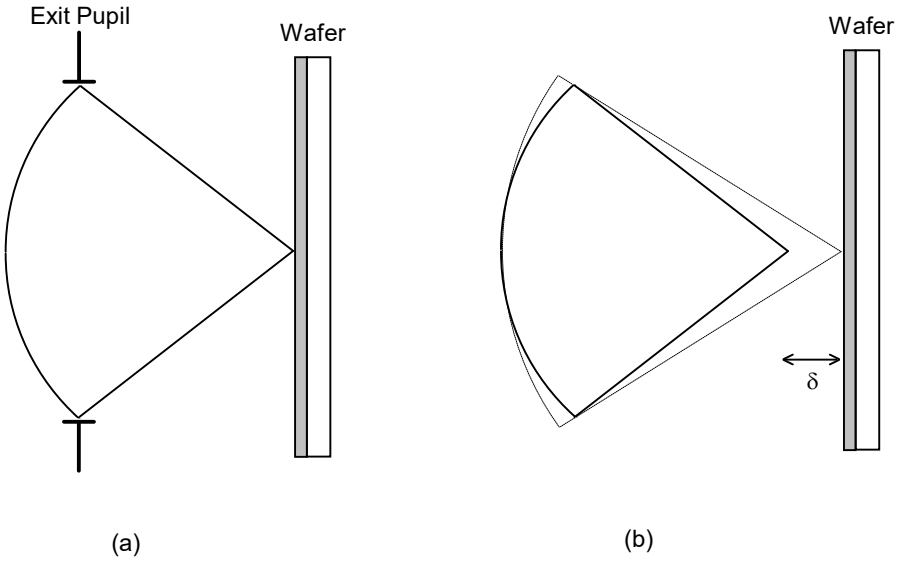

Figure 2-8. Focusing of light can be thought of as a converging spherical wave: a) in focus, and b) out of focus by a distance δ.

As we have seen before, the spatial frequency and the numerical aperture define positions within the pupil as the sine of an angle. Thus, the above expression for optical path difference would be more useful if expressed as a function of $\sin\theta$:

$$OPD = \delta(1-\cos\theta) = \tfrac{1}{2}\delta\left(\sin^2\theta + \frac{\sin^4\theta}{4} + \frac{\sin^6\theta}{8} + \ldots\right) \approx \tfrac{1}{2}\delta\sin^2\theta \quad (2.19)$$

where the final approximation is accurate only for relatively small angles. Figure 2-10 describes the accuracy of this approximation as a function of the angle θ.

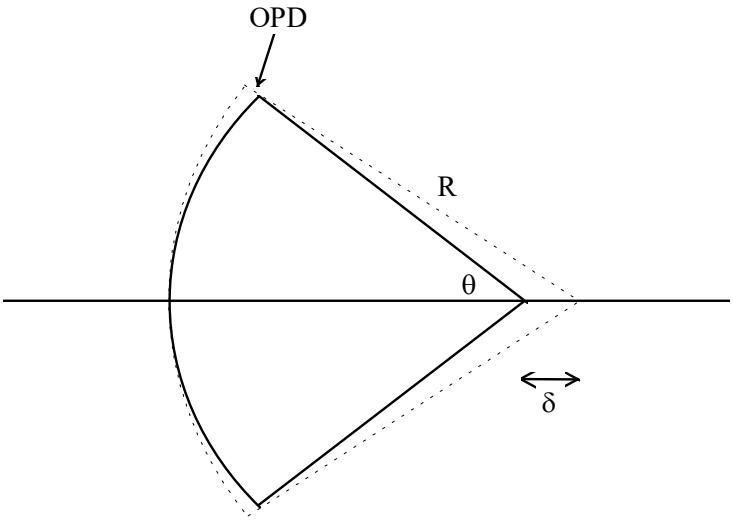

Figure 2-9. Geometry relating the optical path difference (OPD) to the defocus distance δ, the angle θ, and the radius of curvature of the converging wave R.

So how does this optical path difference affect the formation of an image? The OPD acts just like an aberration, modifying the pupil function of the lens. For light, this path length traveled (the OPD) is equivalent to a change in phase. Thus, the OPD can be expressed as a phase error, $\Delta\phi$, due to defocus:

$$\Delta\phi = k\,OPD = 2\pi\delta(1-\cos\theta)/\lambda \approx \pi\delta\sin^2\theta/\lambda \qquad (2.20)$$

where $k = 2\pi/\lambda$ = the *propagation constant* in air and, again, the final approximation is only valid for small angles. We are now ready to see how defocus affects the diffraction pattern and the resulting image. Our interpretation of defocus is that it causes a phase error as a function of radial position within the aperture. Light in the center of the aperture has no error, light at the edge of the aperture has the greatest phase error. This is very important when we remember what a diffraction pattern looks like as it enters

the lens aperture. Figure 2-3b shows such a diffraction pattern for the simple case of equal lines and spaces. Recall that diffraction by periodic patterns results in discrete diffraction orders: the zero order is the undiffracted light passing through the center of the lens, higher orders contain information necessary to reconstruct the image. *Thus, the effect of defocus is to add a phase error to the higher order diffracted light relative to the zero order.* When the lens recombines these orders to form an image, this phase error will result in a degraded image (Figure 2-11).

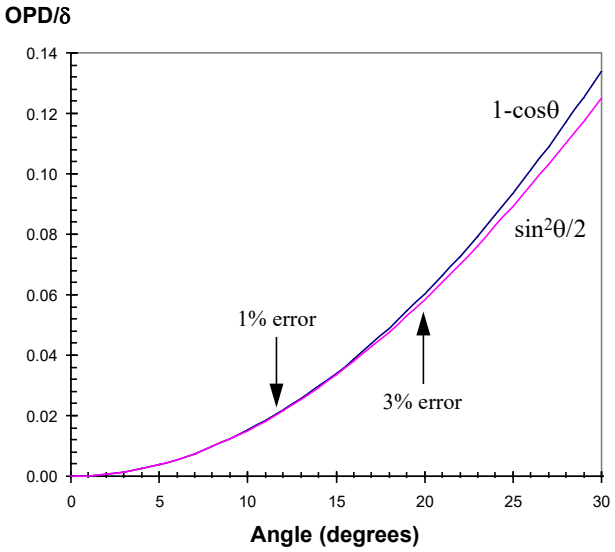

Figure 2-10. Comparison of the exact and approximate expressions for the defocus optical path difference (OPD) shows an increasing error as the angle increases. An angle of 30° (corresponding to the edge of an NA = 0.5 lens) shows an error of 6.7% for the approximate expression, while an angle of 37° (not shown, but corresponding to the edge of an NA = 0.6 lens) gives an error of 10%.

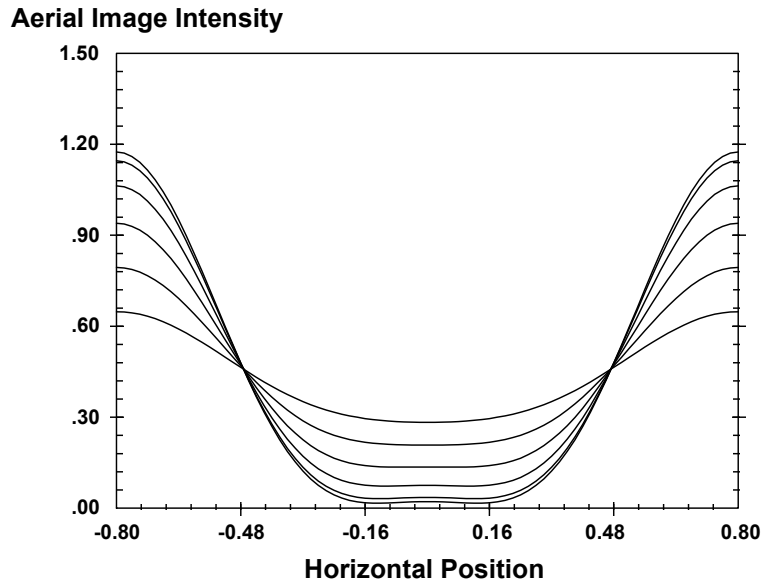

Figure 2-11. Aerial image intensity of a 0.8 λ /NA line and space pattern as focus is changed.

E. Image Calculation Modes

Calculation of an aerial image means, quite literally, determination of the image in air. Of course, in lithography one projects this image into photoresist. The propagation of the image into resist can be quite complicated, so models usually make one or more approximations. This section describes approximations that can be made in determining the intensity of light within the photoresist.

1. Zero Order Scalar Model

The lithography simulator SAMPLE [2.2] and the 1985 version of PROLITH [2.3] used the simple imaging approximation first proposed by Dill [2.4] to calculate the propagation of an aerial image in photoresist. First, an

aerial image $I_i(x)$ is calculated as if projected into air (x being along the surface of the wafer and perpendicular to the propagation direction of the image). Second, a standing wave intensity $I_s(z)$ is calculated assuming a plane wave of light is normally incident on the photoresist coated substrate (where z is defined as zero at the top of the resist and is positive going into the resist). Then, it is assumed that the actual intensity within the resist film $I(x,z)$ can be approximated by

$$I(x,z) \approx I_i(x) I_s(z) \tag{2.21}$$

For very low numerical apertures and reasonably thin photoresists, these approximations are valid. They begin to fail when the aerial image changes as it propagates through the resist (i.e., it defocuses) or when the light entering the resist is appreciably non-normal. Note that if the photoresist bleaches (changes its optical properties during exposure), only $I_s(z)$ changes in this approximation. The zero order scalar model is not used in PROLITH/2.

2. Standard Model of PROLITH/2

The first attempt to correct one of the deficiencies of the zero order model was made by the author [2.5] and, independently, by Bernard [2.6]. The aerial image, while propagating through the resist, is continuously changing focus. Thus, even in air, the aerial image is a function of both x and z. An aerial image simulator calculates images as a function of x and the distance from the plane of best focus, δ. Letting δ_o be the defocus distance of the image at the top of the photoresist, the defocus within the photoresist at any position z is given by

$$\delta(z) = \delta_o + \frac{z}{n} \tag{2.22}$$

where n is the real part of the index of refraction of the photoresist. The intensity within the resist is then given by

$$I(x,z) = I_i(x,\delta(z)) I_s(z) \tag{2.23}$$

Here the assumption of normally incident plane waves is still used when calculating the standing wave intensity. This approximate form of the scalar model is known as the “Standard Model” in PROLITH/2. The standard model

also uses the approximate form of the defocus expression, as found in equation (2.19).

3. High NA Scalar Model in PROLITH/2

The light propagating through the resist can be thought of as various plane waves traveling through the resist in different directions. Consider first the propagation of the light in the absence of diffraction by a mask pattern (that is, exposure of the resist over a large open area). The spatial dimensions of the light source determine the characteristics of the light entering the photoresist. For the simple case of a coherent point source of illumination centered on the optical axis, the light traveling into the photoresist would be the normally incident plane wave used in the calculations presented above. The standing wave intensity within the resist can be determined analytically [2.7] as the square of the magnitude of the electric field given by

$$E(z) = \frac{\tau_{12} E_I \left(e^{-i2\pi \boldsymbol{n}_2 z/\lambda} + \rho_{23} \tau_D^2 e^{i2\pi \boldsymbol{n}_2 z/\lambda} \right)}{1 + \rho_{12}\rho_{23}\tau_D^2} \tag{2.24}$$

where the subscripts 1, 2, and 3 refer to air, the photoresist and the substrate, respectively, D is the resist thickness, E_I is the incident electrical field, λ is the wavelength, and where

complex index of refraction of film j: $\boldsymbol{n}_j = n_j - i\kappa_j$

transmission coefficient from i to j: $\tau_{ij} = \dfrac{2\boldsymbol{n}_i}{\boldsymbol{n}_i + \boldsymbol{n}_j}$

reflection coefficient from i to j: $\rho_{ij} = \dfrac{\boldsymbol{n}_i - \boldsymbol{n}_j}{\boldsymbol{n}_i + \boldsymbol{n}_j}$

internal transmittance of the resist: $\tau_D = e^{-i2\pi \boldsymbol{n}_2 D/\lambda}$

A more complete description of the standing wave equation (2.24) is given in Chapter 3.

The above expression can be easily modified for the case of non-normally incident plane waves. Suppose a plane wave is incident on the resist film at some angle θ_1. The angle of the plane wave inside the resist will be θ_2 as determined from Snell's law. An analysis of the propagation of this plane wave within the resist will give an expression similar to equation (2.24) but with the position z replaced with $z\cos\theta_2$.

$$E(z,\theta_2) = \frac{\tau_{12}(\theta_2)E_I\left(e^{-i2\pi n_2 z\cos\theta_2/\lambda} + \rho_{23}(\theta_2)\tau_D^2(\theta_2)e^{i2\pi n_2 z\cos\theta_2/\lambda}\right)}{1+\rho_{12}(\theta_2)\rho_{23}(\theta_2)\tau_D^2(\theta_2)} \qquad (2.25)$$

The transmission and reflection coefficients are now functions of the angle of incidence and are given by the Fresnel formulas (see Chapter 3). A similar approach was taken by Bernard and Urbach [2.8].

By calculating the standing wave intensity at one incident angle θ_1 to give $I_s(z,\theta_1)$, the full standing wave intensity can be determined by integrating over all angles. Each incident angle comes from a given point in the illumination source, so that integration over angles is the same as integration over the source. Thus, the effect of partial coherence on the standing waves is accounted for (see Figure 2-12). Note that for the model described here the effect of the non-normal incidence is included only with respect to the zero order light (the light which is not diffracted by the mask). This form of the scalar imaging problem is known as the "High NA Scalar" model in PROLITH/2. The high NA scalar model uses the exact defocus expression.

Reduction (or magnification) in an imaging system adds an interesting complication. Light entering the objective lens will leave the lens with no loss in energy (the lossless lens assumption). However, if there is reduction or magnification in the lens, the *intensity* distribution of the light entering will be different from that leaving since the intensity is the energy spread over a changing area. The result is a radiometric correction well known in optics [2.9] and first applied to lithography by Cole and Barouch [2.10]. The amplitude of the electric field passing through the pupil at angle θ is modified by the radiometric correction

$$Radiometric\ Correction\ =\ \left(\frac{1-\frac{\sin^2\theta}{R^2}}{1-\sin^2\theta}\right)^{0.25} \tag{2.26}$$

where R is the reduction factor (for example, 5.0 for a 5X reduction stepper). In PROLITH/2, the radiometric correction is applied in the high NA scalar model but not in the standard model.

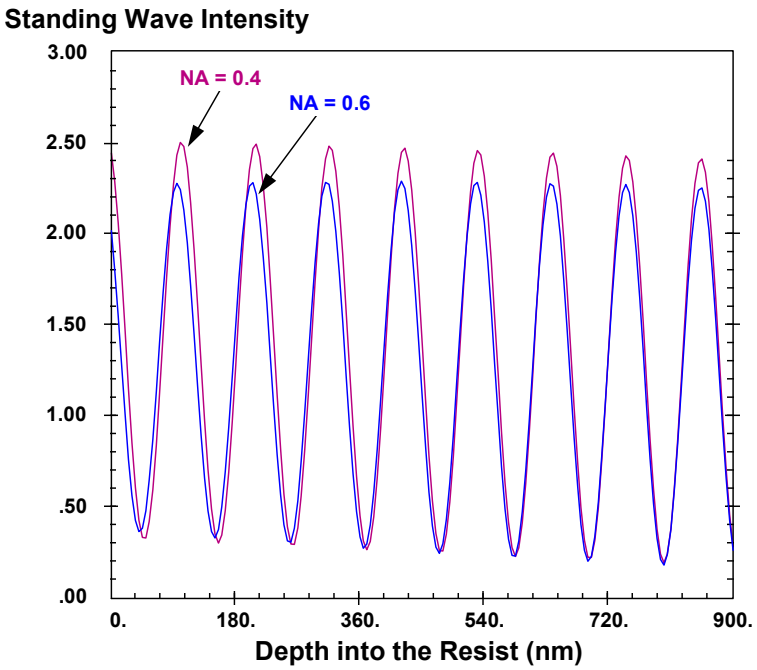

Figure 2-12. Calculation of the standing wave intensity for the high NA scalar model as a function of NA (with σ = 0.7). A numerical aperture equal to 0.4 is very close to the normally incident standing wave pattern, but an NA of 0.6 (corresponding to plane waves incident over a ±25° range) causes a significant decrease in the standing wave amplitude as well as an increase in the period.

4. Full Scalar and Vector Models

The above methods for calculating the image intensity within the resist all make the assumption of separability, that an aerial image and a standing wave intensity can be calculated independently and then multiplied together to give the total intensity. This assumption is not required. Instead, one could calculate the full *I(x,z)* at once making only the standard scalar approximation. The formation of the image can be described as the summation of plane waves. For coherent illumination, each diffraction order gives one plane wave propagating into the resist. Interference between the zero order and the higher orders produces the desired image. Each point in the illumination source will produce another image which will add incoherently (i.e., intensities will add) to give the total image. Equation (2.25) describes the propagation of a plane wave in a stratified media at any arbitrary angle. By applying this equation to each diffraction order (not just the zero order as in the high NA scalar model), an exact scalar representation of the full intensity within the resist is obtained. This model is called the Full Scalar model in PROLITH/2. The Full Scalar model also makes use of the radiometric correction and uses the exact defocus expression.

Light is an electromagnetic wave which can be described by time-varying electric and magnetic field vectors. In lithography, the materials used are generally non-magnetic so that only the electric field is of interest. The electric field vector is described by its three vector components (for example, x, y, and z components). Maxwell's equations, sometimes put into the form of the wave equation, govern the propagation of the electric field vector. The *scalar approximation* assumes that each of the three components of the electric field vector can be treated as a single scalar quantity and that this scalar electric field must satisfy the wave equation. Further, when two fields of light (say, two plane waves) are added together, the scalar approximation means that the sum of the fields would simply be the sum of the scalar amplitudes of the two fields.

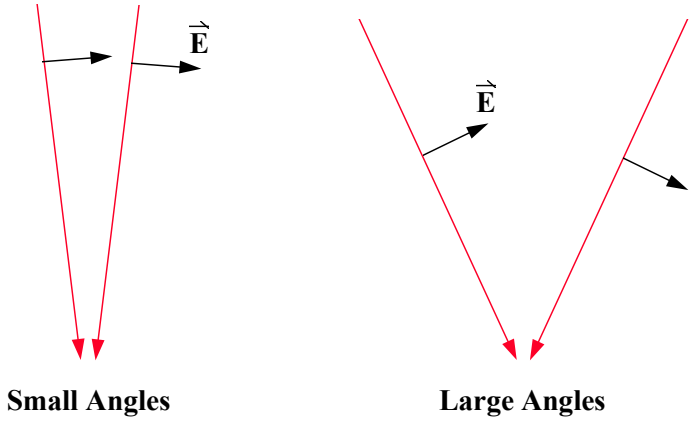

Figure 2-13. Addition of two *p*-polarized plane waves depends on the angle between them.

The scalar approximation is commonly used throughout optics and is known to be accurate under many conditions. There is one simple situation, however, in which the scalar approximation is not adequate. Consider the interference of two plane waves traveling past each other. If each plane wave is treated as a vector, they will interfere only if there is some overlap in their electric field vectors. If the vectors are parallel, there will be complete interference. If, however, their electric fields are at right angles to each other there will be no interference. The scalar approximation essentially assumes that the electric field vectors are always parallel and will always give complete interference. These differences come into play in lithography when considering the propagation of plane waves traveling through the resist at large angles (Figure 2-13). For large angles, the scalar approximation may fail to account for these vector effects. In particular, *s*-polarized light always results in complete overlap of the electric field vectors so that the full scalar approach gives the same result as a vector approach for *s*-polarized illumination. However, *p*-polarized illumination can give a very different result depending on the angle (i.e., on the size of the numerical aperture). Thus, a vector model would keep track of the vector direction of the electric field and use this information when adding two plane waves together [2.11,2.12]. The vector option of PROLITH/2 includes both the Full Scalar model and the Vector model as described above.

References

2.1. J. W. Goodman, Introduction to Fourier Optics, McGraw-Hill (New York: 1968).

2.2. W. G. Oldham, S. N. Nandgaonkar, A. R. Neureuther and M. O'Toole, "A General Simulator for VLSI Lithography and Etching Processes: Part I - Application to Projection Lithography," *IEEE Trans. Electron Devices*, ED-26, No. 4 (April 1979) pp. 717-722.

2.3. C. A. Mack, "PROLITH: A Comprehensive Optical Lithography Model," *Optical Microlith. IV, Proc.*, SPIE Vol. 538 (1985) pp. 207-220.

2.4. F. H. Dill, A. R. Neureuther, J. A. Tuttle, and E. J. Walker "Modeling Projection Printing of Positive Photoresists," *IEEE Trans. Electron Devices*, ED-22, No. 7, (1975) pp. 456-464.

2.5. C. A. Mack, "Understanding Focus Effects in Submicron Optical Lithography," *Optical/Laser Microlithography, Proc.*, SPIE Vol. 922 (March, 1988) pp. 135-148, and *Optical Engineering*, Vol. 27, No. 12 (Dec. 1988) pp. 1093-1100.

2.6. D. A. Bernard, "Simulation of Focus Effects in Photolithography," *IEEE Trans. Semiconductor Manufacturing*, Vol. 1, No. 3 (August, 1988) pp. 85-97.

2.7. C. A. Mack, "Analytical Expression for the Standing Wave Intensity in Photoresist", *Applied Optics*, Vol. 25, No. 12 (15 June 1986) pp. 1958-1961.

2.8. D. A. Bernard and H. P. Urbach, "Thin-film Interference Effects in Photolithography for Finite Numerical Apertures," *Jour. Optical Society of America A*, Vol. 8, No. 1 (Jan., 1991) pp. 123-133.

2.9. M. Born and E. Wolf, Principles of Optics, 6th edition, Pergamon Press, (Oxford, 1980) pp. 113-117.

2.10. D. C. Cole, E. Barouch, U. Hollerbach, and S. A. Orszag, "Extending Scalar Aerial Image Calculations to Higher Numerical Apertures," *Jour. Vacuum Science and Tech*., Vol. B10, No. 6 (Nov/Dec, 1992) pp. 3037-3041.

2.11. D. G. Flagello, A. E. Rosenbluth, C. Progler, J. Armitage, "Understanding High Numerical Aperture Optical Lithography," *Microelectronic Engineering*, Vol 17 (1992) pp. 105-108.

2.12. C. A. Mack and C-B. Juang, "Comparison of Scalar and Vector Modeling of Image Formation in Photoresist," *Optical/Laser Microlithography VIII, Proc.*, SPIE Vol. 2440 (1995).

Chapter 3

Standing Waves

When a thin dielectric film placed between two semi-infinite media (e.g., a thin coating on a thick substrate in air) is exposed to monochromatic light, standing waves are produced in the film. This effect has been well documented for such cases as anti-reflection coatings and photoresist exposure [3.1]-[3.5]. In the former, the standing wave effect is used to reduce reflections from the substrate. In the latter, standing waves are an undesirable side effect of the exposure process. Unlike the anti-reflection application, photolithography applications require a knowledge of the intensity of the light within the thin film itself. Early work [3.4], [3.5] on determining the intensity within a thin photoresist film has been limited to numerical solutions based on Berning's matrix method [3.6]. This section presents an analytical expression for the standing wave intensity within a thin film [3.7]. This film may be homogeneous or of a known small inhomogeneity. The film may be on a substrate or between one or more other thin films. The incident light can be normally incident or incident at some angle.

A. Normally Incident, Single Layer

Consider a thin film of thickness D and complex index of refraction $\boldsymbol{n}_2$ deposited on a thick substrate with complex index of refraction $\boldsymbol{n}_3$ in an ambient environment of index n_1. An electromagnetic plane wave is normally incident on this film. Let E_1, E_2, and E_3 be the electric fields in the ambient, thin film, and substrate, respectively (see Figure 3-1). Assuming monochromatic illumination by a normally incident plane wave, the electric field in each region is a plane wave or the sum of two plane waves traveling in opposite directions (i.e., a standing wave). Maxwell's equations require certain boundary conditions to be met at each interface: specifically, E_j and the magnetic field H_j are continuous across the boundaries $z = 0$ and $z = D$. Solving the resulting equations simultaneously, the electric field in region 2 can be shown to be [3.7]

$$E_2(x,y,z) = E_1(x,y)\frac{\tau_{12}\left(e^{-i2\pi\boldsymbol{n}_2 z/\lambda} + \rho_{23}\tau_D^2 e^{i2\pi\boldsymbol{n}_2 z/\lambda}\right)}{1+\rho_{12}\rho_{23}\tau_D^2} \tag{3.1}$$

where $E_1(x,y)$ = the incident plane wave at $z = 0$,

$\rho_{ij} = (\boldsymbol{n}_i - \boldsymbol{n}_j)/(\boldsymbol{n}_i + \boldsymbol{n}_j)$, the reflection coefficient

$\tau_{ij} = 2\boldsymbol{n}_i/(\boldsymbol{n}_i + \boldsymbol{n}_j)$, the transmission coefficient

$\tau_D = \exp(-i\boldsymbol{k}_2 D)$, the internal transmittance of the film

$\boldsymbol{k}_j = 2\pi\boldsymbol{n}_j/\lambda$, the propagation constant

$\boldsymbol{n}_j = n_j - i\kappa_j$, the complex index of refraction

λ = vacuum wavelength of the incident light.

Equation (3.1) is the basic standing wave expression where film 2 represents the photoresist. Squaring the magnitude of the electric field gives the standing wave intensity. Note that absorption is taken into account in this expression through the imaginary part of the index of refraction. The common absorption coefficient α is related to the imaginary part of the index by

$$\alpha = \frac{4\pi\kappa}{\lambda} \tag{3.2}$$

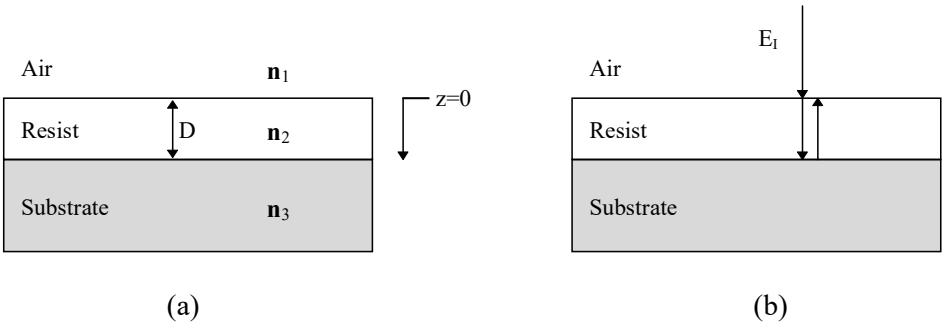

Figure 3-1. Film stack showing the geometry for the standing wave derivation.

The derivation of equation (3.1) required an assumption about the sign convention for the phasor representation of a sinusoidal wave, as discussed in Chapter 2. Unfortunately, the convention commonly used for thin film calculations is the opposite to that normally used for imaging. Thus, for the purposes of this chapter, a plane wave traveling in the +*z*-direction would be represented by exp(-*ikz*) and the imaginary part of the index of refraction must be negative to represent an absorbing media.

B. Multiple Layers

It is very common to have more than one film coated on a substrate. The problem then becomes that of two or more absorbing thin films on a substrate. An analysis similar to that for one film yields the following result for the electric field in the top layer of an *m*-1 layer system:

$$E_2(x,y,z) = E_I(x,y)\frac{\tau_{12}\left(e^{-i2\pi n_2 z/\lambda} + \rho'_{23}\tau_D^2 e^{i2\pi n_2 z/\lambda}\right)}{1+\rho_{12}\rho'_{23}\tau_D^2} \tag{3.3}$$

where

$$\rho'_{23} = \frac{\boldsymbol{n}_2 - \boldsymbol{n}_3 X_3}{\boldsymbol{n}_2 + \boldsymbol{n}_3 X_3}$$

$$X_3 = \frac{1 - \rho'_{34}\,\tau^2_{D3}}{1 + \rho'_{34}\,\tau^2_{D3}}$$

$$\rho'_{34} = \frac{\boldsymbol{n}_3 - \boldsymbol{n}_4 X_4}{\boldsymbol{n}_3 + \boldsymbol{n}_4 X_4}$$

.
.
.

$$X_m = \frac{1 - \rho_{m,m+1}\,\tau^2_{Dm}}{1 + \rho_{m,m+1}\,\tau^2_{Dm}}$$

$$\rho_{m,m+1} = \frac{\boldsymbol{n}_m - \boldsymbol{n}_{m+1}}{\boldsymbol{n}_m + \boldsymbol{n}_{m+1}}$$

$$\tau_{Dj} = e^{-ik_j D_j}$$

and all other parameters are defined previously. The parameter ρ'_{23} is the effective reflection coefficient between the thin resist film and what lies beneath it.

If the thin film in question is not the top film (layer 2), the intensity can be calculated in layer *j* from

$$E_j(x,y,z) = E_{Ieff}(x,y)\,\tau^*_{j-1,j}\,\frac{\left(e^{-i\boldsymbol{k}_j z_j} + \rho'_{j,j+1}\tau^2_{Dj}\,e^{i\boldsymbol{k}_j z_j}\right)}{1 + \rho^*_{j-1,j}\,\rho'_{j,j+1}\tau^2_{Dj}} \qquad (3.4)$$

where $\tau^*_{j-1,j} = 1 + \rho^*_{j-1,j}$. The effective reflection coefficient ρ^* is analogous to the coefficient ρ', looking in the opposite direction. E_{Ieff} is the effective intensity incident on layer j. Both E_{Ieff} and ρ^* are defined in detail in Reference 3.7.

If the film in question is not homogeneous the equations above are, in general, not valid. Let us, however, examine one special case in which the inhomogeneity takes the form of small variations in the imaginary part of the index of refraction of the film in the z-direction, leaving the real part constant. In this case, the absorbance Abs is no longer simply αz, but becomes

$$Abs(z) = \int_0^z \alpha(z')\,dz' \tag{3.5}$$

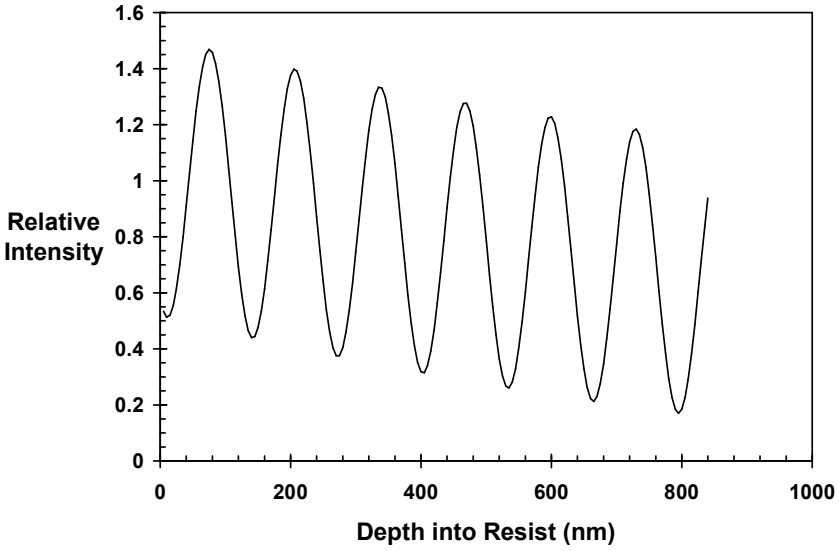

Figure 3-2. Standing wave intensity within a photoresist film at the start of exposure (850nm of resist on 100nm SiO_2 on silicon, λ = 436nm). The intensity shown is relative to the incident intensity.

It can be shown that equations (3.1) - (3.4) are still valid if the anisotropic expression for absorbance (3.5) is used. Thus, *I(z)* can be found if the absorption coefficient is known as a function of *z*. Figure 3-2 shows a typical result of the standing wave intensity within a photoresist film coated on an oxide on silicon film stack.

C. Oblique Incidence

The equation (3.1) can be easily modified for the case of non-normally incident plane waves. Suppose a plane wave is incident on the resist film at some angle θ_1. The angle of the plane wave inside the resist will be θ_2 as determined from Snell's law ($n_1 \sin\theta_1 = n_2 \sin\theta_2$). An analysis of the propagation of this plane wave within the resist will give an expression similar to equation (3.1) but with the position z replaced with $z\cos\theta_2$.

$$E(z,\theta_2) = \frac{\tau_{12}(\theta_2)E_I\left(e^{-i2\pi n_2 z\cos\theta_2/\lambda} + \rho_{23}(\theta_2)\tau_D^2(\theta_2)e^{i2\pi n_2 z\cos\theta_2/\lambda}\right)}{1+\rho_{12}(\theta_2)\rho_{23}(\theta_2)\tau_D^2(\theta_2)} \qquad (3.6)$$

The transmission and reflection coefficients are now functions of the angle of incidence (as well as the polarization of the incident light) and are given by the Fresnel formulas.

$$\rho_{ij\perp}(\theta) = \frac{n_i\cos(\theta_i) - n_j\cos(\theta_j)}{n_i\cos(\theta_i) + n_j\cos(\theta_j)}$$

$$\tau_{ij\perp}(\theta) = \frac{2n_i\cos(\theta_i)}{n_i\cos(\theta_i) + n_j\cos(\theta_j)}$$

$$\rho_{ij\parallel}(\theta) = \frac{n_i\cos(\theta_j) - n_j\cos(\theta_i)}{n_i\cos(\theta_j) + n_j\cos(\theta_i)}$$

$$\tau_{ij\parallel}(\theta) = \frac{2n_i\cos(\theta_i)}{n_i\cos(\theta_j) + n_j\cos(\theta_i)} \qquad (3.7)$$

Here, || represents an electric field vector which lies in a plane defined by the direction of the incident light and a normal to the resist surface. Other names for || polarization include *p* polarization and TM (transverse magnetic) polarization. The polarization denoted by ⊥ represents an electric field vector which lies in a plane perpendicular to that defined by the direction of the incident light and a normal to the resist surface. Other names for ⊥ polarization include *s* polarization and TE (transverse electric) polarization. Note that for light normally incident on the resist surface, both *s* and *p* polarization result in electric fields which lie along the resist surface and the four Fresnel formulae revert to the two standard definitions of reflection and transmission coefficients used earlier. Figure 3-3 shows how the reflectivity (the square of the magnitude of the reflection coefficient) varies with incident angle for both *s* and *p* polarized illumination.

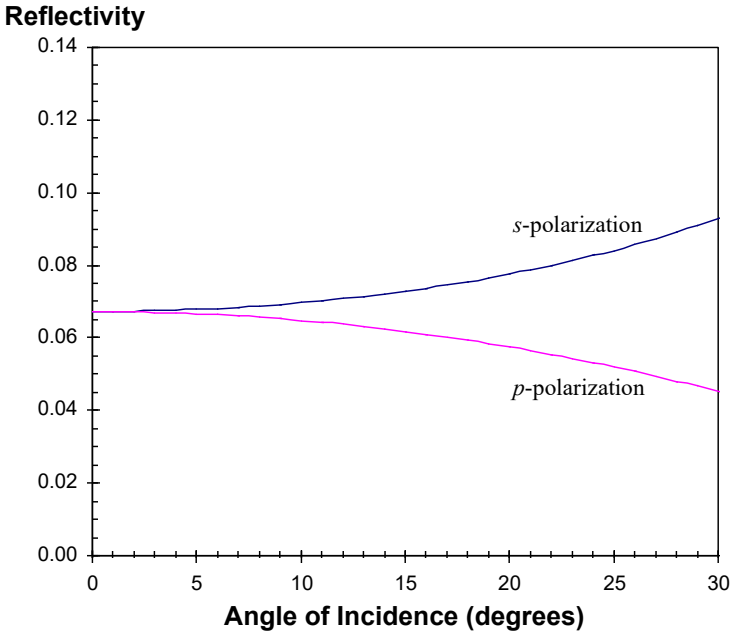

Figure 3-3. Reflectivity (square of the reflection coefficient) as a function of the angle of incidence showing the difference between *s* and *p* polarization (n_1 = 1.0, n_2 = 1.7).

D. Broadband Illumination

The analysis presented above applies to monochromatic illumination. What if broadband (polychromatic) illumination were used? In general, the use of broadband illumination in imaging applications can be thought of as the incoherent superposition of individual monochromatic results. Thus, the standing wave intensity for a single wavelength is integrated over the wavelengths of the source, weighted by the source illumination spectrum. Figure 3-4 shows a typical mercury arc lamp output spectrum (before filtering in the illumination system of the projection tool).

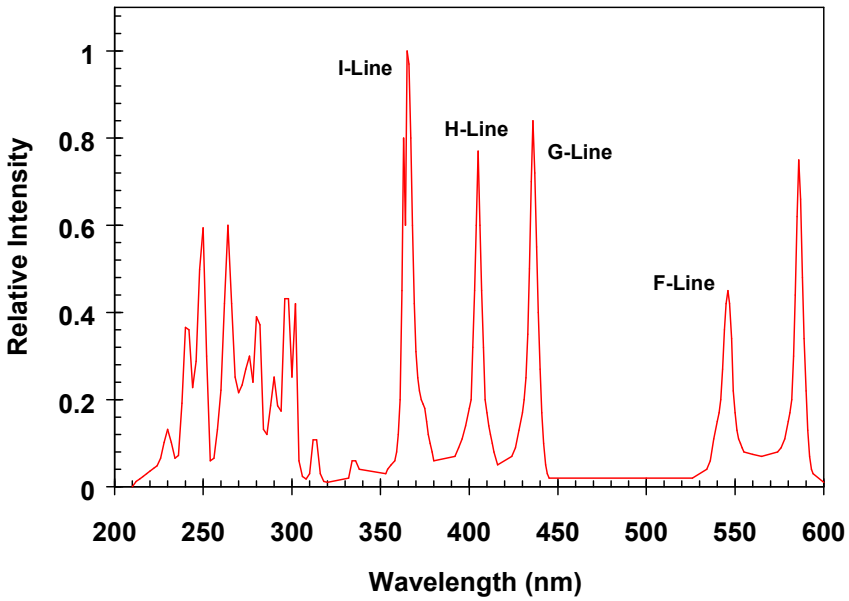

Figure 3-4. Spectral output of a typical high-pressure mercury arc lamp. The illumination spectrum of a lithographic exposure tool is usually a filtered portion of this lamp spectrum.

Although wavelength appears explicitly in the expressions for the standing wave electric field in the resist, an implicit dependence occurs in the indices of refraction of the various resist and substrate materials. The variation of the index of refraction of a material with wavelength, called dispersion, is extremely material dependent. Over a limited range of wavelengths, many materials' dispersion curves can be adequately described by an empirical expression called the Cauchy equation.

$$n(\lambda) = C_1 + \frac{C_2}{\lambda^2} + \frac{C_3}{\lambda^4} \tag{3.8}$$

where C_1, C_2, and C_3 are the empirically derived Cauchy coefficients. It is important to note that any Cauchy fit to refractive index data will be valid only over the wavelength range of the data and should not be extrapolated.

References

3.1. S. Middlehoek, "Projection Masking, Thin Photoresist Layers and Interference Effects," *IBM Jour. Res. Dev*., Vol. 14, (March, 1970) pp. 117-124.

3.2. J. E. Korka, "Standing Waves in Photoresists," *Applied Optics*, Vol. 9, No. 4, (April, 1970) pp. 969-970.

3.3. D. F. Ilten and K. V. Patel, "Standing Wave Effects in Photoresist Exposure," *Image Technology*, (Feb/March, 1971), pp. 9-14.

3.4. D. W. Widmann, "Quantitative Evaluation of Photoresist Patterns in the 1μm Range," *Applied Optics*, Vol. 14, No. 4 (April, 1975), pp. 931-934.

3.5. F. H. Dill, "Optical Lithography," *IEEE Trans. Electron Devices*, Vol. ED-22, No. 7 (July, 1975) pp. 440-444.

3.6. P. H. Berning, "Theory and Calculations of Optical Thin Films," Physics of Thin Films, George Hass, ed., Academic Press (New York: 1963) pp. 69-121.

3.7. C. A. Mack, "Analytical Expression for the Standing Wave Intensity in Photoresist", *Applied Optics*, Vol. 25, No. 12 (15 June 1986) pp. 1958-1961.

Chapter 4

Diffraction for Contact and Proximity Printing

The phenomenon of diffraction has been extensively studied and is well documented in the literature (e.g., ref. [4.1]). However, rigorous treatments of the problem are prohibitively complicated and, thus, practical solutions make one or more simplifying approximations or assumptions. The most common practical treatment of diffraction is that given by Kirchhoff and is outlined in some detail below. As with any approximate solution, Kirchhoff's diffraction theory is appropriate only under certain conditions, and this region of validity must be determined. Of course, theory is more useful if it can be applied to realistic situations. Thus, a method for applying Kirchhoff's theory to heterogeneous media (in particular those media appropriate to contact and proximity printing) will be given.

A. Kirchhoff's Diffraction Theory

The goal of any diffraction theory is to predict the intensity of light that has passed by some object or through some aperture. For the case of contact

printing, this means predicting the intensity of light within a photoresist film after it has passed through an aperture called the mask. As an example, Figure 4-1 shows the geometry for the case of a narrow slit of width w and length l in the x_s-y_s plane. An electric field U_I is incident on the aperture giving rise to an electric field $U(P)$ at point P. Thus, the goal of diffraction theory is to determine $U(P)$ for a given aperture and incident wave.

Kirchhoff's diffraction theory is, in effect, a mathematically rigorous version of Huygens' principle, which states that any wavefront propagating through a medium can be thought of as a series of point sources, each producing its own spherical wavefront which, when superimposed, generates the new wavefront. From a different perspective, the electric field at some point P resulting from some arbitrary wavefront S is the superposition of the electric field at P due to each of an infinite number of point sources along S.

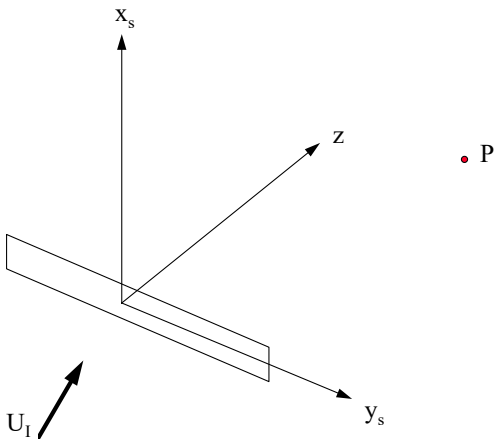

Figure 4-1. Diffraction by a slit.

To prove the above statement, Kirchhoff indirectly solved the homogeneous wave equation at P under certain conditions. Consider a monochromatic scalar wave of the form

$$V(x,y,z,t) = U(x,y,z)e^{-i\omega t} \tag{4.1}$$

where U is the phasor representation of the wave (see Chapter 2, equation 2.4). The time independent homogeneous wave equation (also known as the Helmholtz equation) states that

$$\left(\nabla^2 + k^2\right)U(x,y,z) = 0 \tag{4.2}$$

where $k = 2\pi n/\lambda$, the propagation constant of the medium,
n = index of refraction of the medium, and
λ = vacuum wavelength of the radiation.

The Helmholtz equation is a direct result of Maxwell's equations for any electromagnetic wave in a homogeneous medium in the absence of sources. There are infinitely many solutions to this equation, including the plane wave and the spherical wave.

Consider some arbitrary point P completely enclosed by a surface S of volume V. If $U(x,y,z)$ is continuous and has continuous first and second derivatives within and on the surface S, then Green's theorem states

$$\iiint_V (U\nabla^2 G - G\nabla^2 U)dV = -\iint_S \left(U\frac{\partial G}{\partial n} - G\frac{\partial U}{\partial n}\right)dS \tag{4.3}$$

where $G(x,y,z)$ is any other function with the same continuity requirements as $U(x,y,z)$ and n is the inward normal to S. Further, let us pick G so that it satisfies the homogeneous wave equation (4.2). Thus,

$$\left(\nabla^2 + k^2\right)U = 0 \qquad G\left(\nabla^2 + k^2\right)U = 0$$

$$\left(\nabla^2 + k^2\right)G = 0 \qquad U\left(\nabla^2 + k^2\right)G = 0 \tag{4.4}$$

which leads to

$$U\nabla^2 G - G\nabla^2 U = 0 \tag{4.5}$$

Therefore, the left hand integral in equation (4.3) becomes zero and

$$\iint_S \left(U\frac{\partial G}{\partial n} - G\frac{\partial U}{\partial n} \right) dS = 0 \tag{4.6}$$

For reasons which will be made clear later, let us assume G has a singularity at P, for example

$$G = \frac{e^{-iks}}{s} \tag{4.7}$$

where s is the distance from the point P to the point (x,y,z) on the surface S. Despite our initial assumption, G is not continuous in the volume V, having a singularity at P. To remedy this problem we will define a different volume V^* that excludes the point P, as shown in Figure 4-2. The new surface is $S + S'$ where S' is any surface contained in S which contains P. The function G is continuous in the new volume and equation (4.6) becomes

$$\iint_S \left(U\frac{\partial G}{\partial n} - G\frac{\partial U}{\partial n} \right) dS + \iint_{S'} \left(U\frac{\partial G}{\partial n} - G\frac{\partial U}{\partial n} \right) dS = 0 \tag{4.8}$$

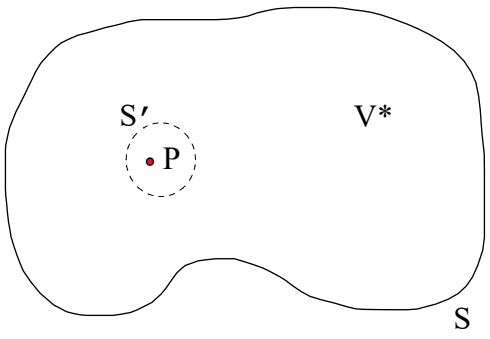

Figure 4-2. Geometry used for the derivation of Kirchhoff's integral.

Since S' can be any surface, let us take it to be a small sphere of radius r. Substituting equation (4.7) into (4.8) and letting r go to zero, the right hand term in equation (4.8) becomes $-4\pi U(P)$. The function U at the point P can be expressed as

$$U(P) = \frac{1}{4\pi}\iint_S \left(U\frac{\partial G}{\partial n} - G\frac{\partial U}{\partial n} \right) dS \tag{4.9}$$

Thus, $U(P)$ may be determined if U is known everywhere on the surface S. Equation (4.9) is known as the *Kirchhoff diffraction integral*.

We will now apply the Kirchhoff diffraction integral to the problem of diffraction. Consider an arbitrary wave U_I incident on an opaque screen (in the x_s-y_s plane) with an aperture of arbitrary shape A (Figure 4-3). To find the value of U a some point P to the right of the screen, we will pick S as pictured in Figure 4-3 and consider the three regions A just under the aperture, B under the opaque screen, and C a hemisphere of radius R, separately. Letting $R \to \infty$, G and $\partial G / \partial n$ become zero on C and this region contributes nothing to the integral. To evaluate the integral (4.9) in regions A and B we must make some assumptions about U in these regions. The standard "black screen" approximations are as follows:

In region A: $U = U_I$

In region B: $U = 0, \quad \partial U / \partial n = 0$ (4.10)

Thus, region B does not contribute to the integral and equation (4.9) becomes

$$U(P) = \frac{1}{4\pi}\iint_A \left(U_I\frac{\partial G}{\partial n} - G\frac{\partial U_I}{\partial n} \right) dS \tag{4.11}$$

If U_I is known at the aperture, $U(P)$ can be determined. The boundary conditions (4.10) are called the "black screen" boundary conditions since an aperture in an infinitely absorbing black body would reproduce these conditions. The accuracy of equation (4.11) is dependent on the applicability of these boundary conditions to the problem being studied. Although the black screen boundary conditions allow for a simple solution to the Kirchhoff diffraction integral, they are less

than physically realizable since the result is a discontinuity of U on S. Of course, other boundary conditions can be used but Kirchhoff's theory provides no assistance in determining the most appropriate boundary conditions for a given problem. The black screen boundary conditions will be used here with their effect on the accuracy of the results discussed later.

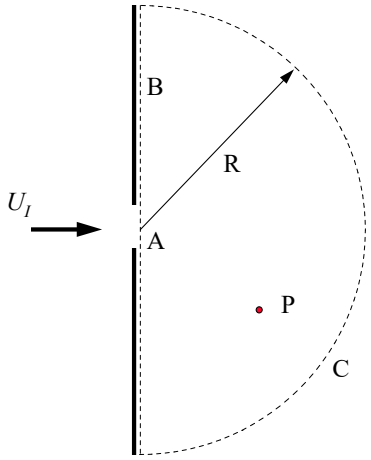

Figure 4-3. Diffraction by an opaque screen.

B. Plane Wave Slit Diffraction

As an example of the use of equation (4.11), consider the case of a uniform plane wave normally incident on a slit of width w and length l. For such a case U_I becomes

$$U_I = E_I e^{-ik_1 z} \tag{4.12}$$

and the integral (4.11) becomes

$$U(P) = \frac{E_I}{4\pi} \int_{-\frac{w}{2}}^{\frac{w}{2}} \int_{-\frac{l}{2}}^{\frac{l}{2}} \left(\frac{\partial G}{\partial z} + ik_1 G \right) dx_S dy_S \tag{4.13}$$

Now, letting l go to infinity (an infinitely long slit), y_s can be integrated out giving a multiplicative constant C.

$$U(P) = C\frac{E_I}{4\pi}\int_{-\frac{w}{2}}^{\frac{w}{2}}\left(\frac{\partial G(x_s,P)}{\partial z} + ik_1 G(x_s,P)\right)dx_s \tag{4.14}$$

For a slit in a homogeneous medium, Green's function is the standard point source distribution of equation (4.7) where s is the distance from P to a point in the aperture x_s. In general, Green's function can be thought of as the response of the medium to a point source located at P.

C. Diffraction In An Inhomogeneous Medium

Consider now an inhomogeneous medium, more specifically, one in which the dielectric constant ε (and thus the index of refraction n) is a function of position. Under these conditions, the wave equation becomes

$$\left(\nabla^2 + k^2\right)U + \nabla(U\nabla\ln\varepsilon) = 0 \tag{4.15}$$

Using this equation in place of the homogeneous wave equation (4.2) in the above analysis, however, does not prove fruitful. A general diffraction integral of the form of equation (4.9) does not seem possible under these conditions.

Thus, we shall not solve the problem of an inhomogeneous medium in general, but will consider the special case of stratified media. Consider a series of homogeneous layers of different materials all perpendicular to the z-direction and parallel to the plane of the aperture (Figure 4-4). The point of interest will lie in the second layer. The last layer, $m + 1$, is infinitely thick. Consider now equation (4.6). As was discussed, this equation will apply to any surface S which contains a homogeneous medium with no sources. This condition can be met by picking an appropriate surface, such as S_1 as shown in Figure 4-5. The integral over S_1 can be divided into four regions A, B, C, and D_{12}. By letting C be at infinity, it contributes nothing to the integral. If we assume the standard boundary conditions for the aperture given in equation (4.10), equation (4.6) becomes

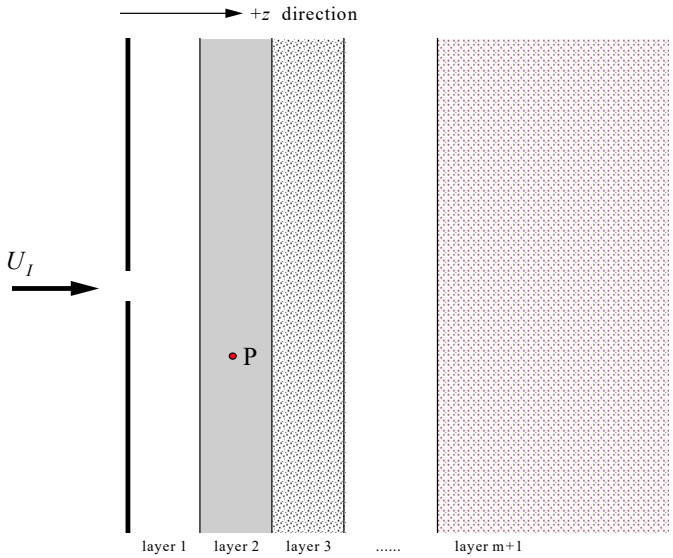

Figure 4-4. Diffraction in a multi-layer medium.

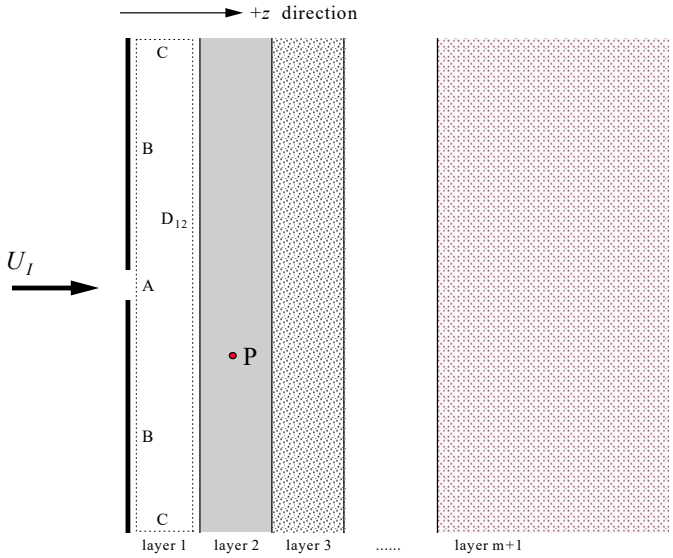

Figure 4-5. Surface S_1 (dotted line) used to evaluate Kirchhoff's diffraction integral.

$$\iint_A \left(\frac{\partial G}{\partial n} - G\frac{\partial U}{\partial n} \right) dxdy \;=\; \iint_{D_{12}} \left(U\frac{\partial G}{\partial n} - G\frac{\partial U}{\partial n} \right) dxdy \qquad (4.16)$$

Consider a second surface S_2 shown in Figure 4-6. The application of equation (4.6) to this surface gives

$$\iint_{D_{21}} + \iint_{D_{23}} + \iint_C + \iint_{S'} \left(U\frac{\partial G}{\partial n} - G\frac{\partial U}{\partial n} \right) dS_2 \;=\; 0 \qquad (4.17)$$

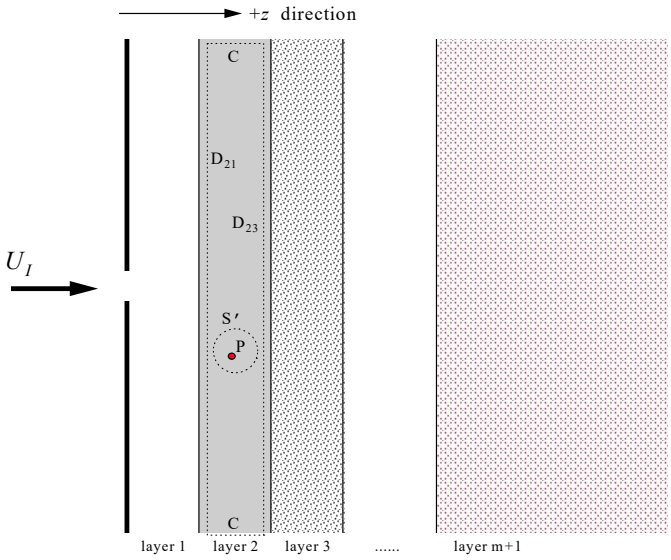

Figure 4-6. Second surface used in Kirchhoff's diffraction integral.

To evaluate the integral over the surface S', we must assume a form for G. Within S_2 (i.e., within the second layer) let us assume that the Green's function is defined by

$$G = \frac{e^{-ik_2 s}}{s} + g(P,Q) \tag{4.18}$$

where Q = a point on S_2,
s = distance from P to Q, and
$k_2 = 2\pi n_2/\lambda$, the propagation constant in layer 2.

Of course, $g(P,Q)$ must be a solution of the wave equation, but we also assume it is continuous and has a continuous first derivative on and within S_2. Letting S' be a sphere of radius r about the point P, and letting r go to zero, the integral on the surface S' can be evaluated as was done previously, yielding a value of $-4\pi U(P)$. Thus, equation (4.17) becomes

$$\iint_{D_{21}} \left(U\frac{\partial G}{\partial n} - G\frac{\partial U}{\partial n} \right) dxdy - \iint_{D_{23}} \left(U\frac{\partial G}{\partial n} - G\frac{\partial U}{\partial n} \right) dxdy = 4\pi U(P) \tag{4.19}$$

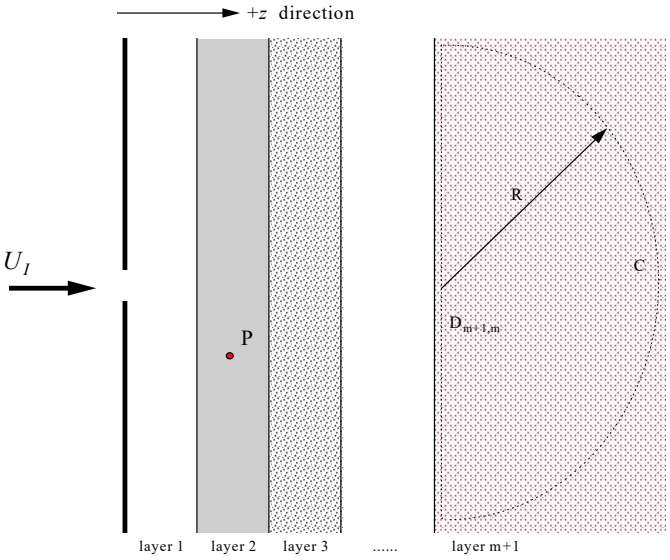

Figure 4-7. Kirchhoff's diffraction in the last layer.

Similarly, in region *j* (which does not contain the point *P*) we obtain

$$\iint_{D_{j,j+1}} \left(U\frac{\partial G}{\partial n} - G\frac{\partial U}{\partial n} \right) dxdy \;=\; \iint_{D_{j,j-1}} \left(U\frac{\partial G}{\partial n} - G\frac{\partial U}{\partial n} \right) dxdy \qquad (4.20)$$

This method can be continued through each layer until the last layer is encountered. In this region we pick S_{m+1} to be a hemisphere of radius R as shown in Figure 4-7. Letting $R \to \infty$,

$$\iint_{D_{m+1,m}} \left(U\frac{\partial G}{\partial n} - G\frac{\partial U}{\partial n} \right) dxdy \;=\; 0 \qquad (4.21)$$

Let us consider the behavior of U at the boundary between two layers. Before doing so, however, we must clarify the difference between scalar and vector quantities. The electric field is a vector and has three components.

$$\mathbf{U} \;=\; U_1\mathrm{a}_1 + U_2\mathrm{a}_2 + U_3\mathrm{a}_3 \qquad (4.22)$$

where U_1, U_2, and U_3 are scalars and a_1, a_2, and a_3 are a unit vector basis set. Equation (4.6), however, applies to a scalar wave function U, not a vector. Since the wave equation (4.2) applies to vectors as well as scalars, if a vector **U** satisfies the homogeneous wave equation, so will each of the scalar components U_1, U_2, and U_3. Thus, equation (4.6) and all the following equations can be applied to each scalar component separately, keeping the analysis in terms of scalars. The unit vectors can be any basis set, but for convenience we shall pick the conventional Cartesian unit vectors a_x, a_y, and a_z for the *x, y,* and *z* directions, respectively.

Electromagnetic theory requires boundary conditions to be met at the interface between two dielectrics. Figure 4-8 shows two vectors **U** and **U**′ at a boundary in the *x*-*y* plane and gives the resulting boundary conditions. If we assume G and $\partial G / \partial z$ are continuous across each boundary, then at the boundary between layers *j* and *j* + 1,

$$\iint_{D_{j,j+1}} \left(U_x\frac{\partial G}{\partial z} - G\frac{\partial U_x}{\partial z} \right) dxdy \;=\; \iint_{D_{j+1,j}} \left(U_x\frac{\partial G}{\partial z} - G\frac{\partial U_x}{\partial z} \right) dxdy$$

$$\iint_{D_{j,j+1}} \left(U_y \frac{\partial G}{\partial z} - G \frac{\partial U_y}{\partial z} \right) dxdy = \iint_{D_{j+1,j}} \left(U_y \frac{\partial G}{\partial z} - G \frac{\partial U_y}{\partial z} \right) dxdy$$

$$\iint_{D_{j,j+1}} \left(U_z \frac{\partial G}{\partial z} - G \frac{\partial U_z}{\partial z} \right) dxdy = \left(\frac{n_{j+1}^2}{n_j^2} \right) \iint_{D_{j+1,j}} \left(U_z \frac{\partial G}{\partial z} - G \frac{\partial U_z}{\partial z} \right) dxdy \quad (4.23)$$

$$U_x = U_x'$$

$$U_y = U_y'$$

$$\varepsilon U_z = \varepsilon' U_z'$$

or, if $\mu = \mu'$:

$$n^2 U_z = n'^2 U_z'$$

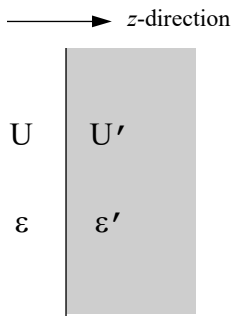

Figure 4-8. Electromagnetic boundary conditions at the interface between two dielectrics.

We can apply these boundary conditions to equations (4.19) - (4.21). Equation (4.21) tells us that the integral along the surface $D_{m+1,m}$ is zero for each component of U. Thus, by the above boundary conditions, the integrals along the surface $D_{m,m+1}$ are also zero. And, by equation (4.20) the integrals along $D_{m,m-1}$ must also be zero. This process can be continued until layer 2 is reached. Equation (4.19) then becomes

$$\iint_{D_{21}} \left(U \frac{\partial G}{\partial z} - G \frac{\partial U}{\partial z} \right) dxdy = 4\pi U(P) \quad (4.24)$$

for each of the three components of U. Using the boundary conditions on equation (4.24) and combining with equation (4.16) yields

$$U_x(P) = \left(\frac{1}{4\pi}\right)\iint_A \left(U_{Ix}\frac{\partial G}{\partial z} - G\frac{\partial U_{Ix}}{\partial z}\right) dS$$

$$U_y(P) = \left(\frac{1}{4\pi}\right)\iint_A \left(U_{Iy}\frac{\partial G}{\partial z} - G\frac{\partial U_{Iy}}{\partial z}\right) dS$$

$$U_z(P) = \left(\frac{n_1^2}{4\pi n_2^2}\right)\iint_A \left(U_{Iz}\frac{\partial G}{\partial z} - G\frac{\partial U_{Iz}}{\partial z}\right) dS \qquad (4.25)$$

As an example of the use of these equations, consider a plane wave normally incident on an infinitely long slit. U_I, the incident wave, has no z component, thus the last of the three equations (4.25) is zero. The first two equations become

$$U_x(P) = C\frac{E_{Ix}}{4\pi}\int_{-\frac{w}{2}}^{\frac{w}{2}} \left(\frac{\partial G(x_s,P)}{\partial z} + ik_1 G(x_s,P)\right) dx_s$$

$$U_y(P) = C\frac{E_{Iy}}{4\pi}\int_{-\frac{w}{2}}^{\frac{w}{2}} \left(\frac{\partial G(x_s,P)}{\partial z} + ik_1 G(x_s,P)\right) dx_s \qquad (4.26)$$

and the intensity at P becomes

$$I(P) = I_o\left[C\frac{1}{4\pi}\int_{-\frac{w}{2}}^{\frac{w}{2}} \left(\frac{\partial G(x_s,P)}{\partial z} + ik_1 G(x_s,P)\right) dx_s\right]^2 \qquad (4.27)$$

It is interesting to note that the above expression for intensity is identical to the expression one would obtain for the case of a homogeneous medium (e.g., from equation (4.14)). The only difference is the choice of the Green's function. In the above discussion we have placed many restrictions on G and the usefulness of equations (4.26) or (4.27) will depend on our ability to determine a suitable function for G. The Green's function must satisfy the homogeneous

wave equation in each layer, it must be continuous and have a continuous first derivative across each boundary, and it must take the form of equation (4.18) in layer 2. As was mentioned previously, the Green's function can be thought of as the response of the system to a point source at *P*. It can be shown that this response meets the three conditions above. In the next section, the Green's function for a specific case is determined.

D. Determining Green's Function

The cases of proximity and contact printing can now be treated using the diffraction theory given above. A mask located above the resist will generate a diffraction pattern which is *z*-dependent in amplitude as well as phase. In this case, the medium consists of air over resist over a reflecting substrate and the electric field distribution due to a point source must be determined. Rather than determining the electric field in the aperture due to a point source at *P*, we shall solve the conceptually simpler though mathematically equivalent problem of finding the electric field at *P* due to a point source in the aperture. Consider the geometry shown in Figure 4-9. For simplicity, a new coordinate system has been defined so that $z = 0$ on the resist surface. A geometrical approach will be used in which the electric field at an arbitrary point in the resist *P* is the sum of the rays emanating from the point source which pass through *P*. The first ray is simply refracted at the resist surface to pass through (*x, z*) (Figure 4-9).

Using Snell's Law and the geometry of the situation,

$$a_o = \frac{z_g}{\cos\phi}$$

$$b_o = \frac{z}{\cos\theta}$$

$$\cos\phi = \left(1 - \frac{n_2^2}{n_1^2}\sin^2\theta\right)^{\frac{1}{2}}$$

$$\cos\theta = \left(1 - \sin^2\theta\right)^{\frac{1}{2}} \tag{4.28}$$

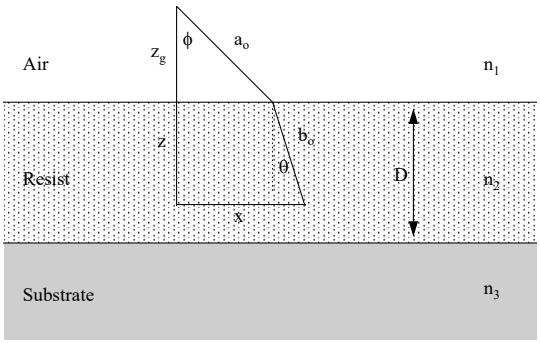

Figure 4-9. Geometry used in determining Green's function.

Determining the angle θ is more complicated than it may seem. The function $\theta(z,z_g,x)$ is of sixth order and must be solved numerically. The standard engineering approach (guess θ, calculate ϕ, then iterate until convergence) does not always converge in a stable manor. The best approach is to apply Fermat's principle, which states that the optical path length $n_1a_o + n_2b_o$ will be a minimum. A suitable algorithm, such as the bisection or Newton's method, can be used to minimize this function and determine the angles.

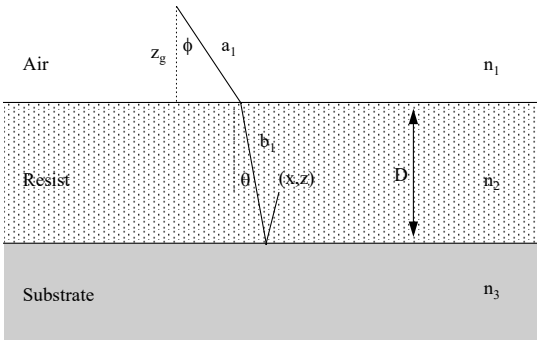

Figure 4-10. Geometry used in determining Green's functions after one reflection.

The transmission and reflection coefficients must be applied for oblique incidence. However, at this point, parallel or perpendicular polarization must be chosen. For the following discussion perpendicular polarization only is used. However, to model the more commonly used unpolarized light, one must calculate the intensity for both polarizations then average the two results. For perpendicular polarization, the Fresnel reflection and transmission coefficients are (see Chapter 3, equation 3.7)

$$\tau_{12} = \frac{2n_1 \cos\phi}{n_2 \cos\theta + n_1 \cos\phi}$$

$$\rho_{21} = \frac{n_2 \cos\theta - n_1 \cos\phi}{n_2 \cos\theta + n_1 \cos\phi}$$

$$\rho_{23} = \frac{n_2 \cos\theta - \left(n_3^2 - n_2^2 \sin^2\theta\right)^{\frac{1}{2}}}{n_2 \cos\theta + \left(n_3^2 - n_2^2 \sin^2\theta\right)^{\frac{1}{2}}} \tag{4.29}$$

The electric field due to a ray with no reflections, E_o, becomes

$$E_o = \frac{\tau_{12}(\theta)}{a_o + b_o} e^{-i\left(k_1 a_o + k_2 b_o\right)} \tag{4.30}$$

where k_1 and k_2 are the propagation constants in media 1 and 2, respectively.

The next ray to be considered has one reflection (Figure 4-10). Let a_1 be the distance the ray travels in air and b_1 the distance the ray travels in the resist. It can be shown that equations (4.28) - (4.29) will give the proper results if the variable z is replaced by z_1 where

$$z_1 = 2D - z \tag{4.31}$$

Similarly, after n reflections equations (4.28) - (4.29) are true when z is replaced by z_n where

$$z_n = nD + z, \quad \textit{for n even}$$

$$= (n+1)D - z, \quad \textit{for n odd} \tag{4.32}$$

The expression for the electric field caused by a ray undergoing n reflections becomes, for n even,

$$E_n = \frac{\tau_{12}(\theta)\left[\rho_{23}(\theta)\rho_{21}(\theta)\right]^{n/2}}{a_n + b_n} e^{-i(k_1 a_n + k_2 b_n)}$$

and for n odd,

$$E_n = \frac{\tau_{12}(\theta)\rho_{23}(\theta)\left[\rho_{23}(\theta)\rho_{21}(\theta)\right]^{(n-1)/2}}{a_n + b_n} e^{-i(k_1 a_n + k_2 b_n)} \tag{4.33}$$

The total electric field at the point (x,z) is then the algebraic sum of each ray.

$$G = \sum_{n=0}^{\infty} E_n \tag{4.34}$$

Fortunately, the series (4.34) converges very rapidly, within five or six terms using typical parameters.

Knowing G, the integral (4.27) can be evaluated numerically. Figure 4-11 shows the solution to this integral as a function of depth into a 1μm photoresist film on a silicon substrate for a 1.0μm isolated space and a 0.1μm mask-wafer gap.

E. Contact Printing

Kirchhoff's integral has been found experimentally to be valid for values of z_g as small as half a wavelength, and for line or space widths of a wavelength or more [4.2], even using the non-physical black screen boundary conditions. For typical photoresist applications this translates into $z_g > 0.2\mu m$. This condition is certainly met during proximity printing, and is quite often true for

contact printing. Usually, the tolerances for wafer and mask flatness are less stringent than 0.2μm. Thus, the above analysis for proximity printing is rigorous enough for most contact printing applications. A notable exception is conformable contact printing, in which a thin mask is allowed to conform to the topography of the wafer, making z_g a small fraction of a wavelength [4.3]. For this case, an accurate diffraction pattern near the top of the resist can be obtained only by finding a solution to the exact electromagnetic boundary value problem using Maxwell's equations. Solutions of this sort can be found [4.4,4.5], but are quite complicated.

Although all of the discussions thus far have been limited to monochromatic radiation, contact and proximity printers almost exclusively employ polychromatic sources (e.g., a mercury arc lamp) for their exposures. The effects of polychromatic illumination can be accounted for using an analysis given previously [4.6], and is easily incorporated into a contact printing model.

Figure 4-11. Typical diffraction image inside a 1μm thick photoresist on a silicon substrate (λ = 436nm, z_g = 0.1 μm, 1.0 μm isolated space).

The above analysis allows one to calculate the intensity of light within a photoresist layer during contact or proximity printing.

References

4.1. M. Born and E. Wolf, Principle of Optics, 6th ed., Pergamon Press (Oxford:1980) pp. 370-386.

4.2. C. L. Andrews, "Diffraction Pattern of a Circular Aperture at Short Distances," *Phys. Rev*., Vol. 71 (1947) pp. 777-786.

4.3. B. J. Lin, 'Deep-UV Conformable Contact Photolithography for Bubble Circuits," *IBM Jour. Res. Dev*., Vol. 20 (May, 1976) pp. 213-221.

4.4. M. Born and E. Wol, Principal of Optics, 6th ed., Pergamon Press (Oxford:1980) pp. 556-592.

4.5. B. J. Lin, "Electromagnetic Near-Field Diffraction o a Medium Slit," *Jour. Opt. Soc. Amer*., Vol. 62, No. 8 (Aug., 1972) pp. 976-981.

4.6. C. A. Mack, "Absorption and Exposure in Positive Photoresist," *Applied Optics*, Vol. 27, No. 23 (1 Dec. 1988) pp. 4913-4919.

Chapter 5

Photoresist Exposure Kinetics

The kinetics of photoresist exposure is intimately tied to the phenomenon of absorption. The discussion below begins with a description of absorption, followed by the chemical kinetics of exposure. Next, the chemistry of chemically amplified resists will be reviewed. Finally, a description of the measurement method for the kinetic exposure parameters will be given.

A. Absorption

The phenomenon of absorption can be viewed on a macroscopic or a microscopic scale. On the macro level, absorption is described by the familiar Lambert and Beer laws, which give a linear relationship between absorbance and path length times the concentration of the absorbing species. On the micro level, a photon is absorbed by an atom or molecule, promoting an electron to a higher energy state. Both methods of analysis yield useful information needed in describing the effects of light on a photoresist.

The basic law of absorption is an empirical one. It was first expressed by Lambert (circa 1760) and can be expressed in differential form as

$$\frac{dI}{dz} = -\alpha I \tag{5.1}$$

where I is the intensity of light traveling in the z-direction through a medium, and α is the absorption coefficient of the medium and has units of inverse length. This law is basically a single photon absorption probability equation: the probability that a photon will be absorbed is proportional to the photon flux. In a homogeneous medium (i.e., α is not a function of z), equation (5.1) may be integrated to yield

$$I(z) = I_0 \exp(-\alpha z) \tag{5.2}$$

where z is the distance the light has traveled through the medium and I_o is the intensity at $z = 0$. If the medium is inhomogeneous, equation (5.2) becomes

$$I(z) = I_0 \exp(-Abs(z)) \tag{5.3}$$

where

$$Abs(z) = \int_0^z \alpha(z')dz' \quad = \quad \textit{the absorbance}$$

When working with electromagnetic radiation, it is often convenient to describe the radiation by its complex electric field vector. The propagation of an electric field through some material can implicitly account for absorption by using a complex index of refraction $\boldsymbol{n}$ for the material such that

$$\boldsymbol{n} = n - i\kappa \tag{5.4}$$

The imaginary part of the index of refraction is related to the absorption coefficient by

$$\alpha = 4\pi\kappa/\lambda \tag{5.5}$$

Note that the sign of the imaginary part of the index in equation (5.4) depends on the sign convention chosen for the phasor representation of the electric field (see equation (3.4) in Chapter 3). For typical absorption calculations in thin films,

the "standard" sign convention most commonly used in the literature results in a negative imaginary part of the index of refraction. If the wrong sign is chosen in equation (5.4), the material will amplify the electric field rather than absorb it!

In 1852, August Beer showed that for dilute solutions the absorption coefficient is proportional to the concentration of the absorbing species in the solution.

$$\alpha_{solution} = ac \tag{5.6}$$

where a is the molar absorption coefficient (sometimes called the extinction coefficient) of the absorbing species (given by $a = \alpha_0 MW/\rho$, where α_0 is the absorption coefficient of the pure material, MW is the molecular weight, ρ is the density) and c is the concentration. The stipulation that the solution be dilute expresses a fundamental limitation of Beer's law. At high concentrations, where absorbing molecules are close together, the absorption of a photon by one molecule may be affected by a nearby molecule [5.1]. Since this interaction is concentration dependent, it causes deviation from the linear relation (5.6). Also, an apparent deviation from Beer's law occurs if the real part of the index of refraction changes appreciably with concentration. Thus, the validity of Beer's law should always be verified over the concentration range of interest.

For an N component homogeneous solid, the overall absorption coefficient becomes

$$\alpha_T = \sum_{j=1}^{N} a_j c_j \tag{5.7}$$

The linear addition of absorption terms presumes that Beer's law holds across components, i.e., that the absorption by one material is not influenced by the presence of the other materials. Of the total amount of light absorbed, the fraction of light which is absorbed by component i is given by

$$\frac{I_{Ai}}{I_{AT}} = \frac{a_i c_i}{\alpha_T} \tag{5.8}$$

where I_{AT} is the total light absorbed by the film, and I_{Ai} is the light absorbed by component *i*.

We will now apply the concepts of macroscopic absorption to a typical positive photoresist. A diazonaphthoquinone positive photoresist (such as AZ1350J) is made up of four major components; a base resin *R* that gives the resist its structural properties, a photoactive compound *M* (abbreviated PAC, this is the light sensitive moiety in the resist), exposure products *P* generated by the reaction of *M* with ultraviolet light, and a solvent *S*. Although photoresist drying during prebake is intended to drive off solvents, thermal studies have shown that a resist may contain up to 10% solvent after a typical prebake [5.2, 5.3]. The absorption coefficient α is then

$$\alpha = a_M M + a_P P + a_R R + a_S S \tag{5.9}$$

If M_o is the initial PAC concentration (i.e., with no UV exposure), the stoichiometry of the exposure reaction gives

$$P = M_o - M \tag{5.10}$$

Equation (5.9) may be rewritten as [5.4]

$$\alpha = Am + B \tag{5.11}$$

where $A = (a_M - a_P)M_o$
$B = a_P M_o + a_R R + a_S S$
$m = M/M_o$

A and *B* are called the bleachable and non-bleachable absorption coefficients, respectively, and make up the first two Dill photoresist parameters [5.4]. Other non-bleachable components of the photoresist (such as a dye additive) are added to the *B* term above.

The quantities *A* and *B* are experimentally measurable [5.4] and can be easily related to typical resist absorbance curves, measured using a UV spectrophotometer. When the resist is fully exposed, $M = 0$ and

$$\alpha_{exposed} = B \tag{5.12}$$

Similarly, when the resist is unexposed, $m = 1$ ($M = M_o$) and

$$\alpha_{unexposed} = A + B \tag{5.13}$$

From this A may be found by

$$A = \alpha_{unexposed} - \alpha_{exposed} \tag{5.14}$$

Thus, $A(\lambda)$ and $B(\lambda)$ may be determined from the UV absorbance curves of unexposed and completely exposed resist (Figure 5-1). A more complete description of the measurement of A and B will be given in a following section.

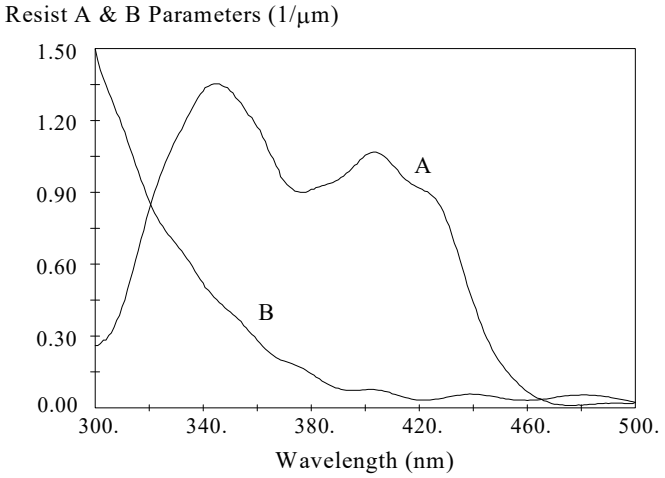

Figure 5-1. Resist parameters *A* and *B* as a function of wavelength measured with a UV spectrophotometer for a typical g-line resist.

As mentioned previously, Beer's law is empirical in nature and, thus, should be verified experimentally. In the case of positive photoresists, this

means formulating resist mixtures with differing photoactive compound to resin ratios and measuring the resulting *A* parameters. Previous work has shown that Beer's law is valid for conventional photoresists over the full practical range of PAC concentrations [5.5].

B. Exposure Kinetics

On a microscopic level, the absorption process can be thought of as photons being absorbed by an atom or molecule causing an outer electron to be promoted to a higher energy state. This phenomenon is especially important for the photoactive compound since it is the absorption of UV light that leads to the chemical conversion of *M* to *P*.

$$M \xrightarrow{UV} P \tag{5.15}$$

This concept is stated in the first law of photochemistry: only the light that is absorbed by a molecule can be effective in producing photochemical change in the molecule. The actual chemistry of diazonaphthoquinone exposure is given below [5.6]:

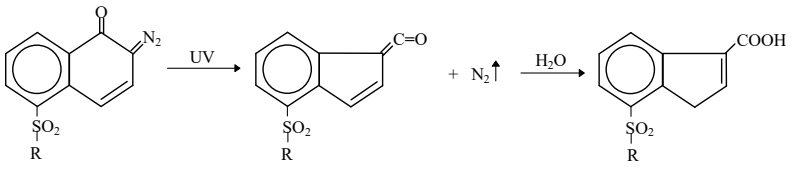

(5.16)

The chemical reaction (5.15) can be rewritten in a more general form as

$$M \underset{k_2}{\overset{k_1}{\rightleftarrows}} M^* \xrightarrow{k_3} P \tag{5.17}$$

where *M* is the photoactive compound (PAC), *M** is the PAC molecule in an excited state, *P* is the carboxylic acid (product), and k_1, k_2, k_3 are the rate constants for each reaction. Simple kinetics can now be applied. The proposed mechanism (5.17) assumes that all reactions are first order. Thus, the rate equation for each species can be written.

$$\frac{dM}{dt} = k_2 M^* - k_1 M$$

$$\frac{dM^*}{dt} = k_1 M - (k_2 + k_3) M^*$$

$$\frac{dP}{dt} = k_3 M^* \tag{5.18}$$

A system of three coupled linear first order differential equations can be solved exactly using Laplace transforms and the initial conditions [5.7]

$$\begin{aligned} M(t=0) &= M_o \\ M^*(t=0) &= P(t=0) = 0 \end{aligned} \tag{5.19}$$

However, if one uses the steady state approximation the solution becomes much simpler. This approximation assumes that in a very short time the excited molecule M^* comes to a steady state, i.e., M^* is formed as quickly as it disappears. In mathematical form,

$$\frac{dM^*}{dt} = 0 \tag{5.20}$$

A previous study has shown that M^* does indeed come to a steady state quickly, on the order of 10^{-8} seconds or faster [5.7]. Thus,

$$\frac{dM}{dt} = -KM \tag{5.21}$$

where

$$K = \frac{k_1 k_3}{k_2 + k_3}$$

Assuming K remains constant with time (an assumption we shall soon dispose of),

$$M = M_o \exp(-Kt) \tag{5.22}$$

The overall rate constant K is a function of the intensity of the exposure radiation. An analysis of the microscopic absorption of a photon predicts that K is directly proportional to the intensity of the exposing radiation [5.5]. The rate constant k_1 in equation (5.17) will be proportional to the rate of photon absorption, which in turn is proportional to the photon flux (by Lambert's law) and thus the intensity. A more useful form of equation (5.21) is then

$$\frac{dm}{dt} = -CIm \tag{5.23}$$

where the relative PAC concentration m (= M/M_o) has been used and C is the standard exposure rate constant and the third Dill photoresist parameter [5.4].

A solution to the exposure rate equation (5.23) is simple if the intensity within the resist is constant throughout the exposure. However, this is generally not the case. In fact, many resists *bleach* upon exposure, that is, they become more transparent as the photoactive compound M is converted to product P. This corresponds to a positive value of A, as seen, for example, in Figure 5-1. Since the intensity varies as a function of exposure time, this variation must be known in order to solve the exposure rate equation. In the simplest possible case, a resist film coated on a substrate of the same index of refraction, only absorption affects the intensity within the resist. Thus, Lambert's law of absorption, coupled with Beer's law, could be applied.

$$\frac{dI}{dz} = -(Am + B)I \tag{5.24}$$

where equation (5.11) was used to relate the absorption coefficient to the relative PAC concentration. Equations (5.23) and (5.24) are coupled, and thus become first order non-linear partial differential equations which must be solved simultaneous. The solution to equations (5.23) and (5.24) was first carried out numerically for the case of lithography simulation [5.4], but in fact was solved analytically by Herrick [5.8] many years earlier. The same solution was also presented more recently by Diamond and Sheats [5.9] and by Babu and Barouch [5.10]. These solutions take the form of a single numerical integration, which is much simpler than solving two differential equations!

Although an analytical solution exists for the simple problem of exposure with absorption only, in more realistic problems the variation of intensity with depth in the film is more complicated than equation (5.24). In fact, the general exposure situation results in the formation of standing waves, as discussed previously. In such a case, equations (4.1) - (4.4) can give the intensity within the resist as a function of the PAC distribution *m(x,y,z,t)*. Initially, this distribution is simply *m(x,y,z,0) = 1* (resulting in a uniform index of refraction). Thus, equation (4.1), for example, would give *I(x,y,z,0)*. The exposure equation (5.23) can then be integrated over a small increment of exposure time Δt to produce the PAC distribution *m(x,y,z,*Δt*)*. The assumption is that over this small increment in exposure time the intensity remains relatively constant, leading to the exponential solution

$$m(x,y,z,t+\Delta t) \;=\; m(x,y,z,t)\exp(-CI\Delta t) \tag{5.25}$$

This new PAC distribution is then used to calculate the new intensity distribution *I(x,y,z,*Δt*)*, which in turn is used to generate the PAC distribution at the next increment of exposure time *m(x,y,z,2*Δt*)*. This process continues until the final exposure time is reached.

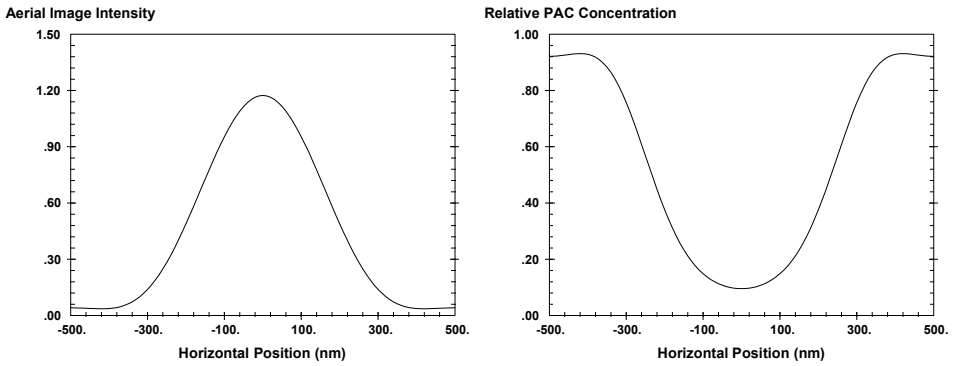

Figure 5-2. The exposure process takes an aerial image (a) and converts it into a latent image (b).

The final result of exposure is the conversion of an aerial image *I(x,y,z)* into a latent image *m(x,y,z)*. Figure 5-2 illustrates a one-dimensional case.

C. Chemically Amplified Resists

Chemically amplified photoresists are composed of a polymer resin (possibly "blocked" to inhibit dissolution), a photoacid generator (PAG), and possibly a crosslinking agent, dye or other additive. As the name implies, the photoacid generator forms a strong acid when exposed to Deep-UV light. Ito and Willson first proposed the use of an aryl onium salt [5.11], and triphenylsulfonium salts have been studied extensively as PAGs. The reaction of a common PAG is shown below:

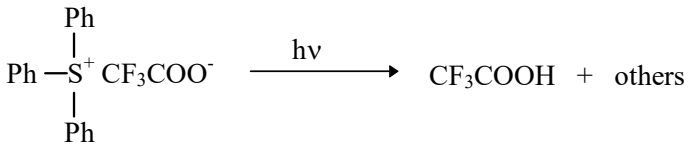

(5.26)

The acid generated in this case (trifluoroacetic acid) is a derivative of acetic acid where the electron-drawing properties of the fluorines are used to greatly increase the acidity of the molecule. The PAG is mixed with the polymer resin at a concentration of typically 5-15% by weight, with 10% as a typical formulation.

The kinetics of the exposure reaction are presumed to be standard first order:

$$\frac{\partial G}{\partial t} = -CIG \tag{5.27}$$

where G is the concentration of PAG at time t (the initial PAG concentration is G_o), I is the exposure intensity, and C is the exposure rate constant. For constant intensity, the rate equation can be solved for G:

$$G = G_o e^{-CIt} \tag{5.28}$$

The acid concentration H is given by

$$H = G_o - G = G_o\left(1 - e^{-CIt}\right) \tag{5.29}$$

If the intensity is not constant throughout the exposure, then the iterative approach described in the section above can certainly be used.

Exposure of the resist with an aerial image *I(x)* results in an acid latent image *H(x)*. A post-exposure bake (PEB) is then used to thermally induce a chemical reaction. This may be the activation of a crosslinking agent for a negative resist or the deblocking of the polymer resin for a positive resist. The reaction is catalyzed by the acid so that the acid is not consumed by the reaction and, to first order, H remains constant. Ito and Willson first proposed the concept of deblocking a polymer to change its solubility [5.11]. A base polymer such as polyhydroxystyrene, PHS, is used which is very soluble in an aqueous base developer. It is the hydroxyl groups which give the PHS its high solubility so by "blocking" these sites (by reacting the hydroxyl group with some longer chain molecule) the solubility can be reduced. Ito and Willson employed a *t*-butoxycarbonyl group (*t*-BOC), resulting in a very slowly dissolving polymer. In the presence of acid and heat, the *t*-BOC blocked polymer will undergo acidolysis to generate the soluble hydroxyl group, as shown below.

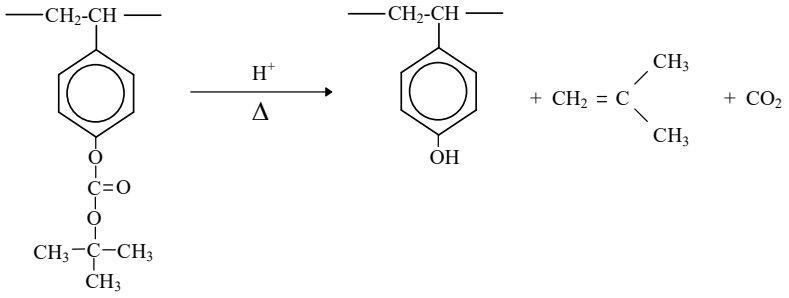

(5.30)

One drawback of this scheme is that the cleaved *t*-BOC is volatile and will evaporate, causing film shrinkage in the exposed areas. Larger molecular weight blocking groups can be used to reduce this film shrinkage to acceptable levels (below 10%). Also, the blocking group is such an effective inhibitor of

dissolution that nearly every blocked site on the polymer must be deblocked in order to obtain significant dissolution. Thus, the photoresist can be made more "sensitive" by only partially blocking the PHS. Typical photoresists use 10-30% of the hydroxyl groups blocked, with 20% a typical value. Molecular weights for the PHS run in the range of 3000 to 5000 giving about 20 to 35 hydroxyl groups per polymer molecule, about 4 to 7 of which are initially blocked.

Using M as the concentration of some reactive site, these sites are consumed (i.e., are reacted) according to kinetics of some unknown order in H and first order in M [5.12]:

$$\frac{\partial M}{\partial t'} = -K_{\text{amp}} M H^n \tag{5.31}$$

where K_{amp} is the rate constant of the amplification reaction (crosslinking, deblocking, etc.) and t' is the bake time. Simple theory would indicate that n = 1, but the general form will be used here. Assuming H is constant, equation (5.31) can be solved for the concentration of reacted sites X:

$$X = M_o - M = M_o \left(1 - e^{-K_{\text{amp}} H^n t'}\right) \tag{5.32}$$

(Note: Although H^+ is not consumed by the reaction, the value of H is not locally constant. Diffusion during the PEB and acid loss mechanisms cause local changes in the acid concentration, thus requiring the use of a reaction-diffusion system of equations. The approximation that H is constant is a useful one, however, which gives insight into the reaction as well as accurate results under some conditions.)

It is useful here to normalize the concentrations to some initial values. This results in a normalized acid concentration h and normalized reacted and unreacted sites x and m:

$$h = \frac{H}{G_o} \qquad x = \frac{X}{M_o} \qquad m = \frac{M}{M_o} \tag{5.33}$$

Equations (5.30) and (5.32) become

$$h = 1 - e^{-CIt}$$
$$m = 1 - x = e^{-\alpha h^n} \tag{5.34}$$

where α is a lumped "amplification" constant equal to $G_o^n K_{amp} t'$. The result of the PEB is an amplified latent image *m(x)*, corresponding to an exposed latent image *h(x)*, resulting from the aerial image *I(x)*.

The above analysis of the kinetics of the amplification reaction assumed a locally constant concentration of acid *H*. Although this could be exactly true in some circumstances, it is typically only an approximation, and is often a poor approximation. In reality, the acid diffuses during the bake. In one dimension, the standard diffusion equation takes the form

$$\frac{\partial H}{\partial t'} = \frac{\partial}{\partial z}\left(D_H \frac{\partial H}{\partial z} \right) \tag{5.35}$$

where D_H is the diffusivity of acid in the photoresist. Solving this equation requires a number of things: two boundary conditions for each dimension, one initial condition, and a knowledge of the diffusivity as a function of position and time.

The initial condition is the initial acid distribution within the film, *H(x,y,z,0)*, resulting from the exposure of the PAG. The two boundary conditions are at the top and bottom surface of the photoresist film. The boundary at the wafer surface is assumed to be impermeable, giving a boundary condition of no diffusion into the wafer. The boundary condition at the top of the photoresist will depend on the diffusion of acid into the atmosphere above the wafer, as described below. In the plane of the wafer (x- and y-directions), boundary conditions will depend on the geometry of the problem.

The solution of equation (5.35) can now be performed if the diffusivity of the acid in the photoresist is known. Unfortunately, this solution is complicated by two very important factors: the diffusivity is a strong function of temperature and, most probably, the extent of amplification. Since the temperature is changing with time during the bake, the diffusivity will be time dependent. The concentration dependence of diffusivity results from an increase in free volume for typical positive resists: as the amplification reaction

proceeds, the polymer blocking group evaporates resulting in a decrease in film thickness but also an increase in free volume (and probably a change in the glass transition temperature as well). Since the acid concentration is time and position dependent, the diffusivity in equation (5.35) must be determined as a part of the solution of equation (5.35) by an iterative method. The resulting simultaneous solution of equations (5.31) and (5.35) is called a *reaction-diffusion* system.

The temperature dependence of the diffusivity can be expressed in a standard Arrhenius form:

$$D_o(T) = A_r \exp\left(-E_a / RT\right) \tag{5.36}$$

where D_o is a general diffusivity, A_r is the Arrhenius coefficient, E_a is the activation energy, R is the universal gas constant, and T is the absolute temperature. A full treatment of the amplification reaction would include a thermal model of the hotplate in order to determine the actual time-temperature history of the wafer [5.13]. To simplify the problem, an ideal temperature distribution will be assumed -- the temperature of the resist is zero (low enough for no diffusion or reaction) until the start of the bake, at which time it immediately rises to the final bake temperature, stays constant for the duration of the bake, then instantly falls back to zero.

The concentration dependence of the diffusivity is less obvious. Several authors have proposed and verified the use of different models for the concentration dependence of diffusion within a polymer. Of course, the simplest form (besides a constant diffusivity) would be a linear model. Letting D_o be the diffusivity of acid in completely unreacted resist and D_f the diffusivity of acid in resist which has been completely reacted,

$$D_H = D_o + x\left(D_f - D_o\right) \tag{5.37}$$

Here, diffusivity is expressed as a function of the extent of the amplification reaction x. Another common form is the Fujita-Doolittle equation [5.14] which can be predicted theoretically using free volume arguments. A form of that equation which is convenient for calculations is shown here:

$$D_H = D_o \exp\left(\frac{\alpha x}{1+\beta x}\right) \tag{5.38}$$

where α and β are experimentally determined constants. Other concentration relationships are also possible [5.15], but only constant, linear, and exponential are used in PROLITH/2.

Through a variety of mechanisms, acid formed by exposure of the resist film can be lost and thus not contribute to the catalyzed reaction to change the resist solubility. There are two basic types of acid loss: loss that occurs between exposure and post-exposure bake, and loss that occurs during the post-exposure bake. The first type of loss leads to delay time effects -- the resulting lithography is affected by the delay time between exposure and post-exposure bake. Delay time effects can be very severe and, of course, are very detrimental to the use of such a resist in a manufacturing environment [5.16, 5.17]. The typical mechanism for delay time acid loss is the diffusion of atmospheric base contaminates into the top surface of the resist. The result is a neutralization of the acid near the top of the resist and a corresponding reduced amplification. For a negative resist, the top portion of a line is not insolublized and resist is lost from the top of the line. For a positive resist, the effects are more devastating. Sufficient base contamination can make the top of the resist insoluble, blocking dissolution into the bulk of the resist (Figure 5-3). In extreme cases, no patterns can be observed after development. Another possible delay time acid loss mechanism is base contamination from the substrate, as has been observed on TiN substrates [5.17].

The effects of acid loss due to atmospheric base contaminants can be accounted for in a straightforward manner [5.18]. The base diffuses slowly from the top surface of the resist into the bulk. Assuming that the concentration of base contaminant in contact with the top of the resist remains constant, the diffusion equation can be solved for the concentration of base, *B*, as a function of depth into the resist film:

$$B = B_o \exp\left(-(z/\sigma)^2\right) \tag{5.39}$$

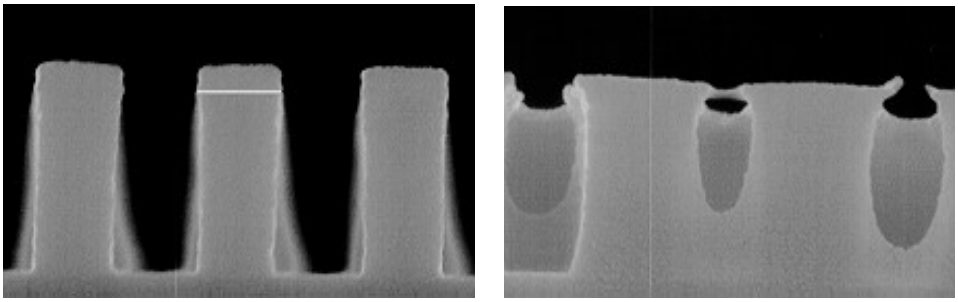

(a) (b)

Figure 5-3. Atmospheric base contamination leads to T-top formation. Shown are line/space features printed in APEX-E for (a) 0.275μm features with no delay and (b) 0.325μm features with 10 minute delay between exposure and post-exposure bake *(courtesy of SEMATECH)*.

where B_o is the base concentration at the top of the resist film, z is the depth into the resist (z=0 at the top of the film) and σ is the diffusion length of the base in resist. The standard assumption of constant diffusivity has been made here so that diffusion length goes as the square root of the delay time.

Since the acid generated by exposure for most resist systems of interest is fairly strong, it is a good approximation to assume that all of the base contaminant will react with acid if there is sufficient acid present. Thus, the acid concentration at the beginning of the PEB, H^*, is related to the acid concentration after exposure, H, by

$$H^* = H - B \qquad or \qquad h^* = h - b \tag{5.40}$$

where the lower case symbols again represent the concentration relative to G_o, the initial photoacid generator concentration.

Acid loss during the PEB could occur by other mechanisms. For example, as the acid diffuses through the polymer, it may encounter sites which "trap" the acid, rendering it unusable for further amplification. If these traps

were in much greater abundance than the acid itself (for example, sites on the polymer), the resulting acid loss rate would be first order,

$$\frac{\partial h}{\partial t'} = - K_{loss}\, h \tag{5.41}$$

where K_{loss} is the acid loss reaction rate constant. Of course, other more complicated acid loss mechanisms can be proposed, but in the absence of data supporting them, the simple first order loss mechanism will be used here.

Acid can also be lost at the top surface of the resist due to evaporation. The amount of evaporation is a function of the size of the acid and the degree of its interaction with the resist polymer. A small acid (such as the trifluoroacetic acid discussed above) may have very significant evaporation. A separate rate equation can be written for the rate of evaporation of acid:

$$\left.\frac{\partial h}{\partial t'}\right|_{z=0} = - K_{evap}\left(h(0,t') - h_{air}(0,t')\right) \tag{5.42}$$

where $z = 0$ is the top of the resist and h_{air} is the acid concentration in the atmosphere just above the photoresist surface. Typically, the PEB takes place in a reasonably open environment with enough air flow to eliminate any buildup of evaporated acid above the resist, making $h_{air} = 0$. If K_{evap} is very small, then virtually no evaporation takes place and we say that the top boundary of the resist is impenetrable. If K_{evap} is very large (resulting in evaporation that is much faster than the rate of diffusion), the effect is to bring the surface concentration of acid in the resist to zero. The significance of K_{evap} is best viewed by comparing the magnitude of K_{evap} to K_{amp} (i.e., how fast does evaporation occur relative to amplification).

The combination of a reacting system and a diffusing system is called a reaction-diffusion system. The solution of such a system is the simultaneous solution of equations (5.31) and (5.35) using equation (5.30) as an initial condition and equation (5.37) or (5.38) to describe the reaction-dependent diffusivity. Of course, any or all of the acid loss mechanisms can also be included. A convenient and straightforward method to solve such equations is the finite difference method (see, for example, reference [5.19]). The equations

are solved by approximating the differential equations by difference equations. By marching through time and solving for all space at each time step, the final solution is the result after the final time step. A key part of an accurate solution is the choice of a sufficiently small time step. If the spatial dimension of interest is Δx (or Δy or Δz), the time step should be chosen such that the diffusion length is less than Δx (using a diffusion length of about one third of Δx is common).

D. Measuring the *ABC* Parameters

Dill proposed a single, simple experiment for measuring the ABC parameters [5.4]. The photoresist to be measured is coated in a non-reflecting substrate (e.g., glass, quartz, or similar material). The resist is then exposed by a normally incident parallel beam of light at the wavelength of measurement. At the same time, the intensity of the light transmitted through the substrate is measured continuously. The output of the experiment, transmitted intensity as a function of exposure time, is then analyzed to determine the resist ABC parameters. A typical experimental setup is shown in Figure 5-4.

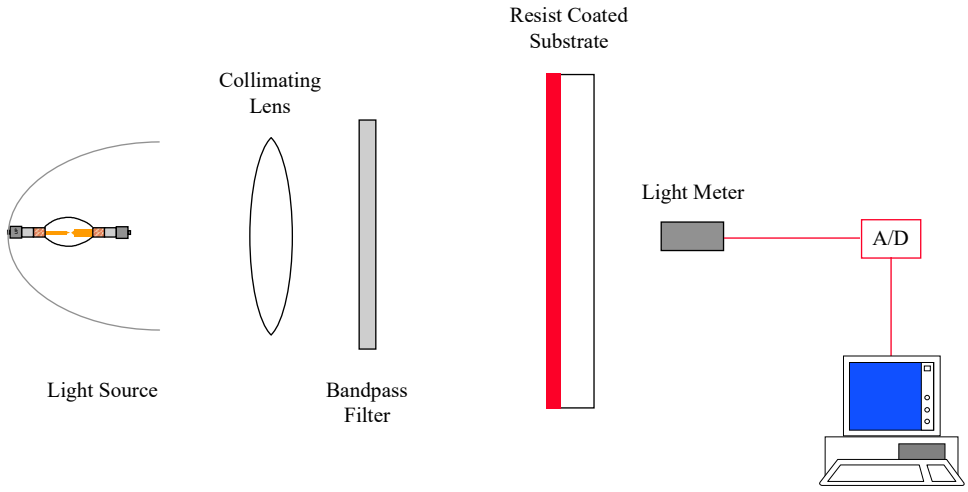

Figure 5-4. Experimental configuration for the measurement of the ABC parameters.

By measuring the incident exposing light intensity, the output of the experiment becomes overall transmittance as a function of incident exposure dose, *T(E)*. Figure 5-5 shows a typical result. Assuming careful measurement of this function, and a knowledge of the thickness of the photoresist, all that remains is the analysis of the data to extract the ABC parameters. Dill proposed two methods for extracting the parameters [5.4]. Those methods will be reviewed here and a third, more accurate approach will be shown.

Note that the effectiveness of this measurement technique rests with the non-zero value of *A*. If the photoresist does not change its optical properties with exposure (i.e., if $A = 0$), then measuring transmittance will provide no insight on the exposure reaction, making *C* unobtainable by this method.

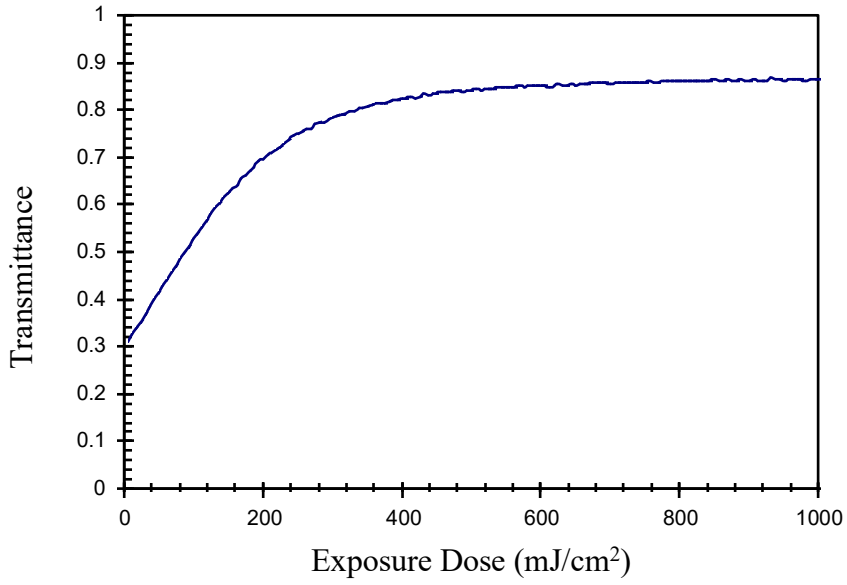

Figure 5-5. Typical transmittance curve of a positive *g*- or *i*-line bleaching photoresist measured using an apparatus similar to that pictured in Figure 5-4.

1. Graphical Data Analysis (Method 1)

Analysis of the experimental data is greatly simplified if the experimental conditions are adjusted so that the simple exposure and absorption equations (5.23) and (5.24) apply exactly. This means that light passing through the resist must not reflect at the resist/substrate interface. Further, light passing through the substrate must not reflect at the substrate/air interface. The first requirement is met by producing a transparent substrate with the same index of refraction as the photoresist. The second requirement is met by coating the backside of the substrate with an interference-type antireflection coating (ARC).

Given such ideal measurement conditions, Dill showed that the ABC parameters can be obtained from the transmittance curve by measuring the initial transmittance *T(0)*, the final (completely exposed) transmittance *T(∞)*, and the initial slope of the curve. The relationships are:

$$A = \frac{1}{D}\ln\left(\frac{T(\infty)}{T(0)}\right) \tag{5.43a}$$

$$B = -\frac{1}{D}\ln\left(T(\infty)\right) \tag{5.43b}$$

$$C = \frac{A+B}{AT(0)\{1-T(0)\}T_{12}}\left.\frac{dT}{dE}\right|_{E=0} \tag{5.43c}$$

where D is the resist thickness and T_{12} is the transmittance of the air-resist interface and is given, for a resist index of refraction n_{resist}, by

$$T_{12} = 1-\left(\frac{n_{resist}-1}{n_{resist}+1}\right)^2 \tag{5.44}$$

2. Differential Equation Solution (Method 2)

Although graphical analysis of the data is quite simple, it suffers from the common problem of errors when measuring the slope of experimental data. As a result, the value of C (and to a lesser extent, A) obtained often contains significant error. Dill also proposed a second method for extracting the ABC parameters from the data. Again assuming that the ideal experimental conditions had been met, the ABC parameters could be obtained by directly solving the two coupled partial differential equations (5.23) and (5.24) and finding the values of A, B, and C for which the solution best fits the experimental data. Obviously, fitting the entire experimental curve is much less sensitive to noise in the data than taking the slope at one point. Several techniques are available to provide a simple numerical solution [5.8-5.10].

3. Full Simulation (Method 3)

Methods 1 and 2 give accurate results only to the extent that the actual experimental conditions match the ideal (no reflection) conditions. In reality, there will always be some deviation from this ideal. Substrates will invariably have an index somewhat different that of the photoresist. And since the index of refraction of the photoresist changes with exposure, even a perfect substrate will be optically matched at only one instant in time during the experiment. Backside ARCs may also be less than perfect. In fact, most experimenters would prefer to use off-the-shelf glass or quartz wafers with no backside ARC. Under these conditions, how accurate are the extracted ABC parameters?

The dilemma can be solved by eliminating the restrictions of the ideal experiment. Rather than solving for the transmitted intensity via equations (5.23) and (5.24), one could use a lithography simulator to solve for the transmittance in a non-ideal case including changes in the resist index of refraction during exposure and reflections from both the top and bottom of the substrate. Then, by adjusting the ABC parameters, a best fit of the model to the data could be obtained. This method provides the ultimate accuracy in obtaining extracted ABC parameters [5.20].

All three methods described above have been incorporated into ProABC.

References

5.1. D. A. Skoog and D. M. West, Fundamentals of Analytical Chemistry, 3rd edition, Holt, Rinehart, and Winston (New York :1976), pp. 509-510.

5.2. J. M. Koyler, et al., "Thermal Properties of Positive Photoresist and their Relationship to VLSI Processing," *Kodak Microelectronics Seminar Interface '79*, (1979) pp. 150-165.

5.3. J. M. Shaw, M. A. Frisch, and F. H. Dill, "Thermal Analysis of Positive Photoresist Films by Mass Spectrometry," *IBM Jour. Res. Dev.*, Vol 21 (May, 1977), pp. 219-226.

5.4. F. H. Dill, W. P. Hornberger, P. S. Hauge, and J. M. Shaw, "Characterization of Positive Photoresist," *IEEE Trans. Electron Devices*, Vol. ED-22, No. 7, (July, 1975) pp. 445-452.

5.5. C. A. Mack, "Absorption and Exposure in Positive Photoresist," *Applied Optics*, Vol. 27, No. 23 (1 Dec. 1988) pp. 4913-4919.

5.6. R. Dammel, Diazonaphthoquinone-based Resists, SPIE Tutorial Texts Vol. TT 11 (Bellingham, WA: 1993).

5.7. J. Albers and D. B. Novotny, "Intensity Dependence of Photochemical Reaction Rates for Photoresists," *Jour. Electrochem. Soc*., Vol. 127, No. 6 (June, 1980) pp. 1400-1403.

5.8. C. E. Herrick, Jr., "Solution of the Partial Differential Equations Describing Photo-decomposition in a Light-absorbing Matrix having Light-absorbing Photoproducts," *IBM Journal of Research and Development*, Vol. 10 (Jan., 1966) pp. 2-5.

5.9. J. J. Diamond and J. R. Sheats, "Simple Algebraic Description of Photoresist Exposure and Contrast Enhancement," *IEEE Electron Device Letters*, Vol. EDL-7, No. 6 (June, 1986) pp. 383-386.

5.10. S. V. Babu and E. Barouch, "Exact Solution of Dill's Model Equations for Positive Photoresist Kinetics," *IEEE Electron Device Letters*, Vol. EDL-7, No. 4 (April, 1986) pp. 252-253.

5.11. H. Ito and C. G. Willson, "Applications of Photoinitiators to the Design of Resists for Semiconductor Manufacturing," in Polymers in Electronics, ACS Symposium Series 242 (1984) pp. 11-23.

5.12 D. Seligson, S. Das, H. Gaw, and P. Pianetta, "Process Control with Chemical Amplification Resists Using Deep Ultraviolet and X-ray Radiation," *Jour. Vacuum Science and Tech*., Vol. B6, No. 6 (Nov/Dec, 1988) pp. 2303-2307.

5.13. C. A. Mack, D. P. DeWitt, B. K. Tsai, and G. Yetter, "Modeling of Solvent Evaporation Effects for Hot Plate Baking of Photoresist," *Advances in Resist Technology and Processing XI, Proc.*, SPIE Vol. 2195 (1994) pp. 584-595.

5.14. H. Fujita, A. Kishimoto, and K. Matsumoto, "Concentration and Temperature Dependence of Diffusion Coefficients for Systems Polymethyl Acrylate and n-Alkyl Acetates," *Transactions of the Faraday Society*, Vol. 56 (1960) pp. 424-437.

5.15. D. E. Bornside, C. W. Macosko and L. E. Scriven, "Spin Coating of a PMMA/Chlorobenzene Solution," *Journal of the Electrochemical Society*, Vol. 138, No. 1 (Jan., 1991) pp. 317-320.

5.16. S. A. MacDonald, et al., "Airborne Chemical Contamination of a Chemically Amplified Resist," *Advances in Resist Technology and Processing VIII, Proc.*, SPIE Vol. 1466 (1991) pp. 2-12.

5.17. K. R. Dean and R. A. Carpio, "Contamination of Positive Deep-UV Photoresists," *OCG Microlithography Seminar Interface '94, Proc*., (1994) pp. 199-212.

5.18. T. Ohfuji, A. G. Timko, O. Nalamasu, and D. R. Stone, "Dissolution Rate Modeling of a Chemically Amplified Positive Resist," *Advances in Resist Technology and Processing X, Proc.*, SPIE Vol. 1925 (1993) pp. 213-226.

5.19. F. P. Incropera and D. P. DeWitt, Fundamentals of Heat and Mass Transfer, 3rd edition, John Wiley & Sons (New York: 1990).

5.20. C. A. Mack, T. Matsuzawa, A. Sekiguchi, Y. Minami, "Resist Metrology for Lithography Simulation, Part 1: Exposure Parameter Measurements," *Metrology, Inspection, and Process Control for Microlithography X, Proc.*, SPIE Vol. 2725 (1996) pp. 34-48.

Chapter 6

Photoresist Bake Effects

Baking a resist may have many purposes, from removing solvent to causing chemical amplification. In addition to the intended results, baking may also cause numerous unintended outcomes. For example, the light sensitive component of the resist may decompose at temperatures typically used to remove solvent. The solvent content of the resist can impact diffusion and amplification rates for a chemically amplified resist. And all aspects of baking will probably affect the dissolution properties of the resist. Baking a photoresist remains one of the most complicated and least understood steps in the lithographic process.

A. Prebake

The purpose of a positive photoresist prebake is to dry the resist after spin coating by removing solvent from the film. However, as with most thermal processing steps, the bake has other effects on the photoresist. When heated to temperatures above about 70ºC, the photoactive compound (PAC) of a diazo-type positive photoresist begins to decompose to a non-photosensitive product.

The initial reaction mechanism is thought to be identical to that of the PAC reaction during ultraviolet exposure [6.1-6.4].

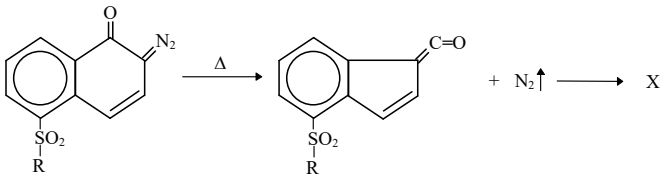

(6.1)

The identity of the product *X* will be discussed in a following section.

To determine the concentration of PAC as a function of prebake time and temperature, consider the first order decomposition reaction,

$$M \xrightarrow{\Delta} X \tag{6.2}$$

where M is the photoactive compound. If we let M'_o be the concentration of PAC before prebake and M_o the concentration of PAC after prebake, simple kinetics tells us that

$$\frac{dM_o}{dt} = -K_T M_o$$

$$M_o = M'_o \exp(-K_T t_b)$$

$$m' = \exp(-K_T t_b) \tag{6.3}$$

where t_b = bake time,
K_T = decomposition rate constant at absolute temperature T, and
m' = M_o/M'_o, the fraction of PAC remaining after the bake.

The dependence of K_T upon temperature may be described by the Arrhenius equation,

$$K_T = A_r \exp(-E_a / RT) \tag{6.4}$$

where A_r = Arrhenius coefficient,
E_a = activation energy, and
R = universal gas constant.

Thus, the two parameters E_a and A_r allow us to know m' as a function of the prebake conditions, provided Arrhenius behavior is followed. In polymer systems, caution must be exercised since bake temperatures near the glass transition temperature sometimes leads to non-Arrhenius behavior. For normal prebakes of typical photoresists, the Arrhenius model appears well founded.

The effect of this decomposition is a change in the chemical makeup of the photoresist. Thus, any parameters which are dependent upon the quantitative composition of the resist are also dependent upon prebake. The most important of these parameters fall into three categories: 1) optical (exposure) parameters such as the resist absorption coefficient, 2) diffusion parameters during post-exposure bake, and 3) development parameters such as the development rates of unexposed and completely exposed resist. A technique will be described to measure E_a and A_r and thus begin to quantify these effects of prebake.

In the model proposed by Dill et al. [6.5], the exposure of a positive photoresist can be characterized by the three parameters A, B, and C. A and B are related to the optical absorption coefficient of the photoresist, α, and C is the overall rate constant of the exposure reaction. More specifically,

$$\alpha = Am + B$$

$$A = (a_M - a_P)M_o \tag{6.5}$$

$$B = a_P M_o + a_R R + a_S S$$

where a_M = molar absorption coefficient of the photoactive compound M,
a_P = molar absorption coefficient of the exposure product P,
a_S = molar absorption coefficient of the solvent S,
a_R = molar absorption coefficient of the resin R,
M_o = the PAC concentration at the start of the exposure (i.e., after prebake), and
$m = M/M_o$, the relative PAC concentration as a result of exposure.

These expressions do not explicitly take into account the effects of prebake on the resist composition. To do so, we can modify equation (6.5) to include absorption by the component *X*.

$$B = a_P M_o + a_R R + a_X X \tag{6.6}$$

where a_X is the molar absorption coefficient of the decomposition product *X* (and the absorption term for the solvent has been neglected for simplicity). The stoichiometry of the decomposition reaction gives

$$X = M'_o - M_o \tag{6.7}$$

Thus,

$$B = a_P M_o + a_R R + a_X(M'_o - M_o) \tag{6.8}$$

Let us consider two cases of interest, no bake (NB) and full bake (FB). When there is no prebake (meaning no decomposition), $M_o = M'_o$ and

$$A_{NB} = (a_M - a_P)M'_o$$

$$B_{NB} = a_P M'_o + a_R R \tag{6.9}$$

We shall define full bake as a prebake which decomposes all PAC. Thus $M_o = 0$ and

$$A_{FB} = 0$$

$$B_{FB} = a_X M'_o + a_R R \tag{6.10}$$

Using these special cases in our general expressions for *A* and *B*, we can show explicitly how these two parameters vary with PAC decomposition:

$$A = A_{NB} m'$$

$$B = B_{FB} - (B_{FB} - B_{NB})m' \tag{6.11}$$

The *A* parameter decreases linearly as decomposition occurs, and *B* typically increases slightly.

The development rate is, of course, dependent on the concentration of PAC in the photoresist. However, the product *X* can also have a large effect on the development rate. Several studies have been performed to determine the composition of the product *X* [6.2-6.4]. The results indicate that there are two possible products and the most common outcome of a prebake decomposition is a mixture of the two. The first product is formed via the reaction (6.12) and is identical to the product of UV exposure.

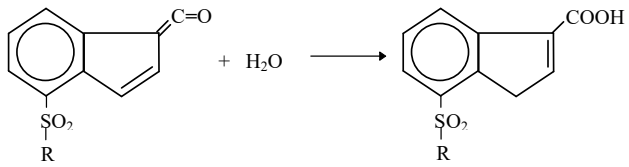

(6.12)

As can be seen, this reaction requires the presence of water. A second reaction, which does not require water, is the esterification of the ketene with the resin.

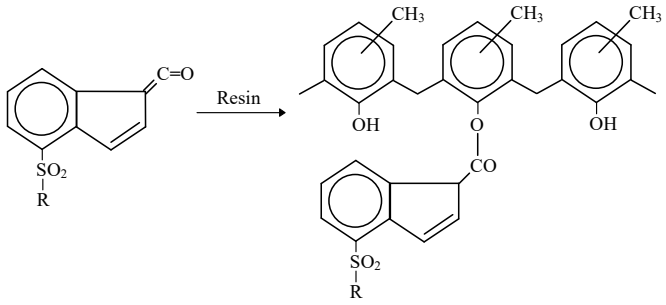

(6.13)

Both possible products have a dramatic effect on dissolution rate. The carboxylic acid is very soluble in developer and enhances dissolution. The formation of carboxylic acid can be thought of as a blanket exposure of the resist. The dissolution rate of unexposed resist (r_{min}) will increase due to the

presence of the carboxylic acid. The dissolution rate of fully exposed resist (r_{max}), however, will not be affected. Since the chemistry of the dissolution process is unchanged, the basic shape of the development rate function will also remain unchanged.

The ester, on the other hand, is very difficult to dissolve in aqueous solutions and thus retards the dissolution process. It will have the effect of decreasing r_{max}, although the effects of ester formation on the full dissolution behavior of a resist are not well known.

If the two mechanisms given in equations (6.12) and (6.13) are taken into account, the rate equation (6.3) will become

$$\frac{dM_o}{dt} = -k_1 M_o - k_2 [H_2O] M_o \tag{6.14}$$

where k_1 and k_2 are the rate constants of equations (6.12) and (6.13), respectively. For a given concentration of water in the resist film this reverts to equation (6.3) where

$$K_T = k_1 + k_2 [H_2O] \tag{6.15}$$

Thus, the relative importance of the two reactions will depend not only on the ratio of the rate constants but on the amount of water in the resist film. The concentration of water is a function of atmospheric conditions during the bake and the past history of the resist coated wafer. Further experimental measurements of development rate as a function of prebake temperature are needed to quantify these effects.

Examining equation (6.11), one can see that the parameter A can be used as a means of measuring m', the fraction of PAC remaining after prebake. Thus, by measuring A as a function of prebake time and temperature, one can determine the activation energy and the corresponding Arrhenius coefficient for the proposed decomposition reaction. Using the technique given by Dill et al. [6.5] and described in the previous chapter, A, B and C can be easily determined by measuring the optical transmittance of a thin photoresist film on a glass substrate while the resist is being exposed.

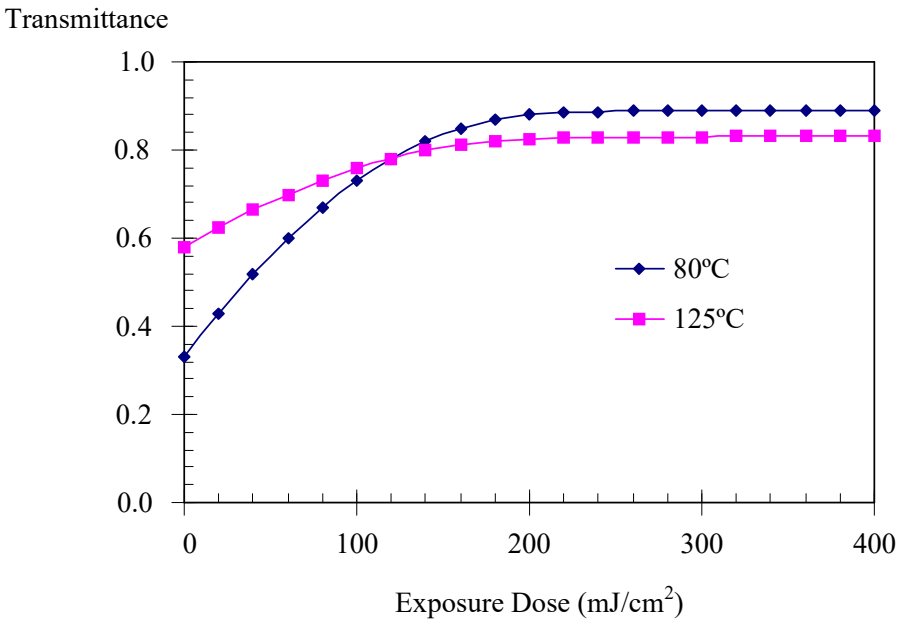

Figure 6-1. Two transmittance curves for Kodak 820 resist at 365nm. The curves are for a convection oven prebake of 30 minutes at the temperatures shown [6.6].

Examples of measured transmittance curves are given in Figure 6-1, where transmittance is plotted versus exposure dose. The different curves represent different prebake temperatures. For every curve, A, B, and C can be calculated. Figure 6-2 shows the variation of the resist parameter A with prebake conditions. According to equations (6.3) and (6.11), this variation should take the form

$$\frac{A}{A_{NB}} = e^{-K_T t_b}$$

$$\ln\left(\frac{A}{A_{NB}}\right) = -K_T t_b \tag{6.17}$$

Thus, a plot of ln(A) versus bake time should give a straight line with a slope equal to -K_T. This plot is shown in Figure 6-3. Knowing K_T as a function of temperature, one can determine the activation energy and Arrhenius coefficient from equation (6.4). One should note that the parameters A_{NB}, B_{NB} and B_{FB} are wavelength dependent, but E_a and A_r are not.

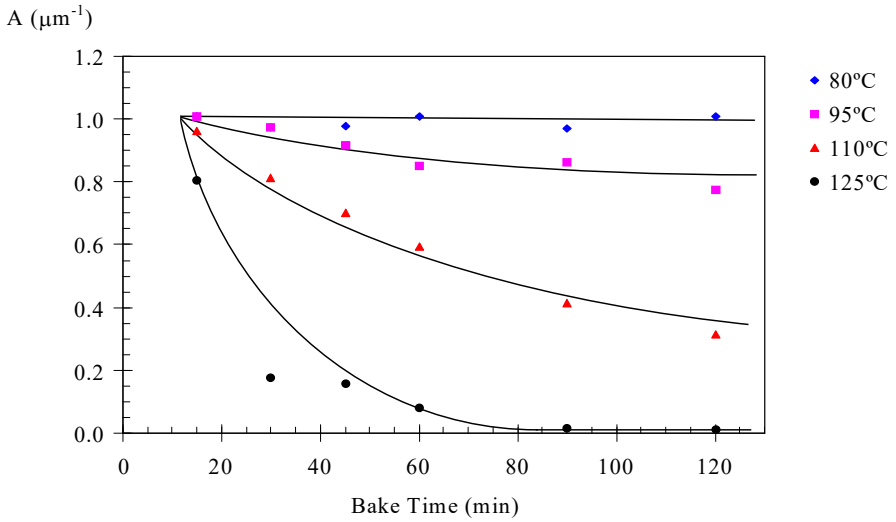

Figure 6-2. The variation of the resist absorption parameter *A* with prebake time and temperature for Kodak 820 resist at 365nm [6.6].

Figure 6-2 shows an anomaly in which there is a lag time before decomposition occurs. This lag time is the time it took the wafer and wafer carrier to reach the temperature of the convection oven. Equation (6.3) can be modified to accommodate this phenomena,

$$m' = e^{-K_T(t_b - t_{wup})} \tag{6.18}$$

where t_{wup} is the warm up time. A lag time of about 11 minutes was observed when convection oven baking a 1/4" thick glass substrate in a wafer carrier. When a 60 mil glass wafer was used without a carrier, the warm-up time was under 5 minutes and could not be measured accurately in this experiment [6.6].

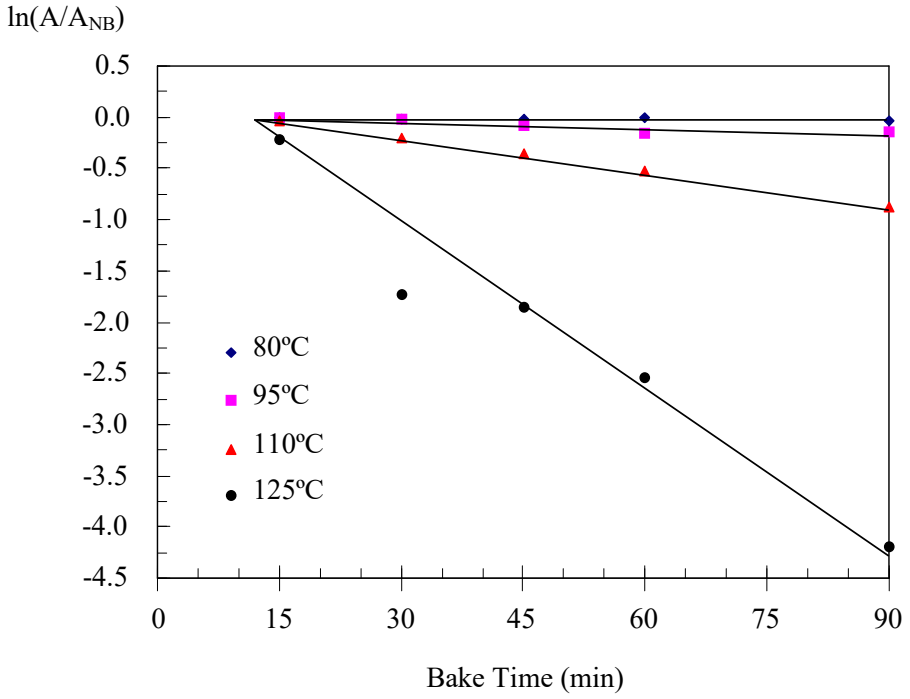

Figure 6-3. Log plot of the resist absorption parameter *A* with prebake time and temperature for Kodak 820 resist at 365 nm [6.6].

Although all the data presented thus far has been for convection oven prebake, the above method of evaluating the effects of prebake can also be applied to hot-plate prebaking. For the data presented in Figure 6-3, the activation energy is 30.3 Kcal/mol and the natural logarithm of the Arrhenius

coefficient (in 1/minutes) is 35.3 [6.6]. Thus, a 100°C, 30 minute convection oven prebake would decompose 11% of the photoactive compound.

B. Post-Exposure Bake

Many attempts have been made to reduce the standing wave effect and thus increase linewidth control and resolution. One particularly useful method is the post-exposure, pre-development bake as described by Walker [6.7]. A 100ºC oven bake for 10 minutes was found to reduce the standing wave ridges on a resist sidewall significantly. This phenomenon can be explained quite simply as the diffusion of photoactive compound (PAC) in the resist during the high temperature bake. A mathematical model which predicts the results of such a post-exposure bake (PEB) is described below.

In general, molecular diffusion is governed by Fick's Second Law of Diffusion, which states (in one dimension)

$$\frac{\partial C_A}{\partial t} = \mathcal{D}\frac{\partial^2 C_A}{\partial t^2} \tag{6.19}$$

where C_A = concentration of species A
$\mathcal{D}$ = diffusion coefficient of A at some temperature T
t = time that the system is at temperature T.

Note that the diffusion coefficient is assumed to be independent of concentration here. This differential equation can be solved given a set of boundary conditions and an initial distribution of A. One possible initial condition is known as the impulse source. At some point x_o there are N moles of substance A and at all other points there is no A. Thus, the concentration at x_o is infinite. Given this initial distribution of A, the solution to equation (6.19) is the Gaussian distribution function,

$$C_A(x) = \frac{N}{\sqrt{2\pi\sigma^2}} e^{-r^2/2\sigma^2} \tag{6.20}$$

where $\sigma = \sqrt{2\mathcal{D}t}$, the diffusion length, and $r = x\text{-}x_o$.

In practice there are no impulse sources. Instead, we can approximate an impulse source as having some concentration C_o over some small distance Δx centered at x_o, with zero concentration outside of this range. An approximate form of equation (6.20) is then

$$C_A(x) \cong \frac{C_o \Delta x}{\sqrt{2\pi\sigma^2}} e^{-r^2/2\sigma^2} \tag{6.21}$$

This solution is fairly accurate if $\Delta x < 3\sigma$. If there are two "impulse" sources located at x_1 and x_2, with initial concentrations C_1 and C_2 each over a range Δx, the concentration of A at x after diffusion is

$$C_A(x) = \left[\frac{C_1}{\sqrt{2\pi\sigma^2}} e^{-r_1^2/2\sigma^2} + \frac{C_2}{\sqrt{2\pi\sigma^2}} e^{-r_2^2/2\sigma^2} \right] \Delta x \tag{6.22}$$

where $r_1 = x\text{-}x_1$ and $r_2 = x\text{-}x_2$.

If there are a number of sources equation (6.22) becomes

$$C_A(x) = \frac{\Delta x}{\sqrt{2\pi\sigma^2}} \sum_n C_n e^{-r_n^2/2\sigma^2} \tag{6.23}$$

Extending the analysis to a continuous initial distribution $C_o(x)$, equation (6.23) becomes

$$C_A(x) = \frac{1}{\sqrt{2\pi\sigma^2}} \int_{-\infty}^{\infty} C_o(x - x') e^{-x'^2/2\sigma^2} \, dx' \tag{6.24}$$

where x' is now the distance from the point x. Equation (6.24) is simply the convolution of two functions.

$$C_A(x) = C_o(x) * f(x) \tag{6.25}$$

where $$f(x) = \frac{1}{\sqrt{2\pi\sigma^2}} e^{-x^2/2\sigma^2}$$

This equation can now be made to accommodate two dimensional diffusion.

$$C_A(x,y) = C_o(x,y) * f(x,y) \tag{6.26}$$

where $$f(x,y) = \frac{1}{2\pi\sigma^2} e^{-r^2/2\sigma^2}$$

$$r = \sqrt{x^2 + y^2}$$

Three-dimensional diffusion can similarly be calculated.

We are now ready to apply equation (6.26) to the diffusion of PAC in a photoresist during a post-exposure bake. For a two-dimensional case, the PAC distribution after exposure can be described by *m(x,z)*, where *m* is the relative PAC concentration. According to equation (6.26) the relative PAC concentration after a post-exposure bake, *m*(x,z)*, is given by

$$m^*(x,z) = \frac{1}{2\pi\sigma^2} \int_{-\infty}^{\infty}\int m(x-x', z-z') e^{-r'^2/2\sigma^2} \, dx'dz' \tag{6.27}$$

In evaluating equation (6.27) it is common to replace the integrals by summations over intervals Δx and Δz. In such a case, the restrictions that $\Delta x < 3\sigma$ and $\Delta z < 3\sigma$ will apply. An alternative solution is to solve the diffusion equation (6.19) directly, for example using a finite difference approach. The boundary conditions typically assume the wafer and air interfaces are impenetrable.

The diffusion model can now be used to simulate the effects of a post-exposure bake. Using PROLITH/2, a simulated resist profile can be generated. By including the model for a post-exposure bake, the profile can be generated showing how the standing wave effect is reduced (Figure 6-4). The only parameter that needs to be specified in equation (6.27) is the diffusion length σ, or equivalently, the diffusion coefficient $\mathcal{D}$ and the bake time *t*. In turn, $\mathcal{D}$ is a function of the bake temperature *T* and, of course, the resist system used. Thus, if the functionality of $\mathcal{D}$ with temperature is known for a given resist system, a

PEB of time t and temperature T can be modeled. A general temperature dependence for the diffusivity $\mathcal{D}$ can be found using the Arrhenius equation (for temperature ranges which do not traverse the glass transition temperature).

$$\mathcal{D} = \mathcal{D}_o e^{-E_a / RT} \tag{6.28}$$

where $\mathcal{D}_o$ = Arrhenius constant (units of nm^2/s),
E_a = activation energy,
R = universal gas constant, and
T = temperature in Kelvin.

Unfortunately, very little work has been done in measuring the diffusivity of photoactive compounds in photoresist. From Walker's work [6.7], one can estimate the values of E_a and $\mathcal{D}_o$ to be about 35 Kcal/mol and 3.2×10^{21} nm^2/s, respectively.

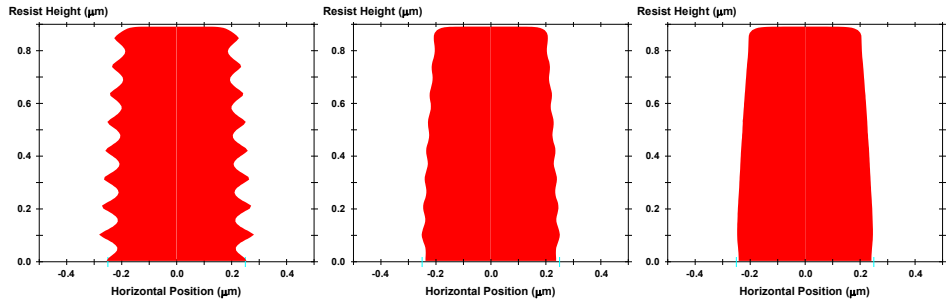

(a) (b) (c)

Figure 6-4. Photoresist profile simulations as a function of the PEB diffusion length: (a) 20nm, (b) 40nm, and (c) 60nm.

References

6.1. F. H. Dill and J. M. Shaw, "Thermal Effects on the Photoresist AZ1350J," *IBM Jour. Res. Dev.*, Vol. 21, No. 3, (May, 1977) pp. 210-218.

6.2. J. M. Shaw, M. A. Frisch and F. H. Dill, "Thermal Analysis of Positive Photoresist Films by Mass Spectrometry," *IBM Jour. Res. Dev*., Vol. 21, No. 3, (May, 1977) pp. 219-226.

6.3. J. M. Koyler, F. Z. Custode and R. L. Ruddell, "Thermal Properties of Positive Photoresist and their relationship to VLSI Processing," *Kodak Interface '79*, (Nov. 1979) pp. 150-165.

6.4. D. W. Johnson, "Thermolysis of Positive Photoresists," *Adv. Resist Tech., Proc*., SPIE Vol. 469, (1984) pp. 72-79.

6.5. F. H. Dill, et al., "Characterization of Positive Photoresists," *IEEE Trans. Electron Devices*, Vol. ED-22, No. 7, (July, 1975) pp. 445-452.

6.6. C. A. Mack and R. T. Carback, "Modeling the Effects of Prebake on Positive Resist Processing," *Kodak Microelectronics Seminar, Proc.*, (1985) pp. 155-158.

6.7. E. J. Walker, "Reduction of Photoresist Standing-Wave Effects by Post-Exposure Bake," *IEEE Trans. Electron Devices*., Vol. ED- 22, No. 7 (July, 1975) pp. 464-466.

Chapter 7

Photoresist Development

An overall resist processing model requires a mathematical representation of the development process. Many previous attempts have taken the form of empirical fits to development rate data as a function of exposure [7.1,7.2]. The model formulated below begins on a more fundamental level, with a postulated reaction mechanism which then leads to a development rate equation [7.3]. The rate constants involved can be determined by comparison with experimental data. An enhanced kinetic model with a second mechanism for dissolution inhibition is also presented [7.4]. Deviations from the expected development rates have been reported under certain conditions at the surface of the resist. This effect, called surface induction or surface inhibition, can be related empirically to the expected development rate, i.e., to the bulk development rate as predicted by a kinetic model.

Unfortunately, fundamental experimental evidence of the exact mechanism of photoresist development is lacking. The model presented below is reasonable, and the resulting rate equation has been shown to describe actual development rates extremely well. However, faith in the exact details of the mechanism is limited by this dearth of fundamental studies.

A. Kinetic Development Model

In order to derive an analytical development rate expression, a kinetic model of the development process will be used. This approach involves proposing a reasonable mechanism for the development reaction and then applying standard kinetics to this mechanism in order to derive a rate equation. We shall assume that the development of a diazo-type positive photoresist involves three processes: diffusion of developer from the bulk solution to the surface of the resist, reaction of the developer with the resist, and diffusion of the product back into the solution. For this analysis, we shall assume that the last step, diffusion of the dissolved resist into solution, occurs very quickly so that this step may be ignored. Let us now look at the first two steps in the proposed mechanism. The diffusion of developer to the resist surface can be described with the simple diffusion rate equation, given approximately by

$$r_D = k_D\left(D - D_S\right) \tag{7.1}$$

where r_D is the rate of diffusion of the developer to the resist surface, D is the bulk developer concentration, D_S is the developer concentration at the resist surface, and k_D is the rate constant.

We shall now propose a mechanism for the reaction of developer with the resist. The resist is composed of large macromolecules of resin R along with a photoactive compound M, which converts to product P upon exposure to UV light. The resin is somewhat soluble in the developer solution, but the presence of the PAC (photoactive compound) acts as an inhibitor to dissolution, making the development rate very slow. The product P, however, is very soluble in developer, enhancing the dissolution rate of the resin. Let us assume that n molecules of product P react with the developer to dissolve a resin molecule. The rate of the reaction is

$$r_R = k_R D_S P^n \tag{7.2}$$

where r_R is the rate of reaction of the developer with the resist and k_R is the rate constant. (Note that the mechanism shown in equation (7.2) is the same as the "polyphotolysis" model described by Trefonas and Daniels [7.5].) From the stoichiometry of the exposure reaction,

$$P = M_o - M \tag{7.3}$$

where M_o is the initial PAC concentration (i.e., before exposure).

The two steps outlined above are in series, i.e., one reaction follows the other. Thus, the two steps will come to a steady state such that

$$r_R = r_D = r \tag{7.4}$$

Equating the rate equations, one can solve for D_S and eliminate it from the overall rate equation, giving

$$r = \frac{k_D k_R D P^n}{k_D + k_R P^n} \tag{7.5}$$

Using equation (7.3) and letting $m = M/M_o$, the relative PAC concentration, equation (7.5) becomes

$$r = \frac{k_D D(1-m)^n}{k_D / k_R M_o^n + (1-m)^n} \tag{7.6}$$

When $m = 1$ (resist unexposed), the rate is zero. When $m = 0$ (resist completely exposed), the rate is equal to r_{max} where

$$r_{\max} = \frac{k_D D}{k_D / k_R M_o^n + 1} \tag{7.7}$$

If we define a constant a such that

$$a = k_D / k_R M_o^n \tag{7.8}$$

the rate equation becomes

$$r = r_{\max} \frac{(a+1)(1-m)^n}{a + (1-m)^n} \tag{7.9}$$

Note that the simplifying constant *a* describes the rate constant of diffusion relative to the surface reaction rate constant. A large value of *a* will mean that diffusion is very fast, and thus less important, compared to the fastest surface reaction (for completely exposed resist).

There are three constants that must be determined experimentally, *a*, *n*, and r_{max}. The constant *a* can be put in a more physically meaningful form as follows. A characteristic of some experimental rate data is an inflection point in the rate curve at about *m* = 0.2-0.7. The point of inflection can be calculated by letting

$$\frac{d^2 r}{dm^2} = 0$$

giving

$$a = \frac{(n+1)}{(n-1)}\left(1 - m_{TH}\right)^n \tag{7.10}$$

where m_{TH} is the value of *m* at the inflection point, called the threshold PAC concentration.

This model does not take into account the finite dissolution rate of unexposed resist (r_{min}). One approach is simply to add this term to equation (7.9), giving

$$r = r_{\max}\frac{(a+1)(1-m)^n}{a+(1-m)^n} + r_{\min} \tag{7.11}$$

This approach assumes that the mechanism of development of the unexposed resist is independent of the above-proposed development mechanism. In other words, there is a finite dissolution of resist that occurs by a mechanism that is independent of the presence of exposed PAC. Note that the addition of the r_{min} term means that the true maximum development rate is actually $r_{max} + r_{min}$. In most cases $r_{max} \gg r_{min}$ and the difference is negligible.

Consider the case when the diffusion rate constant is large compared to the surface reaction rate constant. If $a \gg 1$, the development rate equation (7.11) will become

$$r = r_{\max}(1-m)^n + r_{\min} \tag{7.12}$$

The interpretation of a as a function of the threshold PAC concentration m_{TH} given by equation (7.10) means that a very large a would correspond to a large negative value of m_{TH}. In other words, if the surface reaction is very slow compared to the mass transport of developer to the surface there will be no inflection point in the development rate data and equation (7.12) will apply. It is quite apparent that equation (7.12) could be derived directly from equation (7.2) if the diffusion step were ignored.

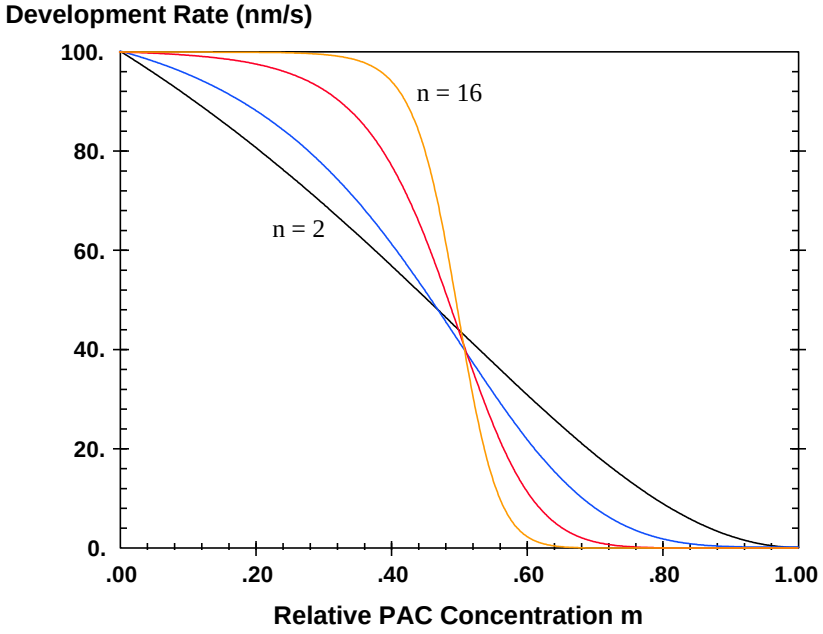

Figure 7-1. Development rate plot of the Original Mack model as a function of the dissolution selectivity parameter (r_{max} = 100 nm/s, r_{min} = 0.1 nm/s, m_{TH} = 0.5, and n = 2, 4, 8, and 16).

Equation (7.11) is called the Original Mack development model in PROLITH/2. Figure 7-1 shows some plots of this model for different values of n. The behavior of the dissolution rate with increasing n values is to make the rate function more "selective" between resist exposed above m_{TH} and resist exposed below m_{TH}. For this reason, n is called the dissolution selectivity parameter. Also from this behavior, the interpretation of m_{TH} as a "threshold" concentration becomes quite evident.

B. Enhanced Kinetic Development Model

The previous kinetic model is based on the principle of dissolution enhancement. The carboxylic acid enhances the dissolution rate of the resin/PAC mixture. In reality this is a simplification -- there are really two mechanisms at work. The PAC acts to inhibit dissolution of the resin while the acid acts to enhance dissolution. Thus, a development rate expression could reflect both of these mechanisms. A new model, call the enhanced kinetic model, was proposed to include both effects [7.4]:

$$R = R_{resin} \frac{1 + k_{enh}(1 - m)^n}{1 + k_{inh}(m)^l} \tag{7.13}$$

where k_{enh} is the rate constant for the enhancement mechanism, n is the enhancement reaction order, k_{inh} is the rate constant for the inhibition mechanism, l is the inhibition reaction order, and R_{resin} is the development rate of the resin alone.

For no exposure, m=1 and the development rate is at its minimum. From equation (7.13),

$$R_{min} = \frac{R_{resin}}{1 + k_{inh}} \tag{7.14}$$

Similarly, when m=0, corresponding to complete exposure, the development is at its maximum.

$$R_{max} = R_{resin}\ (1 + k_{enh}) \tag{7.15}$$

Thus, the development rate expression can be characterized by five parameters: R_{max}, R_{min}, R_{resin}, n, and l.

Obviously, the enhanced kinetic model for resist dissolution is a superset of the original kinetic model. If the inhibition mechanism is not important, then $k_{inh} = 0$. For this case, equation (7.13) is identical to equation (7.12) when

$$R_{min} = R_{resin}, \quad R_{max} = R_{resin}\, k_{enh} \tag{7.16}$$

The enhanced kinetic model of equation (7.13) assumes that mass transport of developer to the resist surface is not significant. Of course, a simple diffusion of developer can be added to this mechanism as was done above with the original kinetic model. Equation (7.13) is called the Enhanced Mack development model in PROLITH/2. Figure 7-2 shows several plots of the Enahnced Mack model.

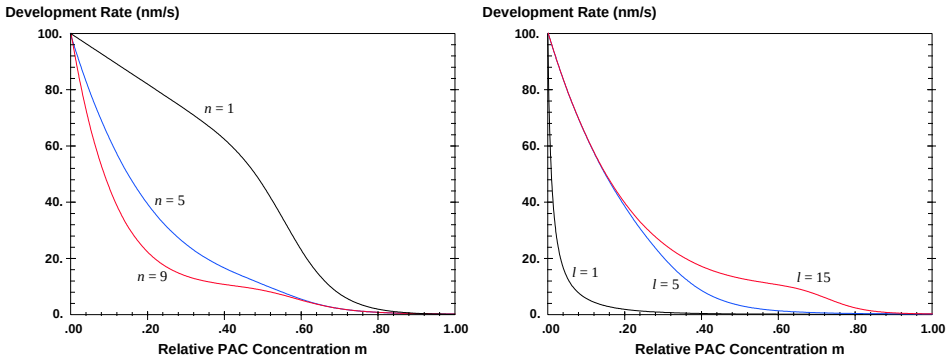

Figure 7-2. Plots of the Enhanced Mack development model for r_{max} = 100 nm/s, r_{resin} = 10 nm/s, r_{min} = 0.1 nm/s and (a) l = 9, and (b) n = 5.

C. Surface Inhibition

The kinetic models given above predict the development rate of the resist as a function of the photoactive compound concentration remaining after the resist has been exposed to UV light. There are, however, other parameters that are known to affect the development rate, but which were not included in this model. The most notable deviation from the kinetic theory is the surface inhibition effect. The inhibition, or surface induction, effect is a decrease in the expected development rate at the surface of the resist [7.6-7.8]. Thus, this effect is a function of the depth into the resist and requires a new description of development rate.

Several factors have been found to contribute to the surface inhibition effect. Baking of the photoresist can produce surface inhibition and two possible mechanisms are thought to be likely causes. One possibility is an oxidation of the resist at the resist surface, resulting in reduced development rate of the oxidized film [7.6-7.8]. Alternatively, the induction effect may be the result of reduced solvent content near the resist surface, which also results from baking the resist [7.9]. Both mechanisms could be contributing to the surface inhibition. Finally, surface inhibition can be induced with the use of surfactants in the developer.

An empirical model can be used to describe the positional dependence of the development rate. If we assume that the development rate near the surface of the resist exponentially approaches the bulk development rate, the rate as a function of depth, *r(z)*, is

$$r(z) = r_B\left(1-\left(1-r_o\right)e^{-z/\delta}\right) \tag{7.17}$$

where r_B is the bulk development rate as given by equation (7.11) or (7.13), r_o is the development rate at the surface of the resist relative to r_B, and δ is the depth of the surface inhibition layer. The induction effect has been found to take place over a depth of about 100 nm [7.6,7.8].

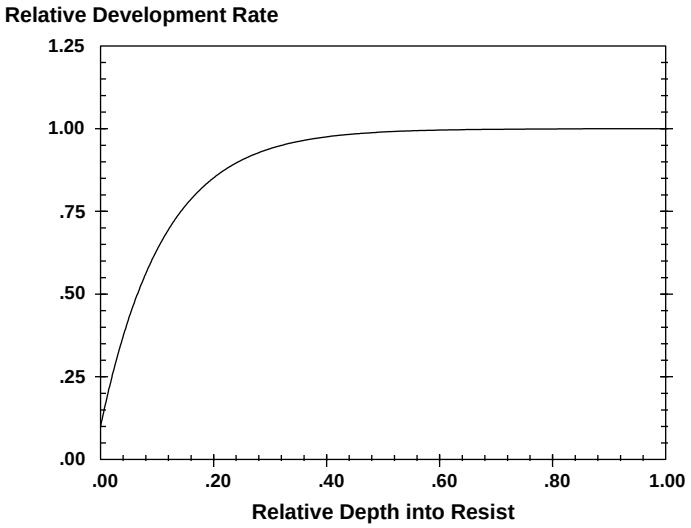

Figure 7-3. Example surface inhibition with r_o = 0.1 and δ = 100 nm.

References

7.1. F. H. Dill, et al., "Characterization of Positive Photoresists," *IEEE Trans. Electron Devices*, Vol. ED-22, No. 7, (July, 1975) pp. 445-452.

7.2. M. A. Narasimham and J. B. Lounsbury, "Dissolution Characterization of Some Positive Photoresist Systems," *Semiconductor Microlithography II, Proc.*, SPIE Vol. 100, (1977) pp. 57-64.

7.3. C. A. Mack, "Development of Positive Photoresist," *Jour. Electrochemical Society*, Vol. 134, No. 1 (Jan. 1987) pp. 148-152.

7.4. C. A. Mack, "New Kinetic Model for Resist Dissolution," *Jour. Electrochemical Society*, Vol. 139, No. 4 (Apr. 1992) pp. L35-L37.

7.5. P. Trefonas and B. K. Daniels, "New Principle for Image Enhancement in Single Layer Positive Photoresists," *Advances in Resist Technology and Processing IV, Proc.*, SPIE Vol. 771 (1987) pp. 194-210.

7.6. F. H. Dill and J. M. Shaw, "Thermal Effects on the Photoresist AZ1350J," *IBM Jour. Res. Dev.*, Vol. 21, No. 3, (May, 1977) pp. 210-218.

7.7. T. R. Pampalone, "Novolac Resins Used in Positive Resist Systems," *Solid State Tech.*, Vol. 27, No. 6 (June, 1984) pp. 115-120.

7.8. D. J. Kim, W. G. Oldham and A. R. Neureuther, "Development of Positive Photoresist," *IEEE Trans. Electron Dev.*, Vol. ED-31, No. 12, (Dec., 1984) pp. 1730-1735.

7.9. C. A. Mack, D. P. DeWitt, B. K. Tsai, and G. Yetter, "Modeling of Solvent Evaporation Effects for Hot Plate Baking of Photoresist," *Advances in Resist Technology and Processing XI, Proc.*, SPIE Vol. 2195 (1994) pp. 584-595.

Chapter 8

Linewidth Measurement

A cross-section of a photoresist profile has, in general, a very complicated two-dimensional shape (Figure 8-1). In order to compare the shapes of two different profiles, one must find a convenient description for the shapes of the profiles which somehow reflects their salient qualities. The most common description is to model the resist profile as a trapezoid. Thus, three numbers can be used to describe the profile: the width of the base of the trapezoid (linewidth, w), its height (profile thickness, D), and the angle that the side makes with the base (sidewall angle, θ). Obviously, to describe such a complicated shape as a resist profile with just three numbers is a great, though necessary, simplification. The key to success is to pick a method of fitting a trapezoid to the profile which preserves the important features of the profile, is numerically practical, and as a result is not overly sensitive to slight changes in the profile. As will be shown below, the method of defining the "best fit" trapezoid will affect the sensitivity of the measured linewidth to profile shape. Such sensitivity is not particular to PROLITH/2, but is a fundamental behavior in any CD measurement system.

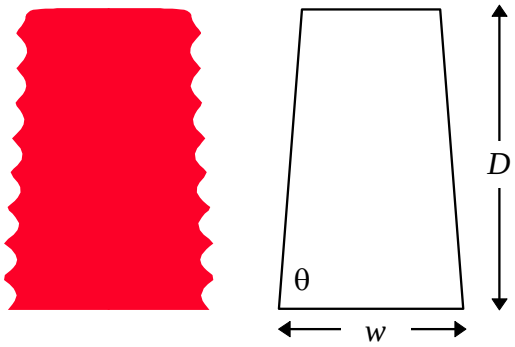

Figure 8-1. Typical photoresist profile and its corresponding “best fit” trapezoid.

PROLITH/2 offers several solutions to the critical dimension (CD) metrology problem of fitting a trapezoid to the resist profile. Each of the three methods available in PROLITH/2 has advantages and disadvantages, depending on the application. The three methods will be compared at the end of this chapter. First, however, a special pre-processing algorithm for the resist profile will be described.

A. Creating The Weighted Profile

PROLITH/2 uses a unique algorithm for analyzing the resist profile. This algorithm, called the *linear weight method*, was created specifically for this application. The goal of this method is to try to mimic the behavior of a top-down linewidth measurement system. The first step is to convert the profile into a “weighted” profile as follows: at any given *x*-position (i.e., along the horizontal axis), determine the “weight” of the photoresist above it. The weight is defined as the total thickness of resist along a vertical line at *x*. Figure 8-2 shows a typical example. The weight at this *x* position would be the sum of the lengths of the line segments which are within the resist profile. This process is then repeated for many x positions. As can be seen, the original profile is complicated and multi-valued whereas the weighted profile is smooth and single-valued.

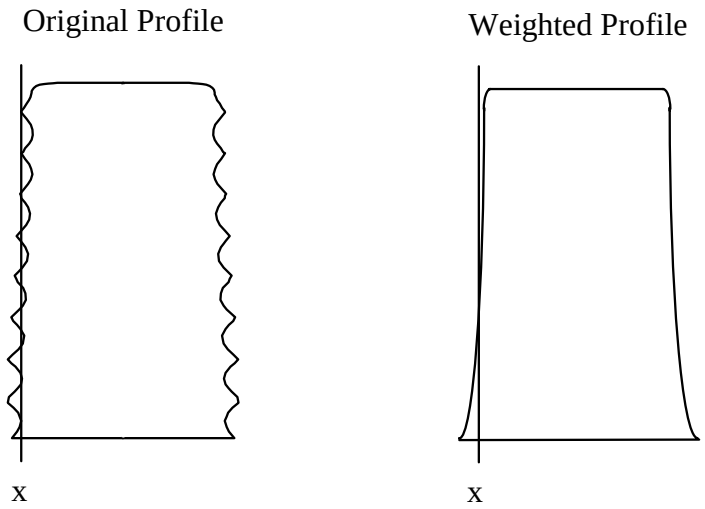

Figure 8-2. Determining the weighted resist profile.

B. Determining Resist Loss and Sidewall Angle

Besides the width of the feature (which will be discussed in the next section), the trapezoid model of the resist profile provides two other parameters: the sidewall angle and the resist loss (the height of the profile, *D*, subtracted from the original resist thickness). In PROLITH/2, the resist loss is defined by setting *D* equal to the tallest part of the resist profile. Note that this definition of *D* is the same for the weighted profile as for the original profile. The sidewall angle is determined using the weighted profile.

Because the weighted profile has smoothed out any standing waves that may be along the edge of the original profile, the weighted profile is ideal for measuring the sidewall angle. A straight line is fitted through the edge of the profile using only the portion of the edge which is between 0.2*D* and 0.8*D* in height. Thus, profile anomalies such as top rounding or a bottom foot in general do not impact the calculation of sidewall angle. The sidewall angle is defined as the angle that this line makes with the substrate.

C. Determining Feature Width

PROLITH/2 can use three different methods for measuring feature width: the standard, raw threshold, and weighted threshold methods.

1. Standard Method

The standard method for linewidth measurement gets its name not from being the preferred method but from being the first method used by PROLITH/2. The first version of PROLITH/2 only used the standard method (the weighted threshold method was added in v2.1 and the raw threshold method was added in v5.0). As will be seen below, the standard method can suffer from some serious flaws and should be used with caution.

The standard method uses the straight line fit to the side of the weighted profile that was used to determine sidewall angle. The intersection of this line with the substrate gives the width of the feature. Thus, the standard method gives the best-fit trapezoid through the middle 60% of the weighted profile and then defines the linewidth as the bottom width of this trapezoid.

2. Raw Threshold Method

The raw threshold method is meant to mimic a cross-sectional measurement. Using the original resist profile, the width of the feature is defined as the width of the original resist profile at a specific height. The height is adjustable and defined by the user, specified as a percentage of *D*. Thus a 5% threshold value means a measurement very close to the bottom of the resist profile. Figure 8-3(a) illustrates the raw threshold method.

3. Weighted Threshold Method

The weighted threshold method works like the raw threshold method except using the weighted resist profile. Thus, the width of the trapezoid is adjusted to match the width of the weighted profile at a given threshold resist thickness. For example, with a threshold of 20%, the trapezoid will cross the weighted profile at a thickness of 20% up from the bottom. Thus, the weighted threshold method can be used to emphasize the importance of one part of the profile. Figure 8-3(b) illustrates this method of linewidth measurement.

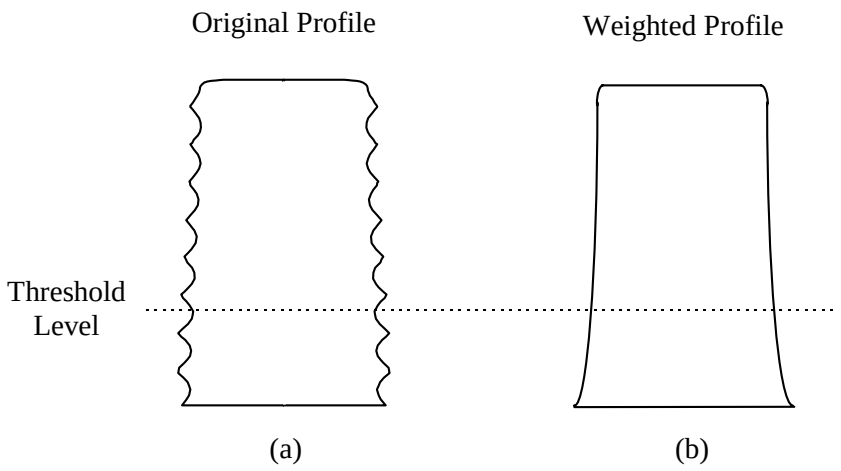

Figure 8-3. Measuring linewidth using (a) the raw threshold method and (b) the weighted threshold method.

In some sense, the weighted threshold method behaves like a top down measurement. Looking at a profile "top-down" would produce a view which blurs or smoothes out standing waves, much like the weighted profile does. Thus, the weighted threshold method is preferred when trying to match simulation to top-down measured data.

D. Comparing Linewidth Measurement Methods

The various linewidth determination methods deviate from one another when the shape of the resist profile begins to deviate from the general trapezoidal shape. Figure 8-4 shows two resist profiles at the extremes of focus (note that in this case the weighted and original profiles are the same). Using a 10% threshold, the linewidths of these two profiles are the same. Using a 50% threshold, however, shows profile (a) to be 20% wider than profile (b). The standard linewidth method, on the other hand, shows profile (a) to be 10% wider than profile (b). Finally, a 1% threshold gives the opposite result, with profile (a) 10% smaller than profile (b).

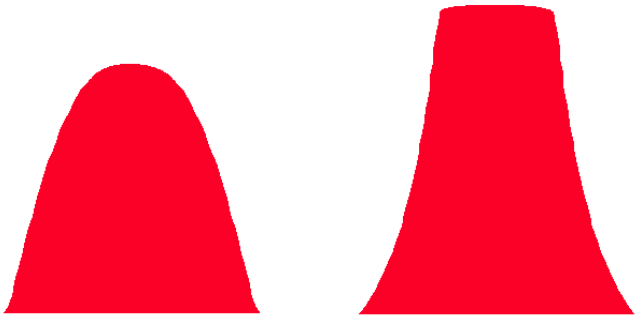

Focus below the resist (a)

Focus above the resist (b)

Figure 8-4. Resist profiles at the extremes of focus.

The profiles of Figure 8-4 show the problem with the standard method. A straight line fit through the sidewall of profile (a) would intersect the base at position wider than the actual resist edge. On the other hand, the straight line fit through profile (b) intersects the base at a position narrower than the actual resist edge. Thus, the standard model seems to give erroneous results whenever the resist profile shows large curvature along the sidewalls.

The effect of changing profile shape on the measured linewidth is further illustrated in Figure 8-5 which shows CD versus focus for the standard, 2%, and 50% weighted threshold CD measurement methods for *one* set of resist profiles. Obviously, the method of measuring the resist profile has a large impact on the linewidth (a single number representing the entire profile) and linewidth trends such as that shown in Figure 8-5. It is important to note that sensitivity of the measured linewidth to profile shape is not particular to PROLITH/2, but is present in any CD measurement system. Fundamentally, this is the result of using the trapezoid model for complicated resist profiles.

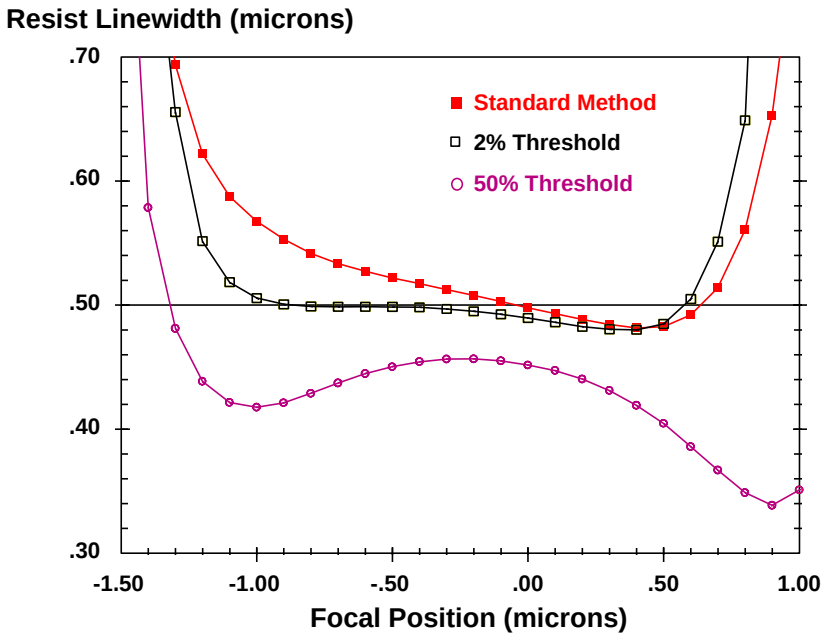

Figure 8-5. Effect of resist profile shape on linewidth measurement in PROLITH/2.

The raw threshold and weighted threshold methods differ whenever there are significant standing waves present on the resist profile. The raw threshold method is overly sensitive to standing waves. A slight change in the raw threshold value can move the measurement point from a minimum to a maximum point of a standing wave ridge. Consider a profile such as the one shown in Figure 8-3(a). If the width of this profile is measured using different raw threshold values, the result looks like that of Figure 8-6(a). The measured linewidth varies greatly with only a small change in threshold value. The weighted threshold method, on the other hand, smoothes out these variations to give the general trend of a smaller width at the top (Figure 8-6(b)).

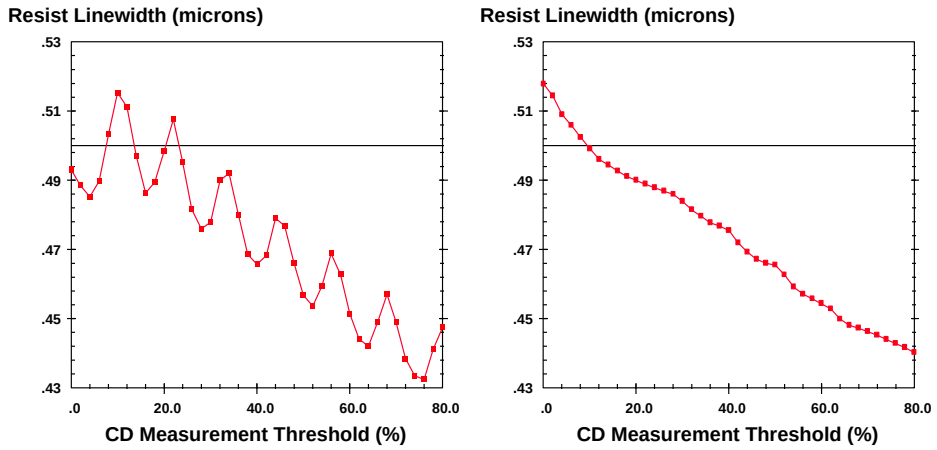

Figure 8-6. Effect of the threshold value on the resulting linewidth for (a) the raw threshold method, and (b) the weighted threshold method when the profile exhibits standing waves.

The weighted profile measurement method suffers from the same drawback as a top-down measurement system. If the resist profile is retrograde (for example, a resist line which is wider at the top than the bottom), a top-down measurement system attempting to measure the bottom of the profile will in fact measure the top. Likewise, the creation of weighted profile will turn a retrograde profile into a normal (non-retrograde) profile, making a measurement of the top appear to be a measurement of the bottom.

As a general rule, the standard method can be used whenever the resist profile is not too curved along the edges. The raw threshold method behaves like a cross-sectional SEM measurement, but is sensitive to standing waves. The weighted threshold method behaves like a top down measurement, and thus has the potential drawback of misinterpreting retrograde profiles.

Obviously, it is difficult to compare resist profiles when the shapes of the profiles are changing. It is very important to use the linewidth method (and proper threshold value, if necessary) which is physically the most significant for

the problems being studied. If the bottom of the resist profile is most important, one of the threshold methods with a small (e.g., 5%) threshold is recommended. It is also possible to "calibrate" PROLITH/2 to a linewidth measurement system. By adjusting the threshold value for CD measurement in PROLITH/2, results comparable to actual measurements can be obtained.

Chapter 9

Lumped Parameter Model

Typically, lithography models make every attempt to describe physical phenomena as accurately as possible. However, in some circumstances speed is more important than accuracy. If a model is reasonably close to correct and is very fast, many interesting applications are possible. With this trade-off in mind, the Lumped Parameter Model (LPM) was developed [9.1-9.3].

A. Development Rate Model

The mathematical description of the resist process incorporated in the lumped parameter model uses a simple photographic model relating development time to exposure, while the aerial image simulation uses the normal PROLITH models as described in Chapter 2. A very simple development rate model is used based on the assumption of a constant contrast. Before proceeding, however, let us define a few terms needed for the derivations that follow. Let E be the nominal exposure energy (i.e., the intensity in a large clear area times the exposure time), $I(x)$ the normalized image intensity, and $I(z)$ the relative intensity variation with depth into the resist. From these definitions, the exposure energy as a function of position within the resist (E_{xz}) is just $EI(x)I(z)$

where x=0 is the center of the mask feature and z=0 is the top of a resist of thickness D. Defining logarithmic versions of these quantities,

$$\varepsilon = \ln[E], \quad i(x) = \ln[I(x)], \quad i(z) = \ln[I(z)] \tag{9.1}$$

and the logarithm of the energy within the resist is

$$\ln[E_{xz}] = \varepsilon + i(x) + i(z) \tag{9.2}$$

The photoresist contrast (γ) is defined theoretically as [9.4]

$$\gamma \equiv \frac{d \ln r}{d \ln E_{xz}} \tag{9.3}$$

where r is the resulting development rate at position (x,z) from an exposure of E_{xz}. Note that the base e definition of contrast is used here. If the contrast is assumed constant over the range of energies of interest, equation (9.3) can be integrated to give a very simple expression for development rate. In order to evaluate the constant of integration, let us pick a convenient point of evaluation. For the standard dose-to-clear measurement, a large clear area is exposed and developed. Let E_o (the dose-to-clear) be the energy required to just clear the photoresist in the allotted development time, t_{dev}, and let r_o be the development rate which results from an exposure of this amount. Carrying out the integration gives

$$r(x,z) = r_o e^{\gamma(\varepsilon + i(x) + i(z) - \varepsilon_o)} = r_o \left[\frac{E_{xz}}{E_o} \right]^{\gamma} \tag{9.4}$$

where

$$\varepsilon_o = \ln[E_0]$$

As an example of the use of the above development rate expression and to further illustrate the relationship between r_o and the dose to clear, consider again the standard dose-to-clear experiment where a large clear area is exposed and the thickness of photoresist remaining is measured. The definition of development rate,

$$r = \frac{dz}{dt} \tag{9.5}$$

can be integrated over the development time. If $\varepsilon = \varepsilon_o$, the thickness remaining is by definition zero, so that

$$t_{dev} = \int_0^D \frac{dz}{r} = \frac{1}{r_o}\int_0^D e^{-\gamma i(z)}\, dz \tag{9.6}$$

where *i(x)* is zero for an open frame exposure. Based on this equation, one can now define an effective resist thickness, D_{eff}, which will be very useful in the derivation of the lumped parameter model which follows.

$$D_{eff} \equiv r(z = D)t_{dev} = r_o t_{dev}\, e^{\gamma i(D)} = e^{\gamma i(D)} \int_0^D e^{-\gamma i(z)}\, dz = \int_0^D \left[\frac{I(z)}{I(D)}\right]^{-\gamma} dz \tag{9.7}$$

As an example, the effective resist thickness can be calculated for the case when only absorption causes a variation in intensity with depth into the resist. For such a case, *I(z)* will decay exponentially with an absorption coefficient α, and equation (9.7) can be evaluated to give

$$D_{eff} = \frac{1}{\alpha\gamma}\left(1 - e^{-\alpha\gamma D}\right) \tag{9.8}$$

If the resist is only slightly absorbing so that $\alpha\gamma D \ll 1$, the exponential can be approximated by the first few terms in its Taylor series expansion.

$$D_{eff} \approx D\left(1 - \frac{\alpha\gamma D}{2}\right) \tag{9.9}$$

Thus, the effect of absorption is to make the resist seem thinner to the development process. The effective resist thickness can be thought of as the following: if an "effective" resist had a constant development rate equal to the rate of the real resist at the bottom, the "effective" resist thickness would be the amount of this effective resist which cleared in the same time as the real resist.

For the case of absorption, the development rate is smaller at the bottom so that a thinner effective resist is required to clear in the same time.

B. Segmented Development

Equation (9.4) is an extremely simple-minded model relating development rate to exposure energy based on the assumption of a constant resist contrast. In order to use this expression, we will develop a phenomenological explanation for the development process. This explanation will be based on the assumption that development occurs in two steps: a vertical development to a depth z, followed by a lateral development to position x (measured from the center of the mask feature) [9.5] as shown in Figure 9-1.

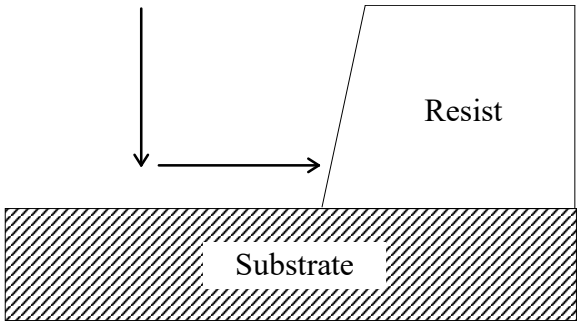

Figure 9-1. Illustration of segmented development: development proceeds first vertically, then horizontally, to the final resist sidewall.

A development ray, which traces out the path of development, starts at the point $(x_o,0)$ and proceeds vertically until a depth z is reached such that the resist to the side of the ray has been exposed more than the resist below the ray (i.e., $E(x_o,z+\Delta z) < E(x_o+\Delta x,z)$). At this point the development will begin horizontally. The time needed to develop in both vertical and horizontal directions, t_z and t_x respectively, can be computed from equation (9.4). The development time per unit thickness of resist is just the reciprocal of the development rate.

$$\frac{1}{r(x,z)} = \tau(x,z) = \tau_o e^{-\gamma(\varepsilon+i(x)+i(z))} \tag{9.10}$$

where

$$\tau_o = \frac{1}{r_o} e^{-\gamma \varepsilon_o} \tag{9.11}$$

The time needed to develop to a depth z is given by

$$t_z = \tau_o e^{-\gamma\varepsilon} e^{-\gamma i(x_o)} \int_0^z e^{-\gamma i(z')} dz' \tag{9.12}$$

Similarly, the horizontal development time is

$$t_x = \tau_o e^{-\gamma\varepsilon} e^{-\gamma i(z)} \int_{x_o}^x e^{-\gamma i(x')} dx' \tag{9.13}$$

The sum of these two times must equal the total development time.

$$t_{dev} = \tau_o e^{-\gamma\varepsilon} \left[e^{-\gamma i(x_o)} \int_0^z e^{-\gamma i(z')} dz' + e^{-\gamma i(z)} \int_{x_o}^x e^{-\gamma i(x')} dx' \right] \tag{9.14}$$

C. Derivation of the Lumped Parameter Model

The above equation can be used to derive some interesting properties of the resist profile. For example, how would a small change in exposure energy $\Delta\varepsilon$ affect the position of the resist profile x? A change in overall exposure energy will not change the depth at which the development ray changes direction for our simple segmented development model. Thus, the depth z in equation (9.14) is constant. Differentiating equation (9.14) with respect to log-exposure energy, the following equation can be derived:

$$\left.\frac{dx}{d\varepsilon}\right|_z = \frac{\gamma\, t_{dev}}{\tau(x,z)} = \gamma\, t_{dev}\, r(x,z) \tag{9.15}$$

Since the x position of the development ray endpoint is just one half of the linewidth, equation (9.15) defines a change in critical dimension (CD) with exposure energy. To put this expression in a more useful form, take the log of both sides and use the development rate expression (9.4) to give

$$\ln\left(\frac{dx}{d\varepsilon}\right) = \ln\left(\gamma\, t_{dev}\, r_o\right) + \gamma\left(\varepsilon + i(x) + i(z) - \varepsilon_o\right) \tag{9.16}$$

Rearranging,

$$\varepsilon = \varepsilon_o - i(x) - i(z) + \frac{1}{\gamma}\ln\left(\frac{dx}{d\varepsilon}\right) - \frac{1}{\gamma}\ln\left(\gamma\, t_{dev}\, r_o\right) \tag{9.17}$$

where ε is the (log) energy needed to expose a feature of width 2x. Equation (9.17) is the differential form of the lumped parameter model and relates the CD versus log-exposure curve and its slope to the image intensity. Although a more useful form of this equation will be given below, some valuable insight can be gained by examining equation (9.17). In the limit of very large γ, one can see that the CD versus exposure curve (i.e., the term ε) becomes controlled only by the aerial image. Thus, exposure latitude becomes *image limited*. For small γ, the other terms become significant and the exposure latitude is *process limited*. Obviously, an image limited exposure latitude represents the best possible case.

A second form of the LPM can also be obtained in the following manner. Applying the definition of development rate to equation (9.15) or, alternatively, solving for the slope in equation (9.17), yields

$$\frac{d\varepsilon}{dx} = \frac{1}{\gamma\, t_{dev} r_o} e^{-\gamma\left(\varepsilon + i(x) + i(z) - \varepsilon_o\right)} \tag{9.18}$$

Before proceeding, let us introduce a slight change in notation that will make the role of the variable ε more clear. As originally defined, ε is just the nominal exposure energy. In equations (9.16) through (9.18), it takes the added meaning

as the nominal energy which gives a linewidth of 2*x*. To emphasize this meaning, we will replace ε by ε(*x*) where the interpretation is not a variation of energy with *x*, but rather a variation of *x* (linewidth) with energy. Using this notation, the energy to just clear the resist can be related to the energy which gives zero linewidth, ε(0).

$$\varepsilon_o = \varepsilon(0) + i(x = 0) \tag{9.19}$$

where $x_o = 0$ has been assumed for simplicity. Using this relation in equation (9.18),

$$\frac{d\varepsilon}{dx} = \frac{1}{\gamma t_{dev} r_o} e^{-\gamma i(z)} e^{\gamma(\varepsilon(0)-\varepsilon(x))} e^{\gamma(i(0)-i(x))} \tag{9.20}$$

Invoking the definitions of the logarithmic quantities,

$$\frac{dE}{dx} = \frac{E(x)}{\gamma D_{eff}} \left[\frac{E(0)I(0)}{E(x)I(x)} \right]^{\gamma} \tag{9.21}$$

where equation (9.7) has been used and the linewidth is assumed to be measured at the resist bottom (i.e., $z = D$). Equation (9.21) can now be integrated.

$$\int_{E(0)}^{E(x)} E^{\gamma-1} dE = \frac{1}{\gamma D_{eff}} [E(0)I(0)]^{\gamma} \int_0^x I(x')^{-\gamma} dx' \tag{9.22}$$

giving

$$\frac{E(x)}{E(0)} = \left[1 + \frac{1}{D_{eff}} \int_0^x \left(\frac{I(x')}{I(0)} \right)^{-\gamma} dx' \right]^{\frac{1}{\gamma}} \tag{9.23}$$

Equation (9.23) is the integral form of the lumped parameter model. Using this equation, one can generate a normalized CD vs. exposure curve by knowing the image intensity, *I(x)*, the effective resist thickness, D_{eff}, and the contrast, γ.

D. Alternate Derivation

The above derivation of the lumped parameter model is not the simplest, but is useful since it leads to both the differential form and the integral form of the LPM. In this section an alternate derivation of the integral form will be presented.

Equations (9.12) - (9.14) apply to general development paths assuming segmented development. Since our interest is to determine the bottom linewidth, consider a path where the depth z is just equal to the resist thickness D. Equation (9.12) for the vertical development time becomes

$$t_z = \tau_o e^{-\gamma\varepsilon} e^{-\gamma i(x_o)} \int_0^D e^{-\gamma i(z')} dz' = \tau_o e^{-\gamma\varepsilon} e^{-\gamma i(x_o)} e^{-\gamma i(D)} \int_0^D \left(\frac{I(z')}{I(D)} \right)^{-\gamma} dz'$$

$$t_z = \frac{1}{r(x_o, D)} \int_0^D \left(\frac{I(z')}{I(D)} \right)^{-\gamma} dz' = \frac{D_{eff}}{r(x_o, D)} \tag{9.24}$$

The result is just a statement of the definition of the effective resist thickness and could have been written down directly from that definition. Similarly, equation (9.13) for the horizontal development time becomes

$$t_x = \tau_o e^{-\gamma\varepsilon} e^{-\gamma i(D)} \int_{x_o}^{x} e^{-\gamma i(x')} dx' = \frac{1}{r(x_o, D)} e^{\gamma i(x_o)} \int_{x_o}^{x} e^{-\gamma i(x')} dx'$$

$$t_x = \frac{1}{r(x_o, D)} \int_{x_o}^{x} \left(\frac{I(x')}{I(x_o)} \right)^{-\gamma} dx' \tag{9.25}$$

The total development time is still the sum of these two components.

$$t_{dev} = \frac{D_{eff}}{r(x_o, D)} \left(1 + \frac{1}{D_{eff}} \int_{x_o}^{x} \left(\frac{I(x')}{I(x_o)} \right)^{-\gamma} dx' \right) \tag{9.26}$$

By applying equations (9.4) and (9.7),

$$\frac{r(x_o,D)t_{dev}}{D_{eff}} = e^{\gamma(\varepsilon-\varepsilon(0))} = \left(\frac{E(x)}{E(0)}\right)^{\gamma} \tag{9.27}$$

Substituting equation (9.27) into (9.26) gives the integral form of the LPM, equation (9.23).

E. Sidewall Angle

The lumped parameter model allows the prediction of linewidth by developing down to a depth z and laterally to a position x, which is one half of the final linewidth. Typically, the bottom linewidth is desired so that the depth chosen is the full resist thickness. By picking different values for z, different x positions will result, giving a complete resist profile. One important result that can be calculated is the resist sidewall slope and the resulting sidewall angle. To derive an expression for the sidewall slope, let us first rewrite equation (9.14) in terms of the development rate.

$$t_{dev} = \int_0^z \frac{dz'}{r(x_o,z')} + \int_{x_o}^x \frac{dx'}{r(x',z)} \tag{9.28}$$

Taking the derivative of this expression with respect to z,

$$0 = \int_0^z \frac{d\tau}{dz}dz' + \frac{1}{r(x_o,z)} + \int_{x_o}^x \frac{d\tau}{dz}dx' + \frac{1}{r(x,z)}\frac{dx}{dz} \tag{9.29}$$

The derivative of the reciprocal development rate can be calculated from equation (9.4) or (9.10),

$$\frac{d\tau}{dz} = -\gamma\,\tau(x,z)\frac{d\ln[E_{xz}]}{dz} \tag{9.30}$$

As one would expect, the variation of development rate with depth into the resist depends on the variation of the exposure dose with depth. Consider a simple example where bulk absorption is the only variation of exposure with z. For an absorption coefficient of α, the Lambert law of absorption gives

$$\frac{d\ln[E_{xz}]}{dz} = -\alpha \tag{9.31}$$

Using equations (9.30) and (9.31) in (9.29),

$$-\alpha\gamma\left(\int_0^z \tau\, dz' + \int_{x_o}^{x} \tau\, dx'\right) = \frac{1}{r(x_o,z)} + \frac{1}{r(x,z)}\frac{dx}{dz} \tag{9.32}$$

Recognizing the term in parentheses as simply the development time, the reciprocal of the resist slope can be given as

$$-\frac{dx}{dz} = \frac{r(x,z)}{r(x_o,z)} + \alpha\gamma\, t_{dev}\, r(x,z) = \frac{r(x,z)}{r(x_o,z)} + \alpha\frac{dx}{d\varepsilon} \tag{9.33}$$

Equation (9.33) shows two distinct contributors to sidewall angle. The first is the development effect. Because the top of the photoresist is exposed to developer longer than the bottom, the top linewidth is smaller resulting in a sloped sidewall. This effect is captured in equation (9.33) as the ratio of the development rate at the edge of the photoresist feature to the development rate at the center. Good sidewall slope is obtained by making this ratio small. The second term in equation (9.33) describes the effect of optical absorption on the resist slope. High absorption or poor exposure latitude will result in a reduction of the resist sidewall angle.

F. Results

The lumped parameter model is based on a simple model for development rate and a phenomenological description of the development process. The result is an equation which predicts the change in linewidth with exposure for a given aerial image. The major advantages of the lumped

parameter model are its extreme ease of application to a lithography process and computational simplicity (i.e., speed). The two parameters of the model, resist contrast and effective thickness, can be determined by the collection of linewidth data from a standard focus-exposure matrix. This data is routinely available in most production and development lithography processes; no extra or unusual data collection is required. The result is a simple and fast model which can be used as an initial predictor of results or as the engine of a lithographic control scheme.

Additionally, the lumped parameter model can be used to predict the sidewall angle of the resulting photoresist profile. The model shows the two main contributors to resist slope: development effects due to the time required for the developer to reach the bottom of the photoresist, and absorption effects resulting in a reduced exposure at the bottom of the resist.

Figure 9-2 shows an example of the output of the LPM. A complete focus-exposure matrix can be simulated by calculating the aerial image through focus. Since aerial image calculations tend to be quite fast, a typical LPM focus-exposure matrix calculation can be completed in about a second on a typical personal computer. From this data, the process window can be generated and the depth of focus determined. The speed of the calculations makes the LPM ideal for optimizing aerial image related quantities. Examples include numerical aperture/partial coherence optimization, aberration tolerancing, off-axis illumination studies, phase shifting mask design, and optical proximity correction.

Finally, the lumped parameter model presents a simple understanding of the optical lithography process. The potential of the model as a learning tool should not be underestimated. In particular, the model emphasizes the competing roles of the aerial image and the photoresist process in determining linewidth control and describes the basic development properties of a resist. This fundamental knowledge lays the foundation for further investigations into the behavior of optical lithography systems.

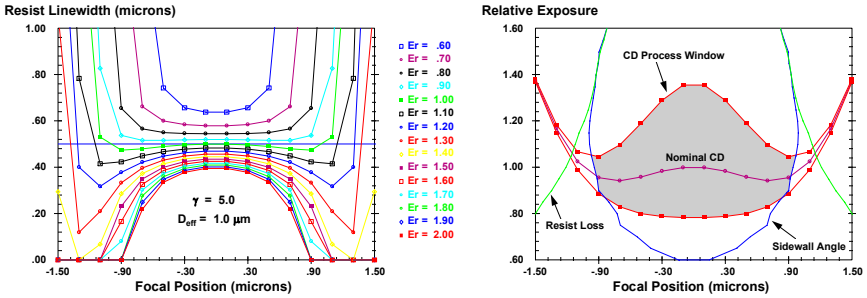

Figure 9-2. Examples of the output of the Lumped Parameter Model. By calculating the aerial image through focus, an entire focus-exposure matrix can be calculated. Shown are (a) the Bossung curves and (b) the process window. The exposure scale on both plots are relative to the nominal exposure at best focus.

References

9.1. R. Hershel and C. A. Mack, "Lumped Parameter Model for Optical Lithography," Chapter 2, Lithography for VLSI, VLSI Electronics - Microstructure Science, R. K. Watts and N. G. Einspruch, eds., Academic Press (New York: 1987) pp. 19-55.

9.2. C. A. Mack, A. Stephanakis, R. Hershel, "Lumped Parameter Model of the Photolithographic Process," *Kodak Microelectronics Seminar, Proc.*, (1986) pp. 228-238.

9.3. C. A. Mack, "Enhanced Lumped Parameter Model for Photolithography," *Optical/Laser Microlithography VII, Proc.*, SPIE Vol. 2197 (1994) pp. 501-510.

9.4. C. A. Mack, "Lithographic Optimization Using Photoresist Contrast," *KTI Microlitho-graphy Seminar, Proc.*, (1990) pp. 1-12, and *Microelectronics Manufacturing Technology*, Vol. 14, No. 1 (Jan. 1991) pp. 36-42.

9.5. M. P. C. Watts and M. R. Hannifan, "Optical Positive Resist Processing II, Experimental and Analytical Model Evaluation of Process Control," *Advances in Resist Technology and Processing II, Proc.*, SPIE Vol. 539 (1985) pp. 21-28.

Chapter 10

Lithographic Analysis

Characterizing and understanding a lithography process is an important part of using processes effectively in manufacturing. Unfortunately, the requisite characterization experiments are expensive and time-consuming. Simulation provides an ideal tool to enhance experimental characterization and improve the understanding of a given process. The ease and flexibility of modeling tools also allow for quick process changes leading to optimization studies. The sections below describe a few examples of how lithography simulation can be used to characterize a lithography process and understand the complex interaction among parameters.

A. Focus Effects

The effect of focus on a projection lithography system (such as a stepper) is a critical part of understanding and controlling a lithographic process. This section will address the importance of focus by providing definitions of the *process window* and *depth of focus* (DOF). Simulation proves an invaluable tool for predicting focus effects, generating process windows, and determining realistic values for the DOF.

In general, DOF can be thought of as the range of focus errors that a process can tolerate and still give acceptable lithographic results. Of course, the key to a good definition of DOF is in defining what is meant by tolerable. A change in focus results in two major changes to the final lithographic result: the photoresist profile changes and the sensitivity of the process to other processing errors is increased. Typically, photoresist profiles are described using three parameters: the linewidth (or critical dimension, CD), the sidewall angle, and the final resist thickness (see Chapter 8). The variation of these parameters with focus can be readily determined for any given set of conditions. The second effect of defocus is significantly harder to quantify: as an image goes out of focus, the process becomes more sensitive to other processing errors such as exposure dose and develop time. Of these secondary process errors, the most important is exposure.

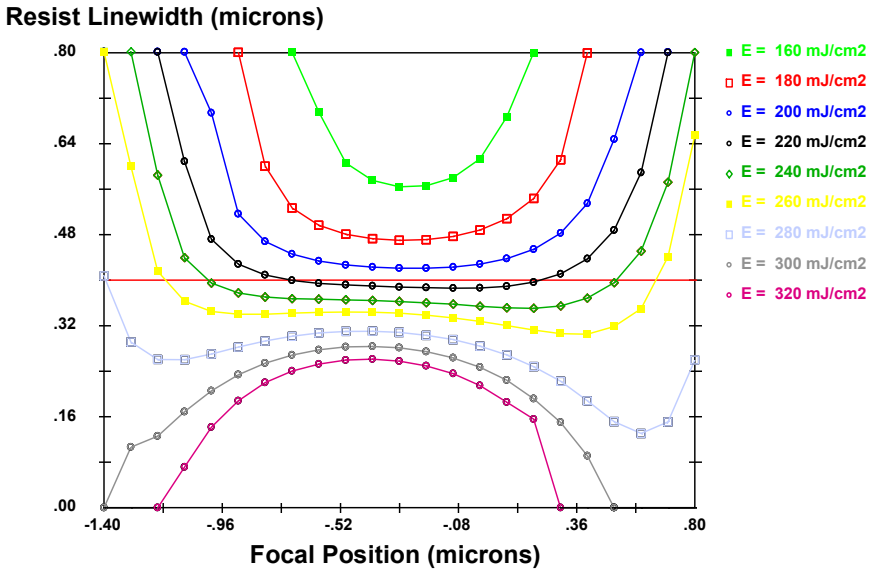

Figure 10-1. Example of the effect of focus and exposure on the resulting resist linewidth. Focal position is defined as zero at the top of the resist with a negative focal position indicating that the plane of focus is inside the resist.

Since the effect of focus is dependent on exposure, the only way to judge the response of the process to focus is to simultaneously vary both focus and exposure in what is known as a *focus-exposure matrix*. Figure 10-1 shows a typical example of the output of a focus-exposure matrix using linewidth as the response (sidewall angle and resist loss can also be plotted in the same way) in what is called a Bossung plot [10.1]. Of course, one output as a function of two inputs can be plotted in several different ways. For example, the Bossung curves could also be plotted as exposure latitude curves (linewidth versus exposure) for different focus settings. Probably the most useful way to plot this two-dimensional data set is a contour plot – contours of constant linewidth versus focus and exposure (Figure 10-2).

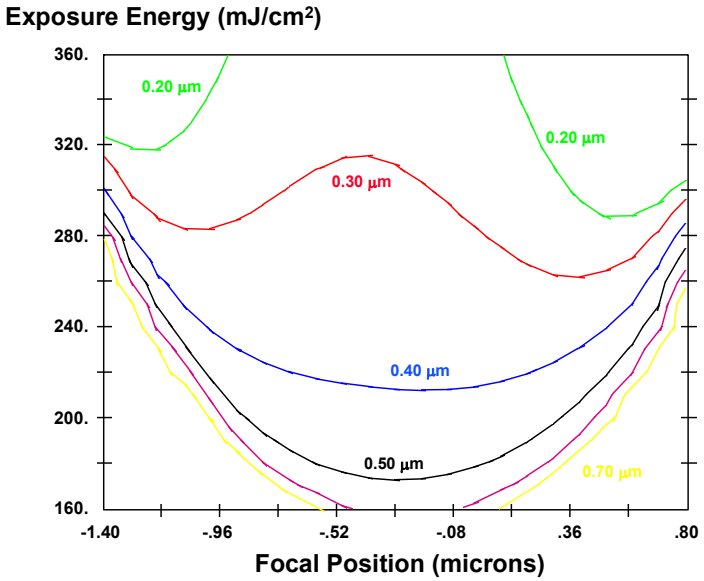

Figure 10-2. Displaying the data from a focus-exposure matrix in an alternate form, contours of constant CD versus focus and exposure.

The contour plot form of data visualization is especially useful for establishing the limits of exposure and focus that allow the final image to meet certain specifications. Rather than plotting all of the contours of constant CD,

one could plot only the two CDs corresponding to the outer limits of acceptability – the CD specifications. Because of the nature of a contour plot, other variables can also be plotted on the same graph. Figure 10-3 shows an example of plotting contours of CD (nominal ±10%), 80° sidewall angle, and 10% resist loss all on the same graph. The result is a *process window* – the region of focus and exposure that keeps the final resist profile within all three specifications.

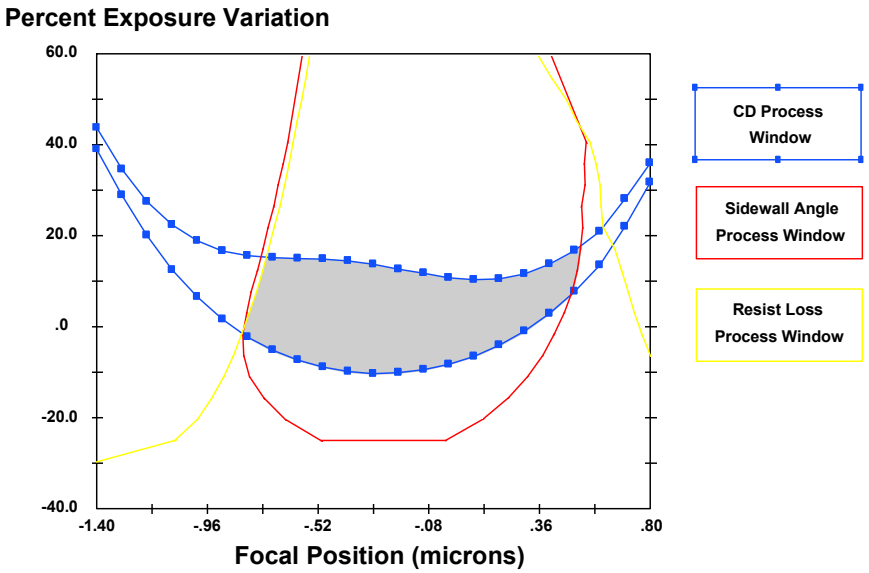

Figure 10-3. The focus-exposure process window is constructed from contours of the specifications for linewidth, sidewall angle, and resist loss. The shaded area shows the overall process window.

The focus-exposure process window is one of the most important plots in lithography since it shows how exposure and focus work together to affect linewidth, sidewall angle, and resist loss. The process window can be thought of as a *process capability* – how the process responds to changes in focus and exposure. How can we determine if a given process capability is good enough?

An analysis of the error sources for focus and exposure in a given process will give a *process requirement* [10.2]. If the process capability exceeds the process requirements, yield will be high. If, however, the process requirement is too large to fit inside the process capability, yield will suffer. A thorough analysis of the effects of exposure and focus on yield can be accomplished with yield modeling (for example, using ProCD) [10.3], but a simpler analysis can give useful insight and can be used to derive a number for depth of focus.

What is the maximum range of focus and exposure (that is, the maximum process requirement) that can fit inside the process window? A simple way to investigate this question is to graphically represent errors in focus and exposure as a rectangle on the same plot as the process window. The width of the rectangle represents the built-in focus errors of the processes, and the height represents the built-in dose errors. The problem then becomes one of finding the maximum rectangle that fits inside the process window. However, there is no one answer to this question. There are many possible rectangles of different widths and heights that are "maximum", i.e., they cannot be made larger in either direction without extending beyond the process window. (Note that the concept of a "maximum area" is meaningless here.) Each maximum rectangle represents one possible trade-off between tolerance to focus errors and tolerance to exposure errors. Larger DOF can be obtained if exposure errors are minimized. Likewise, exposure latitude can be improved if focus errors are small. The result is a very important trade-off between exposure latitude and DOF.

If all focus and exposure errors were systematic, then the proper graphical representation of those errors would be a rectangle. The width and height would represent the total ranges of the respective errors. If, however, the errors were randomly distributed, then a probability distribution function would be needed to describe them. For the completely random case, a Gaussian distribution with standard deviations in exposure and focus is used to describe the probability of a given error. In order to graphically represent the errors of focus and exposure, one should describe a surface of constant probability of occurrence. All errors in focus and exposure inside the surface would have a probability of occurring that is greater than the established cutoff. What is the shape of such a surface? For fixed systematic errors, the shape is a rectangle. For a Gaussian distribution, the surface is an ellipse. If one wishes to describe a

"three-sigma" surface, the result would be an ellipse with major and minor axes equal to the three-sigma errors in focus and exposure.

Using either a rectangle for systematic errors or an ellipse for random errors, the size of the errors that can be tolerated for a given process window can be determined. Taking the rectangle as an example, one can find the maximum rectangle that will fit inside the processes window. Figure 10-4 shows an analysis of the process window where every maximum rectangle is determined and its height (the exposure latitude) plotted versus its width (depth of focus). Likewise, assuming random errors in focus and exposure, every maximum ellipse that fits inside the processes window can be determined. The horizontal width of the ellipse would represent a three-sigma error in focus, while the vertical height of the ellipse would give a three-sigma error in exposure. Plotting the height versus the width of all the maximum ellipses gives the second curve of exposure latitude versus DOF in Figure 10-4.

Figure 10-4. The process window of Figure 10-3 is analyzed by fitting all the maximum rectangles and all the maximum ellipses, then plotting their height (exposure latitude) versus their width (depth of focus).

The exposure latitude versus DOF curves of Figure 10-4 provide the most concise representation of the coupled effects of focus and exposure on the lithography process. Each point on the exposure latitude - DOF curve is one possible operating point for the process. The user must decide how to balance the trade-off between DOF and exposure latitude. One approach is to define a minimum acceptable exposure latitude, and then operate at this point; this has the effect of maximizing the DOF of the process. In fact, this approach allows for the definition of a single value for the DOF of a given feature for a given process. The depth of focus of a feature can be defined as *the range of focus that keeps the resist profile of a given feature within all specifications (linewidth, sidewall angle, and resist loss) over a specified exposure range*. For the example given in Figure 10-4, a minimum acceptable exposure latitude of 15%, in addition to the other profile specifications, would lead to the following depth of focus results:

DOF (rectangle) = 0.85 μm

DOF (ellipse) = 1.14 μm

DOF (average) = 1.00 μm

As one might expect, systematic errors in focus and exposure are more problematic than random errors, leading to a smaller DOF. Most actual processes would have a combination of systematic and random errors. Thus, one might expect the rectangle analysis to give a pessimistic value for the DOF, and the ellipse method to give an optimistic view of DOF. The average value of the two will be a more realistic number in most cases.

The definition of depth of focus also leads naturally to the determination of best focus and best exposure. The DOF value read off from the exposure latitude versus DOF curve corresponds to one maximum rectangle or ellipse that fit inside the process window. The center of this rectangle or ellipse would then correspond to best focus and exposure for this desired operating point.

All of the above graphs were generated using simulation, which can not only generate focus-exposure data, but can analyze the data to determine the process window and DOF as well.

B. Point Optimization

Full optimization of a lithographic process requires thorough and time consuming calculations of many effects. One simplified approach to this optimization problem is to perform limited calculations at one point in space, say at a point in the resist corresponding to the nominal line edge, and try to optimize certain important properties of the resist feature at this point. Such a point optimization method, by its very nature, is somewhat limiting, since any interesting and important lithographic effects that occur elsewhere in the photoresist are not accounted for. However, if the point used is of interest (such as the nominal line edge) and the method used has physical significance, the results can be very useful.

To further simplify the analysis of a lithographic process, it is highly desirable to separate the effects of the lithographic tool from those of the photoresist process. This can be done with reasonable accuracy only if the interaction of the tool (i.e., the aerial image) with the photoresist is known. Consider an aerial image of relative intensity *I(x)*, where *x* is the horizontal position (i.e., in the plane of the wafer and mask) and is zero at the center of a symmetric mask feature. The aerial image exposes the photoresist to produce some chemical distribution *m(x)* within the resist. This distribution is called the *latent image*. Many important properties of the lithographic process, such as exposure latitude and development latitude, are a function of the gradient of the latent image $\partial m / \partial x$. Larger gradients result in improved process latitude. By taking the derivative of equation (5.22), it can be shown that the latent image gradient is related to the aerial image by [10.4]

$$\frac{\partial m}{\partial x} = m \ln(m) \frac{\partial \ln I}{\partial x} \tag{10.1}$$

where the slope of the logarithm of the aerial image is often called simply the *log-slope*. The development properties of the photoresist translate the latent image gradient into a development gradient, which then allows for the generation of a photoresist image. Optimum photoresist image quality is obtained with a large development rate gradient. A lumped parameter called the photoresist contrast, γ, can be defined that relates the aerial image and the development rate *r*:

$$\frac{\partial \ln r}{\partial x} = \gamma \frac{\partial \ln I}{\partial x} \tag{10.2}$$

Equation (10.2) is called the *lithographic imaging equation* and shows in a concise form how a gradient in aerial image intensity results in a solubility differential in photoresist. The development rate gradient is maximized by higher resist contrast and by a larger log-slope of the aerial image.

The above discussion clearly indicates that the aerial image log-slope is a logical metric by which to judge the quality of the aerial image. In particular, the image log-slope, when normalized by multiplication with the feature width *w*, is directly proportional to exposure latitude expressed as a percent change in exposure to give a percent change in linewidth. This normalized image log-slope (*NILS*) is given by

$$NILS = w \frac{\partial \ln I}{\partial x} \tag{10.3}$$

This metric was first discussed by Levenson et al. [10.5], and later in a related form by Levinson and Arnold [10.6,10.7], before being explored to great extent by this author [10.8 - 10.11, 10.2]. Simulation allows for the simple calculation of the NILS and thus its convenient use as an aerial image metric.

The well known effect of defocus on the aerial image was shown previously in Figure 2-11. Both the edge slope of the image and the center space intensity decrease with defocus, and the intensity at the mask edge remains nearly constant or increases slightly. To compare aerial images using the log-slope, one must pick an *x* value to use. An obvious choice is the mask edge (or more correctly, the nominal feature edge). Thus, all subsequent reference to the slope of the log-aerial image will be at the nominal feature edge. Now the effect of defocus on the aerial image can be expressed by plotting log-slope as a function of defocus, as shown in Figure 10-5. The log-slope defocus curve has proven to be a powerful tool for understanding focus effects.

Some useful information can be obtained from a plot of log-slope versus defocus. As was previously discussed, exposure latitude varies directly with the log-slope of the image. Thus, a minimum acceptable exposure latitude

specification translates directly into a minimum acceptable value of the NILS. The log-slope defocus curve can then be used to give a maximum defocus to keep the process within this specification. If, for example, the minimum acceptable normalized log-slope of a given process was determined to be 3.5, the maximum allowable defocus of 0.5 μm lines and spaces on a 0.53 NA i-line stepper would be, from Figure 10-5, about ±0.8 μm. This gives a practical definition of the depth of focus that separates the effects of the aerial image and the photoresist process. The projection printer determines the shape of the log-slope defocus curve, and the process determines the range of operation (i.e., the minimum NILS value). If the minimum log-slope needed was 6, one would conclude from Figure 10-5 that this printer could not adequately resolve 0.5 μm lines and spaces. Thus, resolution can also be estimated from a log-slope defocus curve.

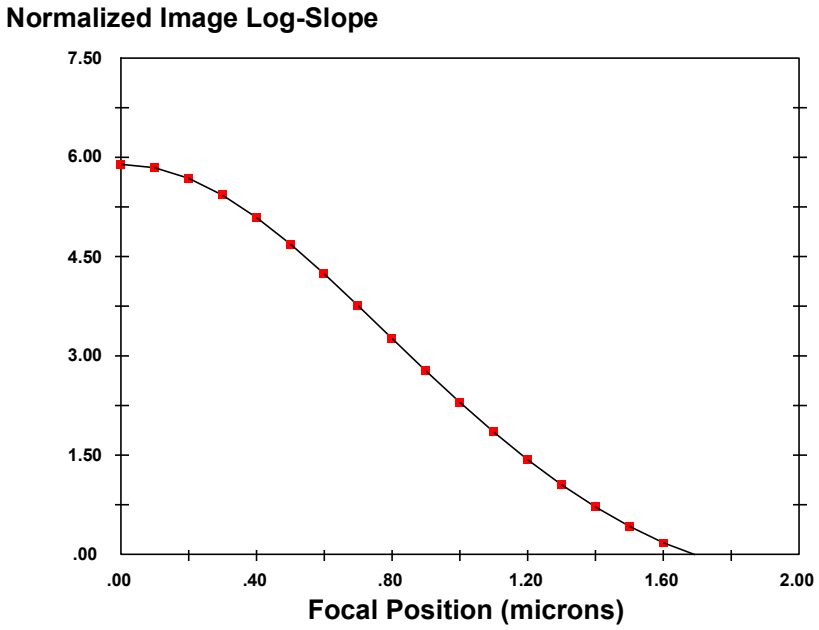

Figure 10-5. An example of the log-slope defocus curve (0.5 μm lines and spaces, NA = 0.53, i-line, σ = 0.5).

To define a resolution metric based on the image log-slope, consider Figure 10-6, which shows the effect of feature size on the log-slope defocus curve. If, for example, a particular photoresist process requires a NILS of 3.8, one can see that the 0.4 μm features will be resolved only when in perfect focus, the 0.5μm features will have a DOF of ±0.7 μm, and the 0.6 μm features will have a DOF of ±0.9 μm. Obviously, the DOF is extremely sensitive to feature size, a fact that is not evident in the common Rayleigh definition. Since DOF is a strong function of feature size, it is logical that resolution is a function of the required DOF. Thus, in the situation shown in Figure 10-6, if the minimum acceptable DOF is ±0.8 μm and the required NILS is 3.8, the practical resolution is about 0.55μm for equal lines and spaces. Resolution and DOF cannot be independently defined, but rather are interdependent. To summarize, DOF can be estimated as the range of focus that keeps the log-slope above some specification for a given feature. Resolution can be estimated as the smallest feature that keeps the log-slope above some specification over a given range of focus.

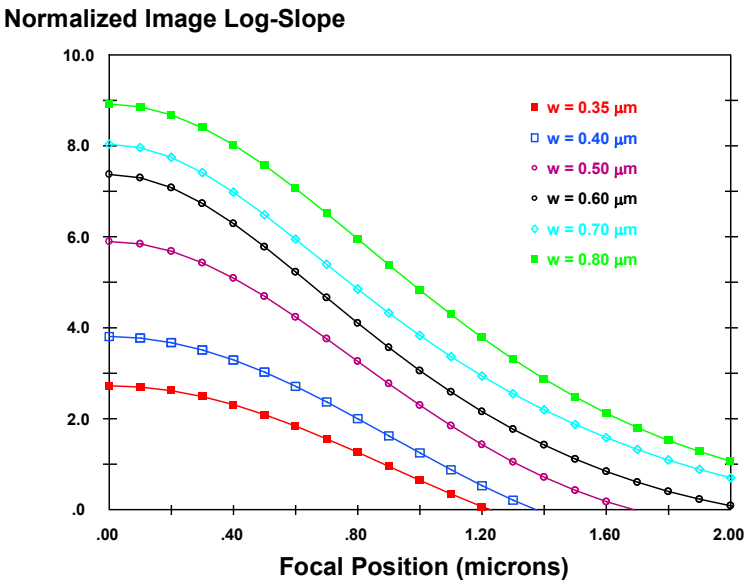

Figure 10-6. Log-slope defocus curves showing the effect of linewidth (equal lines and spaces, NA = 0.53, i-line, σ = 0.5).

The key to the above image-based definitions for resolution and DOF is the linear correlation between the NILS and exposure latitude. But in order to make quantitative estimates, one must have a reasonable estimate for the minimum acceptable normalized log-slope. How is such an estimate obtained? By measuring a focus-exposure matrix, one can obtain an experimental plot of exposure latitude (EL) versus defocus (exposure latitude being defined as the range of exposure which keeps the linewidth within specification, divided by the nominal exposure, and multiplied by 100%). This can be repeated for many different feature types and sizes, if desired. By comparing such experimental data with the log-slope defocus curves as in Figure 10-6, a correlation between NILS and exposure latitude can be obtained. For example, one might find for a particular process that data and simulated NILS are empirically correlated by the simple expression

$$EL = 8.1(NILS - 1.1) \tag{10.4}$$

Equation (10.4) in and of itself leads to very revealing interpretations. First, note that in this example a NILS of at least 1.1 must be used before an image in photoresist is obtained even at one exposure level. Above a NILS of 1.1, each increment in NILS adds 8.1% exposure latitude. Finally, if a minimum required exposure latitude is specified for a process, this value will translate directly into a minimum required NILS. For example, if an *EL* of 20% is required, the NILS that just achieves this level is 3.6. Thus, all images with a NILS in excess of 3.6 would be considered acceptable from an exposure latitude point of view. Correlations like equation (10.4) are very process dependent. However, for a given process, such a correlation allows imaging parameters to be studied by simply examining the log-slope defocus behavior.

Many image-related parameters can be easily studied using the log-slope defocus curves. The differences between imaging dense and isolated features, or lines versus contacts, for example, can be examined. The log-slope defocus approach has been used to optimize the numerical aperture and partial coherence of a stepper [10.12] (as seen in Figure 10-7), examine the differences between imaging in positive and negative tone resist [10.13] and study the advantages of off-axis illumination [10.14].

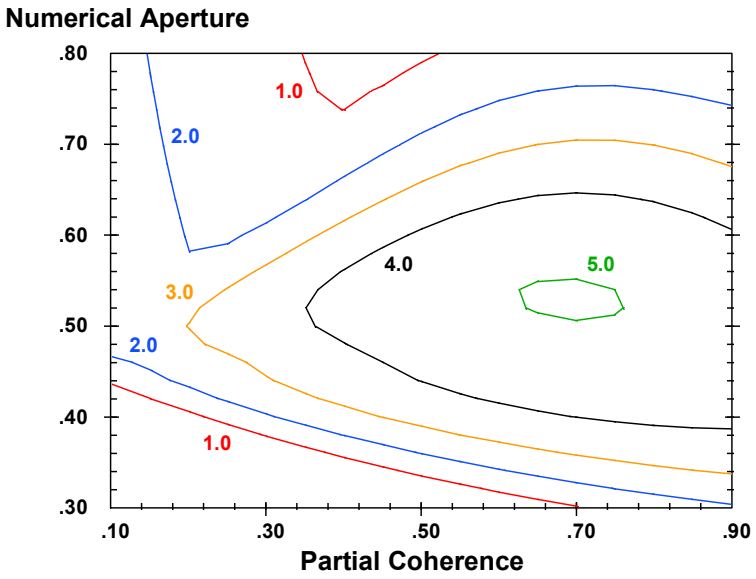

Figure 10-7. The log-slope can be used to "optimize" a stepper by finding the values of numerical aperture and partial coherence which maximize the log-slope of a given feature at a given level of defocus (*i*-line, 0.4μm lines and spaces, defocus = 0.8μm).

Although defocus is strictly an optical phenomenon, the photoresist plays a significant role in determining the effects of defocus. As one might imagine, a better photoresist will provide greater depth of focus. In light of the above description of defocus using log-slope defocus curves, the photoresist impacts the DOF by changing the minimum acceptable log-slope specification. A better photoresist will have a lower log-slope specification, resulting in a greater usable focus range. This relationship between the photoresist and the log-slope specification is determined experimentally as described above by measuring exposure latitude versus defocus. In general, the resulting correlation between the NILS and the exposure latitude is given by

$$EL = \alpha\,(NILS - \beta) \tag{10.5}$$

where β is the minimum NILS required to give any image at all in photoresist, and α is the percent increase in exposure latitude per unit increase in *NILS*. Thus, to a first degree, the effect of the photoresist on depth of focus can be characterized by the two parameters α and β.

Consider for a moment an ideal, infinite contrast photoresist. For such a case, the slope of the exposure latitude curve will be exactly 2/NILS [10.15]. Thus, using a typical linewidth specification of ±10%, an infinite contrast resist would make α=10 and β=0. The quality of a photoresist with respect to focus and exposure latitude can be judged by how close α and β are to these ideals.

References

10.1. J. W. Bossung, "Projection Printing Characterization," *Developments in Semiconductor Microlithography II, Proc*., SPIE Vol. 100, pp. 80-84 (1977).

10.2. C. A. Mack, "Understanding Focus Effects in Submicron Optical Lithography: a Review," *Optical Engineering*, Vol. 32, No. 10, pp. 2350-2362 (Oct., 1993).

10.3. E. W. Charrier and C. A. Mack, "Yield Modeling and Enhancement for Optical Lithography," *Optical/Laser Microlithography VIII, Proc*., SPIE Vol. 2440, pp. 435-447 (1995).

10.4. C. A. Mack, "Photoresist Process Optimization," *KTI Microelectronics Seminar, Proc*., pp. 153-167 (1987).

10.5. M. D. Levenson, D. S. Goodman, S. Lindsey, P. W. Bayer, and H. A. E. Santini, "The Phase-Shifting Mask II: Imaging Simulations and Submicrometer Resist Exposures," *IEEE Trans. Electron Devices*, Vol. ED-31, No. 6, pp. 753-763 (June 1984).

10.6. H. J. Levinson and W. H. Arnold, "Focus: the critical parameter for submicron lithography," *Jour. Vac. Sci. Tech*., Vol. B5, No. 1, pp. 293-298 (1987).

10.7. W. H. Arnold and H. J. Levinson, "Focus: the critical parameter for submicron optical lithography: Part 2," *Optical Microlithography VI, Proc*., SPIE Vol. 772, pp. 21-34 (1987).

10.8. C. A. Mack, "Understanding Focus Effects in Submicron Optical Lithography," *Optical/Laser Microlithography, Proc*., SPIE Vol. 922, pp. 135-148 (1988), and *Optical Engineering*, Vol. 27, No. 12, pp. 1093-1100 (Dec., 1988).

10.9. C. A. Mack, "Comments on 'Understanding Focus Effects in Submicrometer Optical Lithography'," *Optical Engineering*, Vol. 29, No. 3, p. 252 (Mar. 1990).

10.10. C. A. Mack and P. M. Kaufman, "Understanding Focus Effects in Submicron Optical Lithography, part 2: Photoresist effects," *Optical/Laser Microlithography II, Proc*., SPIE Vol. 1088, pp. 304-323 (1989).

10.11. C. A. Mack, "Understanding Focus Effects in Submicron Optical Lithography, part 3: Methods for Depth-of-Focus Improvement," *Optical/Laser Microlithography V, Proc*., SPIE Vol. 1674, pp. 272-284 (1992).

10.12. C. A. Mack, "Algorithm for Optimizing Stepper Performance Through Image Manipulation," *Optical/Laser Microlithography III, Proc*., SPIE Vol. 1264, pp. 71-82 (1990).

10.13. C. A. Mack and J. E. Connors, "Fundamental Differences Between Positive and Negative Tone Imaging," *Optical/Laser Microlithography V, Proc.*, SPIE Vol. 1674, pp. 328-338 (1992), and *Microlithography World*, Vol. 1, No. 3, pp. 17-22 (Jul/Aug 1992).

10.14. C. A. Mack, "Optimization of the Spatial Properties of Illumination," *Optical/Laser Microlithography VI, Proc.*, SPIE Vol. 1927, pp. 125-136 (1993).

10.15. C. A. Mack, A. Stephanakis, R. Hershel, "Lumped Parameter Model of the Photolithographic Process," *Kodak Microelectronics Seminar, Proc.*, pp. 228-238 (1986).

Chapter 11

Uses of Lithography Modeling

In the twenty three years since optical lithography modeling was first introduced to the semiconductor industry, it has gone from a research curiosity to an indispensable tool for research, development and manufacturing. There are numerous examples of how modeling has had a dramatic impact on the evolution of lithography technology, and many more ways in which it has subtly, but undeniably, influenced the daily routines of lithography professionals. There are four major uses for lithography simulation: 1) as a research tool, performing experiments that would be difficult or impossible to do any other way, 2) as a development tool, quickly evaluating options, optimizing processes, or saving time and money by reducing the number of experiments in the fab, 3) as a manufacturing tool, for troubleshooting process problems and determining optimum process settings, and 4) as a learning tool, to help provide a fundamental understanding of all aspects of the lithography process. These four applications of lithography simulation are not distinct – there is much overlap among these basic categories.

A. Research Tool

Since the initial introduction of lithography simulation in 1974, modeling has had a major impact on research efforts in lithography. Here are some examples of how modeling has been used in research.

Modeling was used to suggest the use of dyed photoresist in the reduction of standing waves [11.1]. Experimental investigation into dyed resists didn't begin until 10 years later [11.2,11.3].

After phase-shifting masks were first introduced [11.4], modeling has proven to be indispensable in their study. Levenson used modeling extensively to understand the effects of phase masks [11.5]. One of the earliest studies of phase-shifting masks used modeling to calculate images for Levenson's original alternating phase mask, then showed how phase masks increased defect printability [11.6]. The same study used modeling to introduce the concept of the outrigger (or assist slot) phase mask. Since these early studies, modeling results have been presented in nearly every paper published on phase-shifting masks.

Off-axis illumination was first introduced as a technique for improving resolution and depth of focus based on modeling studies [11.7]. Since then, this technique has received widespread attention and has been the focus of many more simulation and experimental efforts.

Using modeling, the advantages of having a variable numerical aperture, variable partial coherence stepper were discussed [11.7,11.8]. Since then, all major stepper vendors have offered variable NA, variable coherence systems. Modeling remains a critical tool for optimizing the settings of these flexible new machines.

The use of pupil filters to enhance some aspects of lithographic performance have, to date, only been studied theoretically using lithographic models [11.9]. If such studies prove the usefulness of pupil filters, experimental investigations may also be conducted.

Modeling has been used in photoresist studies to understand the depth of focus loss when printing contacts in negative resists [11.10], the reason for artificially high values of resist contrast when surface inhibition is present [11.11], the potential for exposure optimization to maximize process latitude [11.12,11.13], and the role of diffusion in chemically amplified resists [11.14]. Lithographic models are now standard tools for photoresist design and evaluation.

Modeling has always been used as a tool for quantifying optical proximity effects and for defining algorithms for geometry dependent mask biasing [11.15,11.16]. Most people would consider modeling to be a required element of any optical proximity correction scheme.

Defect printability has always been a difficult problem to understand. The printability of a defect depends considerably on the imaging system and resist used, as well as the position of the defect relative to other patterns on the mask and the size and transmission properties of the defect. Modeling has proven itself a valuable and accurate tool for predicting the printability of defects [11.17,11.18].

Modeling has also been used to understand metrology of lithographic structures [11.19-11.22] and continues to find new application in virtually every aspect of lithographic research. In fact, modeling has proven an indispensable tool for predicting future lithographic performance and evaluating the theoretical capabilities and limitations of extensions for optical lithography far into the future.

One of the primary reasons that lithography modeling has become such a standard tool for research activities is the ability to simulate such a wide range of lithographic conditions. While laboratory experiments are limited to the equipment and materials on hand (a particular wavelength and numerical aperture of the stepper, a given photoresist), simulation gives an almost infinite array of possible conditions. From high numerical apertures to low wavelengths, hypothetical resists to arbitrary mask structures, simulation offers the ability to run “experiments” on steppers that you do not own with photoresists that have yet to be made. How else can one explore the shadowy boundary between the possible and the impossible?

B. Process Development Tool

Lithography modeling has also proven to be an invaluable tool for the development of new lithographic processes or equipment. Some of the more common uses include the optimization of dye loadings in photoresist [11.23,11.24], simulation of substrate reflectivity [11.25,11.26], the applicability and optimization of top and bottom antireflection coatings [11.27,11.28], and simulation of the effect of bandwidth on swing curve amplitude [11.29,11.30]. In addition, simulation has been used to help understand the use of thick resists for thin film head manufacture [11.31] as well as other non-semiconductor applications.

Modeling is used extensively by makers of photoresist to evaluate new formulations [11.32,11.33] and to determine adequate measures of photoresist performance for quality control purposes [11.34]. Resist users often employ modeling as an aid for new resist evaluations. On the exposure tool side, modeling has become an indispensable part of the optimization of the numerical aperture and partial coherence of a stepper [11.35-11.37] and in the understanding of the print bias between dense and isolated lines [11.38]. The use of optical proximity correction software requires rules on how to perform the corrections, which are often generated with the help of lithography simulation [11.39].

As a development tool, lithography simulation excels due to its speed and cost-effectiveness. Process development usually involves running numerous experiments to determine optimum process conditions, shake out possible problems, determine sensitivity to variables, and write specification limits on the inputs and outputs of the process. These activities tend to be both time consuming and costly. Modeling offers a way to supplement laboratory experiments with simulation experiments to speed up this process and reduce costs. Considering that a single experimental run in a wafer fabrication facility can take from hours to days, the speed advantage of simulation is considerable. This allows a greater number of simulations than would be practical (or even possible) in the fab.

C. Manufacturing Tool

Although you will find less published material on the use of lithography simulation in manufacturing environments [11.40-11.42], the reason is the limited publications by people in manufacturing rather than the limited use of lithography modeling. The use of simulation in a manufacturing environment has three primary goals: to reduce the number of test or experimental wafers which must be run through the production line, to troubleshoot problems in the fab, and to aid in decision making by providing facts to support engineering judgment and intuition.

Running test wafers through a manufacturing line is costly not so much due to the cost of the test, but due to the opportunity cost of not running product [11.43]. If simulation can reduce the time a manufacturing line is not running product even slightly, the return on investment can be significant. Simulation can also aid in the time required to bring a new process on-line and in the establishment of the base-line capability of a new process.

D. Learning Tool

Although the research, development and manufacturing applications of lithography simulation presented above give ample benefits of modeling based on time, cost and capability, the underlying power of simulation is its ability to act as a learning tool. Proper application of modeling allows the user to learn efficiently and effectively. There are many reasons why this is true. First, the speed of simulation versus experimentation makes feedback much more timely. Since learning is a cycle (an idea, an experiment, a measurement, then comparison back to the original idea), faster feedback allows for more cycles of learning. Since simulation is very inexpensive, there are fewer inhibitions and more opportunities to explore ideas. And, as the research application has shown us, there are fewer physical constraints on what “experiments” can be performed.

All of these factors allows the use of modeling to gain an understanding of lithography. Whether learning fundamental concepts or exploring subtle nuances, the value of improved knowledge can not be overstated.

Epilogue...

The impact of simulation on optical lithography has been undeniably dramatic. However, the best is yet to come. The continuing improvement in models, software, and measured input parameters results in greater use of simulation almost on a daily basis. Like a lithography calculator, lithography simulation is becoming a commonplace tool that engineers rely on to do their jobs. I hope this book will make the use of the PROLITH family of lithography simulation tools more enjoyable, productive and rewarding.

References

11.1. A. R. Neureuther and F. H. Dill, "Photoresist Modeling and Device Fabrication Applications," Optical And Acoustical Micro-Electronics, Polytechnic Press (New York: 1974) pp. 233-249.

11.2. H. L. Stover, M. Nagler, I. Bol, and V. Miller, "Submicron Optical Lithography: I-line Lens and Photoresist Technology," *Optical Microlith. III*, Proc., SPIE Vol. 470 (1984) pp. 22-33.

11.3. I. I. Bol, "High-Resolution Optical Lithography using Dyed Single-Layer Resist," *Kodak Microelec. Seminar Interface '84* (1984) pp. 19-22.

11.4. M. D. Levenson, N. S. Viswanathan, R. A. Simpson, "Improving Resolution in Photolithography with a Phase-Shifting Mask," *IEEE Trans. Electron Devices*, Vol. ED-29, No. 12 (Dec. 1982) pp. 1828-1836.

11.5. M. D. Levenson, D. S. Goodman, S. Lindsey, P. W. Bayer, and H. A. E. Santini, "The Phase-Shifting Mask II: Imaging Simulations and Submicrometer Resist Exposures," *IEEE Trans. Electron Devices*, Vol. ED-31, No. 6 (June 1984) pp. 753-763.

11.6. M. D. Prouty and A. R. Neureuther, "Optical Imaging with Phase Shift Masks," *Optical Microlith. III*, Proc., SPIE Vol. 470 (1984) pp. 228-232.

11.7. C. A. Mack, "Optimum Stepper Performance Through Image Manipulation," *KTI Micro-electronics Seminar, Proc.*, (1989) pp. 209-215.

11.8. C. A. Mack, "Algorithm for Optimizing Stepper Performance Through Image Manipulation," *Optical/Laser Microlithography III, Proc.*, SPIE Vol. 1264 (1990) pp. 71-82.

11.9. H. Fukuda, T. Terasawa, and S. Okazaki, "Spatial Filtering for Depth-of-focus and Resolution Enhancement in Optical Lithography," *Journal of Vacuum Science and Technology*, Vol. B9, No. 6 (Nov/Dec 1991) pp. 3113-3116.

11.10. C. A. Mack and J. E. Connors, "Fundamental Differences Between Positive and Negative Tone Imaging," *Optical/Laser Microlithography V, Proc.*, SPIE Vol. 1674 (1992) pp. 328-338, and *Microlithography World*, Vol. 1, No. 3 (Jul/Aug 1992) pp. 17-22.

11.11. C. A. Mack, "Lithographic Optimization Using Photoresist Contrast," *KTI Microlithography Seminar, Proc.*, (1990) pp. 1-12, and *Microelectronics Manufacturing Technology*, Vol. 14, No. 1 (Jan. 1991) pp. 36-42.

11.12. C. A. Mack, "Photoresist Process Optimization," *KTI Microelectronics Seminar, Proc.*, (1987) pp. 153-167.

11.13. P. Trefonas and C. A. Mack, "Exposure Dose Optimization for a Positive Resist Containing Poly-functional Photoactive Compound," *Advances in Resist Technology and Processing VIII, Proc.*, SPIE Vol. 1466 (1991).

11.14. J. S. Petersen, C. A. Mack, J. Sturtevant, J. D. Byers and D. A. Miller, "Non-constant Diffusion Coefficients: Short Description of Modeling and Comparison to Experimental Results," *Advances in Resist Technology and Processing XII, Proc.*, SPIE Vol. 2438 (1995).

11.15. C. A. Mack and P. M. Kaufman, "Mask Bias in Submicron Optical Lithography," *Jour. Vac. Sci. Tech.*, Vol. B6, No. 6 (Nov./Dec. 1988) pp. 2213-2220.

11.16. N. Shamma, F. Sporon-Fielder and E. Lin, "A Method for Correction of Proximity Effect in Optical Projection Lithography," *KTI Microelectronics Seminar, Proc.*, (1991) pp. 145-156.

11.17. A. R. Neureuther, P. Flanner III, and S. Shen, "Coherence of Defect Interactions with Features in Optical Imaging," *Jour. Vac. Sci. Tech.*, Vol. B5, No. 1 (Jan./Feb. 1987) pp. 308-312.

11.18. J. Wiley, "Effect of Stepper Resolution on the Printability of Submicron 5x Reticle Defects," *Optical/Laser Microlithography II, Proc.*, SPIE Vol. 1088 (1989) pp. 58-73.

11.19. L.M. Milner, K.C. Hickman, S.M. Gasper, K.P. Bishop, S.S.H. Naqvi, J.R. McNeil, M. Blain, and B.L. Draper, "Latent Image Exposure Monitor Using Scatterometry," SPIE Vol. 1673 (1992) pp. 274-283.

11.20. K.P. Bishop, L.M. Milner, S.S.H. Naqvi, J.R. McNeil, and B.L. Draper, "Use of Scatterometry for Resist Process Control," SPIE Vol. 1673 (1992) pp. 441-452

11.21. L.M. Milner, K.P. Bishop, S.S.H. Naqvi, and J.R. McNeil, "Lithography Process Monitor Using Light Diffracted from a Latent Image," SPIE Vol. 1926 (1993) pp. 94-105.

11.22. S. Zaidi, S.L. Prins, J.R. McNeil, and S.S.H. Naqvi, "Metrology Sensors for Advanced Resists," SPIE Vol. 2196 (1994) pp. 341-351

11.23. J.R. Johnson, G.J. Stagaman, J.C. Sardella, C.R. Spinner III, F. Liou, P. Tiefonas, and C. Meister, "The Effects of Absorptive Dye Loading and Substrate Reflectivity on a 0.5 μm I-line Photoresist Process," SPIE Vol. 1925 (1993) pp. 552-563.

11.24. W. Conley, R. Akkapeddi, J. Fahey, G. Hefferon, S. Holmes, G. Spinillo, J. Turtevant, and K. Welsh, "Improved Reflectivity Control of APEX-E Positive Tone Deep-UV Photoresist," SPIE Vol. 2195 (1994) pp. 461-476.

11.25. N. Thane, C. Mack, and S. Sethi, "Lithographic Effects of Metal Reflectivity Variations," SPIE Vol. 1926 (1993) pp. 483-494.

11.26. B. Singh, S. Ramaswami, W. Lin, and N. Avadhany, "IC Wafer Reflectivity Measurement in the UV and DUV and Its Application for ARC Characterization," SPIE Vol. 1926 (1993) pp. 151-163.

11.27. S.S. Miura, C.F. Lyons, and T.A. Brunner, "Reduction of Linewidth Variation over Reflective Topography," SPIE Vol. 1674 (1992) pp. 147-156.

11.28. H. Yoshino, T. Ohfuji, and N. Aizaki, "Process Window Analysis of the ARC and TAR Systems for Quarter Micron Optical Lithography," SPIE Vol. 2195 (1994) pp. 236-245.

11.29. G. Flores, W. Flack, and L. Dwyer, "Lithographic Performance of a New Generation I-line Optical System: A Comparative Analysis," SPIE Vol. 1927 (1993) pp. 899-913.

11.30. B. Kuyel, M. Barrick, A. Hong, and J. Vigil, "0.5 Micron Deep UV Lithography Using a Micrascan-90 Step-And-Scan Exposure Tool," SPIE Vol. 1463 (1991) pp. 646-665.

11.31. G.E. Flores, W.W. Flack, and E. Tai, "An Investigation of the Properties of Thick Photoresist Films," SPIE Vol. 2195 (1994) pp. 734-751.

11.32. H. Iwasaki, T. Itani, M. Fujimoto, and K. Kasama, "Acid Size Effect of Chemically Amplified Negative Resist on Lithographic Performance," SPIE Vol. 2195 (1994) pp. 164-172.

11.33. U. Schaedeli, N. Münzel, H. Holzwarth, S.G. Slater, and O. Nalamasu, "Relationship Between Physical Properties and Lithographic Behavior in a High Resolution Positive Tone Deep-UV Resist," SPIE Vol. 2195 (1994) pp. 98-110.

11.34. K. Schlicht, P. Scialdone, P. Spragg, S.G. Hansen, R.J. Hurditch, M.A. Toukhy, and D.J. Brzozowy, "Reliability of Photospeed and Related Measures of Resist Performances," SPIE Vol. 2195 (1994) pp. 624-639.

11.35. R.A. Cirelli, E.L. Raab, R.L. Kostelak, and S. Vaidya, "Optimizing Numerical Aperture and Partial Coherence to Reduce Proximity Effect in Deep-UV Lithography," SPIE Vol. 2197 (1994) pp. 429-439.

11.36. B. Katz, T. Rogoff, J. Foster, B. Rericha, B. Rolfson, R. Holscher, C. Sager, and P. Reynolds, "Lithographic Performance at Sub-300 nm Design Rules Using High NA I-line Stepper with Optimized NA and σ in Conjunction with Advanced PSM Technology," SPIE Vol. 2197 (1994) pp. 421-428.

11.37. P. Luehrmann, and S. Wittekoek, "Practical 0.35 μm I-line Lithography," SPIE Vol. 2197 (1994) pp. 412-420.

11.38. V.A. Deshpande, K.L. Holland, and A. Hong, "Isolated-grouped Linewidth Bias on SVGL Micrascan," SPIE Vol. 1927 (1993) pp. 333-352.

11.39. R.C. Henderson, and O.W. Otto, "Correcting for Proximity Effect Widens Process Latitude," SPIE Vol. 2197 (1994) pp. 361-370.

11.40. H. Engstrom and J. Beacham, "Online Photolithography Modeling Using Spectrophotometry and PROLITH/2," SPIE Vol. 2196 (1994) pp. 479-485.

11.41. J. Kasahara, M. V. Dusa, and T. Perera, "Evaluation of a Photoresist Process for 0.75 Micron, G-line Lithography," SPIE Vol. 1463 (1991) pp. 492-503.

11.42. E. A. Puttlitz, J. P. Collins, T. M. Glynn, L. L. Linehan, "Characterization of Profile Dependency on Nitride Substrate Thickness for a Chemically Amplified I-line Negative Resist," SPIE Vol. 2438 (1995) pp. 571-582.

11.43. P. M. Mahoney and C. A. Mack, "Cost Analysis of Lithographic Characterization: An Overview," *Optical/Laser Microlithography VI, Proc.*, SPIE Vol. 1927 (1993) pp. 827-832.

Glossary

ABC Parameters — See Dill Parameters

Aberrations, Lens — Any deviation of the real performance of an optical system (lens) from its ideal performance. Examples of lens aberrations include coma, spherical aberration, field curvature, astigmatism, distortion, and chromatic aberration. One way to describe lens aberrations is through a Zernike polynomial fit to the wavefront error at the exit pupil of the lens.

Aerial Image — An image of a mask pattern that is projected onto the photoresist by an optical system.

Annular Illumination — A type of off-axis illumination where a doughnut-shaped (annular) ring of light is used as the source.

Antireflective Coating (ARC) — A coating which is placed on top or below the layer of resist to reduce the reflection of light, and hence, reduce the detrimental

effects of standing waves or thin film interference.

Bandwidth The range of wavelengths that is used to illuminate the resist.

Bias See Mask Bias

Binary Mask A mask made up of opaque and transparent regions (for example, composed of chrome and glass) such that the transmittance of the mask is either 0 or 1.

Bleaching The decrease in optical absorption of a photoresist due to the chemical changes that occur upon exposure to light.

Bossung Curves See Focus-Exposure Matrix

Bottom Antireflective Coating An antireflective coating placed just below the photoresist to reduce reflections from the substrate.

Cauchy Coefficients Coefficients of the Cauchy equation, which gives an emperical variation of the index of refraction of a material as a function of wavelength.

Chemically Amplified Resist A type of photoresist, most commonly used for deep-UV processes, which, upon post-exposure bake, will multiply the number of chemical reactions through the use of chemical catalysis.

Clearing Dose (E_o) See Dose to Clear

Coherent Illumination A type of illumination resulting from a point source of light which illuminates the mask with light from only one direction.

Condenser Lens Lens system in an optical projection system which prepares light to illuminate the mask.

Contrast See Photoresist Contrast

Contrast Enhancement Layer (CEL) A highly bleachable coating on top of the photoresist which serves to enhance the contrast of an aerial image projected through it.

Critical Dimension (CD) The size of a feature printed in resist.

Critical Shape Error (CSE) A metric used to determine the quality of a two dimensional feature as compared to the desired feature. See also Image Critical Shape Error.

Depth of Focus (DOF) The total range of focus which can be tolerated, that is, the range of focus that keeps the resulting printed feature within a variety of specifications (such as linewidth, sidewall angle, resist loss, and exposure latitude).

Development The process by which a liquid, called the developer, selectively dissolves a photoresist as a function of the exposure energy.

Development Rate The rate (change in thickness per unit time) that the photoresist dissolves in developer for a given set of conditions.

Development Rate Monitor (DRM) An instrument used to measure the development rate of a photoresist by measuring the thickness of the resist *in situ* as the development proceeds.

Diffusion Length The average distance that a particle will diffuse during post-exposure bake. This distance is defined to be:

$$Diffusion\ Length = \sqrt{2Dt}$$

where D = diffusivity, t = bake time

Diffraction The property of light which causes the wavefront to bend as it passes a boundary.

Diffraction Pattern The pattern of light entering the objective lens due to diffraction by a mask.

Dill Parameters The name of the exposure modeling parameters for photoresists which were developed by Frederick Dill at IBM in the 1970s. Also called the ABC parameters, these parameters apply to any photoresist which undergoes first order exposure kinetics.

Dose See exposure energy

Dose to Clear (E_o) The amount of exposure energy required to just clear the resist in a large clear area for a given process.

Dose to Size The amount of exposure energy required to produce the proper dimension of the photoresist feature.

DRM See Development Rate Monitor

Duty Cycle The ratio of the width of the feature of interest to the pitch of the repeating pattern.

E-D Tree See Image E-D Tree

Exposure Dose See Exposure Energy

Exposure Energy The amount of light energy (per unit area) that the photoresist is subjected to upon exposure by a projection system. It is equal to the light intensity times the exposure time.

Exposure Latitude The range of exposure energies (usually expressed as a percent variation from the nominal) which keeps the linewidth within the specified limits.

Exposure Margin The ratio of the dose to size to the dose to clear.

Flare The unwanted light that reaches the photoresist as a result of scattering and reflection off surfaces in the optical system that are meant to transmit light. Also called background scattered intensity.

Focal Position See Focus

Focus The position of the plane of best focus of the optical system relative to some reference plane, such as the top surface of the resist.

Focus-Exposure Matrix The variation of linewidth (and possibly other parameters) as a function of both

	focus and exposure energy. The data is typically plotted as linewidth versus focus for different exposure energies.
Frequency Plane	A term taken from Fourier Optics to describe the entrance pupil to an imaging lens.
Gaussian Illumination	A type of illumination with a Gaussian intensity distribution, such as is often obtained from a laser source.
GDS-II	An industry standard file format for mask information.
H-D (contrast) Curve	The standard form of the H-D or contrast curve is a plot of the relative thickness of resist remaining after exposure and development of a large clear area as a function of log-exposure energy. The theoretical H-D curve is a plot of log-development rate versus log-exposure energy. (H-D stands for Hurter-Driffield, the two scientists who first used a related curve in 1890).
Illumination System	The light source and optical system designed to illuminate the mask for the purpose of forming an image on the wafer.
Image Critical Shape Error	The value of the error of the resulting 2-D aerial image as compared to the desired pattern.
Image E-D Trees	A contour plot of constant linewidth versus exposure and defocus generated under the assumption of an infinite contrast resist. It

	can be calculated using only the aerial image as a function of defocus.
Image Log-Slope	The slope of the logarithm of the aerial image at the nominal line edge.
Image Placement Error	The difference between the center of the image and the nominal center of the feature.
Incoherent Illumination	A type of illumination resulting from an infinitely large source of light which illuminates the mask with light from all possible directions.
Index of Refraction	See Refractive Index
Iso-Dense Print Bias	The difference between the CDs of a dense line and an isolated line holding all other parameters constant.
Latent Image	The reproduction of the aerial image in resist as a spatial variation of chemical species (for example, the variation of photoactive compound concentration).
Linewidth	See Critical Dimension.
Log-Slope	See Image Log Slope
Lumped Parameter Model	A simple model of photoresist exposure and development which lumps all effects into two lumped parameters: an effective resist thickness and a lumped photoresist contrast.
Mask	A glass or quartz plate containing information (encoded as a variation in

transmittance and/or phase) about the features to be printed. Also called a photomask or a reticle.

Mask Biasing The process of changing the size or shape of the mask feature in order for the printed feature size to more closely match the nominal or desired feature size.

Metrology The process of measuring structures on the wafer, such as the width of a printed resist feature.

Modeling See Simulation

Negative Photoresist A photoresist whose chemical structure allows for the areas which are exposed to light to develop at a slower rate than those areas not exposed to light.

Normalized Image Log-Slope (NILS) The image log-slope multiplied by the nominal feature width.

Numerical Aperture The sine of the maximum half-angle of light which can make it through a lens, multiplied by the index of refraction of the media.

Objective Lens The main imaging lens of an optical projection system. Also called the projection lens or the reduction lens.

Off-Axis Illumination Illumination which has no on-axis component, i.e., which has no light which is normally incident on the mask. Examples of off-axis illumination include annular and quadrupole illumination.

Optical Path Difference (OPD) The difference in optical path (related to the difference in phase) between an actual wavefront emerging from a lens and the ideal wavefront, as a function of position on the wavefront.

Optical Proximity Correction (OPC) A method of selectively changing the shapes of patterns on the mask in order to more exactly obtain the desired printed patterns on the wafer.

PAC See Photoactive Compound

PAC Gradient The slope of the latent image at the bottom of the resist and at the nominal line edge.

Partial Coherence The ratio of the sine of the maximum half-angle of illumination striking the mask to the numerical aperture of the objective lens. Also called the degree of coherence and the pupil filling function, this term is usually given the symbol σ.

Partially Coherent Illumination A type of illumination resulting from a finite size source of light which illuminates the mask with light from a limited range of directions.

Pattern Placement Error The difference between the center of a simulated resist pattern from the nominal (designed) center.

PEB See Post-Exposure Bake

PEB Diffusion Length The diffusion length of chemical species during a post-exposure bake. (See also Diffusion Length)

Phase-Shifting Mask — A mask which contains a spatial variation not only in intensity transmittance but phase transmittance as well.

Photoactive Compound (PAC) — The component of a photoresist which is sensitive to light (also called a sensitizer).

Photoacid Generator (PAG) — The light sensitive component of a chemically amplified resist which generates an acid upon exposure to light.

Photolithography — The process of creating a three-dimensional relief image in a photoresist by exposure of the photoresist to light.

Photomask — See Mask

Photoresist — A photosensitive material which forms a three-dimensional relief image by exposure to light and allows the transfer of the image into the underlying substrate (for example, by resisting an etch).

Photoresist Contrast — A measure of the resolving power of a photoresist, the photoresist contrast is defined in one of two ways. The measured contrast is the slope of the standard H-D curve as the thickness of resist approaches zero. The theoretical contrast is the maximum slope of a plot of log-development rate versus log-exposure energy. The photoresist contrast is usually given the symbol γ.

Pitch — The sum of the linewidth and spacewidth for a repeating pattern of lines and spaces.

Point Spread Function The aerial image resulting from an infinitely small isolated pinhole on the mask.

Positive Photoresist A photoresist whose chemical structure allows for the areas which are exposed to light to develop at a faster rate than those areas not exposed to light.

Post-Exposure Bake (PEB) The process of heating the wafer immediately after exposure in order to stimulate diffusion of the PAC and reduce the effects of standing waves. For a chemically amplified resist, this bake also causes a catalyzed chemical reaction.

Prebake The process of heating the wafer after application of the photoresist in order to drive off the solvents in the resist (also called softbake and post-apply bake).

Process Window A window made by plotting contours corresponding to various specification limits as a function of exposure and focus. One simple process window, called the CD process window, is a contour plot of the high and low CD specifications as a function of focus and exposure. Other typical process windows include sidewall angle and resist loss. Often, several process windows are plotted together to determine the overlap of the windows.

Pupil Also called an aperture, this is the opening at the entrance or the exit of a lens. The size of a circular pupil is defined by its numerical aperture.

Pupil Filter — A device used to alter the transmission and/or phase of the light as it passes through the pupil of the objective lens.

Quadrupole Illumination — A type of off-axis illumination where four circles of light are used as the source. These four circles are spaced evenly around the optical axis.

Reduction Ratio — The ratio of the size of the features on the mask to the size of the features printed on the wafer.

Refractive Index — The real part of the refractive index of a material is the ratio of the speed of light in vacuum to the speed of light in the material. The imaginary part of the refractive index is determined by the absorption coefficient of the material α and is given by $\alpha\lambda/4\pi$ where λ is the vacuum wavelength of the light.

Resist — See Photoresist

Resist Linewidth — See Critical Dimension

Resist Gamma — See Photoresist Contrast

Resist Reflectivity — The reflectivity of a photoresist coated wafer. This reflectivity corresponds to the reflectivity that would be measured by bouncing light off of the resist coated wafer. If a Top ARC or CEL is used, the reflectivity could include these films as well.

Reticle — See Mask

Scalar Image Model — A mode of image calculation based on scalar descriptions of light.

SEM — Scanning Electron Microscope which is used to inspect photoresist profiles and measure critical dimensions.

SEM Array — An array of SEM cross-sections of photoresist profiles through focus and exposure.

Sensitizer — See Photoactive Compound

Sidewall Angle — The angle that a photoresist profile makes with the substrate.

Simulation — The process of using physical models to predict the behavior of a complex process. These models are usually implemented as computer software.

Smiley Plot — See Focus-Exposure Matrix

Standing Waves — A periodic variation of high and low intensity as a function of depth into the resist that results from interference between a plane wave of light traveling down through the photoresist and one which is reflected up from the substrate.

Substrate — The film stack, including the wafer, on which the photoresist is coated.

Substrate Reflectivity — The total reflectivity of the substrate beneath the resist. This is the reflectivity that light experiences after it passes through the resist and strikes the substrate.

Surface Inhibition — A reduction of the development rate at the top surface of a photoresist relative to the bulk development rate.

Swing Curve — A sinusoidal variation of a parameter, such as linewidth or E_o, as a function of resist thickness caused by thin film interference effects.

Swing Ratio — Determined from the linewidth swing curve, the linewidths of the first two maximums are averaged together to give CD_{max}. Then using the linewidth at the minimum between these two maximums, called CD_{min}, the swing ratio is defined as:

$$SR = 2*(CD_{max} - CD_{min})/(CD_{max} + CD_{min}) \text{ X } 100\%$$

TAR — A top antireflection coating used to reduce swing curves.

Vector Image Model — A mode of image calculation based on vector descriptions of light.

Zernike Coefficients — The coefficients of the Zernike polynomial.

Zernike Polynomial — A specific polynomial, usually cut off at 36 terms, used to fit the wavefront error of a lens for a given field point. This polynomial characterizes the aberrations of the lens.